Characterization and fate of lipofibroblasts during lung development and fibrosis

Inaugural Dissertation
submitted to the
Faculty of Medicine
in partial fulfillment of the requirements
for the PhD-Degree
of the Faculties of Veterinary Medicine and Medicine
of the Justus Liebig University Giessen

by
Vahid Kheirollahi
of
Khoy, IRAN

Giessen 2019

From the Department of Internal Medicine and
Excellence Cluster Cardio-Pulmonary System (ECCPS)
Director / Chairman: Prof. Dr. Werner Seeger
Faculty of Medicine of the Justus Liebig University Giessen

First Supervisor and Committee Member: Prof. Dr. Saverio Bellusci
Second Supervisor and Committee Member: Prof. Dr. Georgios Scheiner-bobis
Committee Members (Chair): Prof. Dr. Norbert Weissman
Committee Member:Prof. Dr. Jörg Distler

Date of Doctoral Defense: 29.05.2019

Declaration

“I declare that I have completed this dissertation single-handedly without the unauthorized help of a second party and only with the assistance acknowledged therein. I have appropriately acknowledged and referenced all text passages that are derived literally from or are based on the content of published or unpublished work of others, and all information that relates to verbal communications. I have abided by the principles of good scientific conduct laid down in the charter of the Justus Liebig University of Giessen in carrying out the investigations described in the dissertation.”

_____

Vahid Kheirollahi

Giessen June, 2019

Table of contents

List of figures

List of tables

Abbreviations and Acronyms

ACTA2	Alpha smooth muscle actin
ACTB	Beta-actin
ADRP	Adipose Differentiation-Related Protein
AECII	Alveolar Epithelial type II cells
ATP	Adenosine triphosphate
BCA	Bicinchoninic acid
BCS	Bovine Calf Serum
BMP2	Bone Morphogenesis Protein 2
BSA	Bovine Serum Albumin
CDH1	E-cadherin
CEBP	CCAAT Enhancer Binding Protein Beta
COPD	Chronic Obstructive Pulmonary Diseases
DAPI	4′,6-diamidino-2-phenylindole
DMEM	Dulbecco's Modified Eagle's Medium
d.p.i.	Day post instillation
DTT	Dithiothreitol
ECM	Extra Cellular Matrix
EMT	Epithelial to Mesenchymal Transition
ERK	Extracellular signal-regulated kinase
FACS	Fluorescent Activated Cell Sorting
FDA	Food and Drug Administration

FGF10	Fibroblast Growth Factor 10
FGFR	Fibroblast Growth Factor receptor
FITC	Fluorescein isothiocyanate
FOXJ1	Forkhead Box J1
FVC	Forced Vital Capacity
GPx3	Glutathione Peroxidase 3
HRP	Horse Radish peroxidase
IPF	Idiopathic Pulmonary Fibrosis
LIF	Lipofibroblast
LOXL2	Lysyl Oxidase Like 2
LPA	LysoPhosphatidic Acid
LPS	Lipopolysaccharide
MAPK	Mitogen-Activated Protein Kinase
mT/mG	Membrane-targeted tdTomato/membrane-targeted green fluorescent protein
mTOR	Mammalian Target Of Rapamycin
NG2	Neural/Glial antigen 2
PAH	Pulmonary Arterial Hypertension
PBGD	Porphobilinogen deaminase
PBS	Phosphate buffered saline
PCLS	Precision-cut lung slices
PCR	Polymerase chain reaction
PDGFrα	Platelet Derived Growth Factor receptor alpha

PDGFrβ	Platelet Derived Growth Factor receptor beta
PARP1	Aoly(ADP-ribose) Polymerase 1
PI3K	PhosphoInositide 3-Kinase
PLIN2	Perilipin 2
PPARa	Peroxisome Proliferator Activated Receptor alpha
PPARb	Peroxisome Proliferator Activated Receptor beta
PPARg	Peroxisome Proliferator Activated Receptor gamma
PPARd	Peroxisome Proliferator Activated Receptor delta
PPRE	PPAR Responsive Element
PTK	Phospho-Tyrosin Kinase
PVDF	Polyvinylidene Fluoride
PTEN	Phosphatase and tensin homologue deleted on chromosome 10
ROCK2	Rho associated Coiled-coil containing protein Kinase 2
SDS-PAGE	Sodium dodecyl sulfate-polyacrylamide gel electrophoresis
siRNA	Small interfering RNA
SPF	Specific Pathogen-Free
STK	Serine/Threonine Kinase
TGFβ1	Transforming Growth Factor beta 1
THY-1	Thy-1 Cell Surface Antigen
WT	Wild type

1. Introduction

1.1. Idiopathic Pulmonary Fibrosis

1.1.1. Overview

Idiopathic pulmonary fibrosis (IPF) is a fatal lung disease of unknown etiology. This disease is more common among the elderly and the average survival rate following diagnosis is only 2-3 years (Sgalla et al., 2016). Histopathological examination of IPF lungs typically reveals extensive alveolar scarring; i.e. replacement of normal alveoli by fibrous scars containing myofibroblasts. The latter cells are considered to be the main source of excessive extracellular matrix (ECM) protein deposition, particularly collagen (Todd et al., 2012), not only in IPF lungs but also in fibrosis of other organs. Due to its progressive nature and since the process of scar formation is part of natural wound healing, IPF is widely regarded as an aberrant wound healing response to repetitive epithelial injury (Günther et al., 2012).

1.1.2. Clinical manifestation and diagnosis

Due to excessive amount of ECM during progression of IPF, patients manifest reduced Forced Vital Capacity (FVC), reduced DLco (Diffusion capacity of lung for carbon monoxide), impaired gas exchange and dyspnea combined with dry cough (Sgalla et al., 2016). Manifestation of sub-pleural/ basal predominance, reticular abnormality and honeycombing with or without traction bronchiectasis in high resolution computed tomography and histology are the current clinical criteria for IPF diagnosis (Sgalla et al., 2016).

1.1.3. Management of IPF

Currently, there are only two FDA-approved medications for IPF which have been proven to be effective in slowing the progression of IPF: Pirfenidone, which is considered as anti-inflammatory and anti-oxidant, exerts its antifibrotic effects by antagonizing TGFβ1 signaling (Sgalla et al., 2018). Analysis of data from the CAPACITY and the ASCEND trials showed that patients who received Pirfenidone experienced much slower rate of FVC decline compared to the placebo group (Nathan et al., 2016). Nintedanib is a multi-

tyrosine kinase receptor inhibitor that was shown to be effective in reducing IPF progression (Richeldi et al., 2014). In spite of efficacy of the aforementioned medications, neither of them can reverse ongoing fibrosis and at best can only retard its progression.

Despite the initial promising results of Pirfenidone, recent re-evaluation revealed that it cannot prevent DLco reduction in patients with advanced IPF even though it significantly reduces FVC decline (Yoon et al., 2018). The published report from the ASCEND trial showed that Pirfenidone is safe to use with acceptable side effect and it can significantly reduce progression of IPF (King et al., 2014). It is worthy to note that the same trial showed that about 16% of patients experienced decline of FVC after 52 months of treatment (King et al., 2014). Moreover, about 15% of patients discontinued the trials due to side effects (King et al., 2014). Another retrospective data analysis reported that Pirfenidone efficacy may diminish after 6 months in patients with severe IPF (Tzouvelekis et al., 2017). Considering that the conducted clinical trials were limited to only 52 weeks, the possible development of drug resistance to Pirfenidone or reduction of its efficacy due to longer treatment period is currently unknown.

Investigating the efficacy of Nintedanib in the clinical trials unveiled its promising effects in reduction of FVC decline in IPF patients. It seems to be safe and generally well tolerated (Richeldi et al., 2014). Despite success of Nintedanib in reducing FVC decline by about 50%, one should note that it only retards the progress of IPF. Thus, eventual worsening of the disease or development of drug resistance ultimately lead to lung transplantation.

1.1.4. Emerging novel therapeutic targets

As mentioned above, neither Pirfenidone nor Nintedanib can reverse lung fibrosis. Therefore, a huge amount of research resources has been directed towards finding novel therapeutic targets for IPF. Hence, finding new medications which can actually reverse the fibrosis is now the focus of researchers around the globe. However, couple of dark spots make this journey far more difficult. Due to interspecies differences between rodent bleomycin injury and human IPF, use of rodent models for the preclinical studies isn’t the best option, but only available one. Furthermore, being a rare disease makes accessibility

of human based research material very limited. Last but not least, due to idiopathic nature of this disease and lack of substantial knowledge about major cells involved in the progression of IPF, finding new therapeutic targets is more difficult. Table 1. lists several of these attempts.

Table 1. Novel therapeutic targets for IPF

Reagents	Molecular mechanism	Reference	Results of clinical trial
GC1008	neutralizing antibody against TGFβ1	(Madala et al., 2014)	Phase 1 (Terminated)(Low efficacy)(NCT00125385)
BG00011	humanized antibody against αvβ6	(Raghu et al., 2018a)	Phase 2A (completed) (promising results), currently at phase 2B
Tralokinumab Lebrikizumab SAR156597	neutralizing antibody against Interleukin 13 and Interleukin 13/14	(Parker et al., 2018; Raghu et al., 2018b; Swigris et al., 2018)	Phase 2A (stopped due to lack of efficacy)
GLPG1690	antagonist of the LPA1 receptor	(Maher et al., 2018)	Phase 1 completed (NCT02738801)(Promising results)
BMS-986020	antagonist of the LPA1 receptor	(Palmer et al., 2018)	Phase 1 (completed) (promising results) Phase 2 completed (Promising results) (NCT01766817)
cocktail of dasatinib and quercetin	cell senescence inducing cocktail	(Schafer et al., 2017)	NA

Pamrevlumab (FG-3019)	monoclonal antibody to reduce Connective Tissue Growth Factor activity	(Raghu et al., 2016)	Phase 2 (completed) (Positive results) (NCT01890265) Phase 3 (Planned)
Omipalisib (GSK2126458)	highly selective dual inhibitor of PI3K and mTOR	(Maher et al., 2017)	Phase 1B (completed) (positive results)((NCT01725139))
Simtuzumab	humanized monoclonal antibody to LOXL2	(Barry-Hamilton et al., 2010)	Phase 2 , RAINER (NCT01769196) and ATLAS (NCT01759511) (Terminated) (Lack of efficacy)
KD025	selective inhibitor of ROCK2	(Averill et al., 2018)	Phase 2 (completed) (positive results) (NCT02688647)
Nintedanib plus Sildenafil		(Kolb et al., 2018)	Phase 2 (completed) (No beneficial effect of sildenafil)(NCT02802345)

1.1.5. Animal models used to study lung fibrosis

Several animal models have been developed to study the progression of lung fibrosis:

Administration of bleomycin, which initially introduced as a chemotherapeutic antibiotic, resulted in development of pulmonary fibrosis in the recipients (Tashiro et al., 2017). It's believed that bleomycin causes single and double stranded breaks in the DNA which ultimately results in increasing level of reactive oxygen species followed by epithelial cell death, excessive infiltration of inflammatory cells, activation of fibroblasts and extra cellular matrix deposition. Despite being regarded as the best fibrosis model, it has been subjected to sever criticism for the inability of this model to fully recapitulate fibrosis in humans. Majority of these criticisms concern rapid pace of its development, initiation of

fibrosis following inflammation and auto resolution mechanism of this model (Tashiro et al., 2017). Despite the aforementioned limitations, during this project we have opted to use this model, simply due to being the best model available to study progression and pathogenesis of the lung fibrosis.

Administration of silica to the lung results development of fibrosis. Despite mimicking some aspects of human lung fibrosis, long waiting period usually 4-16 week, lack of reproducibility and fibroblastic foci, wide heterogeneity and hyperplastic epithelium in addition to requirement for expensive equipment's used to aerosolize the silica dramatically limits applicability of this method (Tashiro et al., 2017). Administration of asbestosis also leads to fibrotic lungs which are very distinct from IPF lungs. Bronchial wall fibrosis, presence of fewer myofibroblastic foci and development of fibrosis in the central areas of the lung rather than sub-plural area are among the caveats of this model (Tashiro et al., 2017). Overexpression of cytokines such as TGF-β, TNF-α, IL-13 leads to increased apoptosis rate of alveolar epithelial cells and activation of fibroblasts. Even though these models result a highly variable and heterogeneous fibrotic response, they tend to mimic human disease features much better. However, these models developed recently, thus aren't as well established as bleomycin model. Hence, they are currently more useful to study role of a specific signaling pathway in the pathogenesis of disease rather than recapitulating the complexity of human fibrosis (Tashiro et al., 2017).

Induction of fibrosis via administration of fluorescent isothiocyanate, radiation-induced fibrosis and intravenous instillation of human IPF fibroblasts which results humanized model of lung fibrosis are among the other model which have been developed recently. They also share their own fair share of limitations and caveats.

1.1.6. Cellular origin of activated myofibroblasts

Exploring the cellular origin of activated myofibroblasts, which are the main culprit in the formation of fibrotic foci and deposition of ECM (Zhang et al., 1996b), is important for exploring novel therapeutic options to treat IPF patients. Several cell populations have been proposed to be the cell-of-origin for activated myofibroblasts in lung fibrosis. Resident fibroblasts are a heterogeneous population of cells located in the lung

interstitium. These cells are plastic and play important roles during both normal lung homeostasis and repair after injury (Sontake et al., 2019). Several groups have already shown major contribution of these resident cells to activated myofibroblasts at the event of lung injury (Barron et al., 2016; Hung et al., 2013; Kendall and Feghali-Bostwick, 2014). However, identity of these cells and the molecular mechanisms involved in the process are not sufficiently studied.

Fibrocytes are mesenchymal progenitor cells originated from bone marrow which can be found in the fibrotic foci. However, their contribution to activated myofibroblast pool in the IPF via transdifferentiation is controversial (Maharaj et al., 2013). Moore et al., provided evidences that these cells migrate to the area with active fibrosis and can produce cytokines which are crucial for the progression of fibrosis (Moore et al., 2006). However, direct differentiation of fibrocytes to activated myofibroblasts is the topic of debates in the scientific community.

Pericytes are another group of perivascular, mesenchymal like cells which contribute to progression of lung fibrosis. Like fibrocytes, they are subject of many scientific debates regarding their ability to transdifferentiate to activated myofibroblasts. Using lineage tracing tools Rock et al., didn't observe transdifferentiation of $NG2^+$ and $Foxj1^+$ cells to activated myofibroblasts (Rock et al., 2011). On the other hand, a more recent study managed to provide evidences regarding contribution of $NG2^+$/ $Pdgfrb\beta^+$ double positive pericytes to the pool of activated myofibroblast (Hung et al., 2013). Considering published reports, further research is required to resolve these controversies.

Another one of controversial sources which have been described to contribute to the pool of activated myofibroblasts are epithelial cells. Based on evidence provided in one study, epithelial cells undergo Epithelial to Mesenchymal Transition (EMT) and differentiate to activated myofibroblasts following exposure to TGFβ1 signaling pathway (Tanjore et al., 2009). In comparison, using lineage tracing tools, Kim et al., didn't observed a major transition of epithelial cells to activated myofibroblasts (Kim et al., 2006). These discrepancies might be due to difference in animal models which have been used in the previous studies and warrant further research.

1.2. Lipofibroblasts in the developing lung: overview

The lung mesenchyme consists of serval different cell types that play various roles during homeostasis. One of the understudied mesenchymal cell types in the lung is the lipid droplet-containing interstitial fibroblast, also known as the lipofibroblast (LIF). LIFs were first identified in 1970 via electron microscopy imaging of the developing lung (O'Hare and Sheridan, 1970). They have been described as lipid droplet-containing fibroblasts residing in close proximity to type II alveolar epithelial cells (AECII). However, detailed characterization of these cells during normal development of lung, homeostasis and disease progression is still lacking substantial details. Initial reports provided evidence regarding their heterogeneity and suggested potential role of LIFs in alveolarization and restructuring of the lung (Brody and Kaplan, 1983; Maksvytis et al., 1981). Furthermore, Tordet et al. reported that increasing level of diacylglycerols and triacylglycerols starting at E17.5 in the rats lung coincides with the appearance of lipofibroblasts (Tordet et al., 1981). Considering all the available information at that time, it was proposed that these cells support AECIIs in the process of pulmonary surfactant production via storing and transferring lipid molecules to these cells as was later demonstrated by Torday et al. (Torday et al., 1995). Torday et al, revealed that labeled fatty acids accumulated in the lipofibroblasts shuttle to AECIIs (Torday et al., 1995). Several pieces of evidence revealed that LIFs require active PPARg signaling pathway which leads to expression of *PLIN2*, also known as *ADRP* (Adipocyte Differentiation Related Protein), as well as other lipid binding proteins and finally accumulation of lipid droplets (McGowan et al., 1997; Schultz et al., 2002). In an attempt to study the molecular mechanisms involved in formation and maintenance of the lipofibroblasts, Schultz et al., isolated AECII and lipofibroblasts and assessed expression level of *Plin2*. Their data showed increased level of *Plin2* as a downstream target of Pparg, which binds and encapsulated lipid droplets in lipofibroblasts that harbor active fatty acid synthesis and storage mechanism. On the other hand, AECIIs which dont store lipid droplets, express minimal levels of *Plin2*. In addition to *PLIN2* and *PPARg*, *THY-1* (Friedmacher et al., 2014), parathyroid hormone-related protein (Rehan and Torday, 2014) and leptin are among other markers of LIFs. Overexpression of *Thy-1* in *Thy-1* negative cells, increases expression of *Pparg* and its co-receptor, *RXR-α*, and eventually *Plin2* (Varisco et al., 2012). Despite increasing level of attention toward LIFs in the past years, their origin and potential role in pulmonary diseases remain unclear. El Agha et al. carried out genetic

lineage tracing using a novel *Fgf10Cre-ERT2; tomato^{flox}* line to show that FGF10^{+} cells labeled at either E11.5 or E15.5 give rise lipofibroblasts at the end of gestation (E18.5) (El Agha et al., 2014). It's worthy to note that only a fraction of lipofibroblasts derives from the FGF10^{+} lineage. Recently, it has been shown that mesenchymal cells expressing *Tcf21* are also progenitors for LIFs during embryonic lung development (Park et al., 2019). It remains to be established how distinct the FGF10^{+} and TCF21^{+} cell populations are, and whether there are other unknown cellular sources for LIFs in the developing lung.

1.2.1. PPARg signaling pathway

The signature signaling pathway that is believed to be required for the formation and maintenance of lipofibroblasts is the PPARg signaling cascade (El Agha et al., 2017; McGowan et al., 1997). PPARg is part of a bigger family of PPARs (PPARa, PPARb, PPARg and PPARd) that after shuttling into the nucleus exert their function via binding to PPAR Responsive Element (PPRE) in the promoter region of their target genes. Although they share similarities in their structure, each member of the PPAR family has unique functions as reflected by distinct tissue distribution and differential response to distinct ligands (Poulsen et al., 2012). The *PPARg* gene encodes two variants, PPARg1 and PPARg2 as a result of having two transcription start sites as well as alternative splicing. *PPARg1* is expressed ubiquitously in various cell types in the body while *PPARg2* is exclusively expressed in adipocytes (Medina-Gomez et al., 2007; Tontonoz and Spiegelman, 2008).

1.2.2. PPARg signaling plays different roles in different pulmonary cells

Since its discovery, due to the complexity and importance of this signaling cascade, PPARg signaling has been an interesting research topic. Several crucial roles have been described for PPARg signaling including but not limited to various roles in adipogenesis, differentiation and maintenance of adipocytes (Tontonoz and Spiegelman, 2008), cellular metabolism (Tomaru et al., 2009), cell cycle control and tumorigenesis (Penna et al., 2016; Sjodahl et al., 2019), obesity and insulin resistance (Marginean et al., 2018),

modulation of immune system and immune response (Martin, 2010; Speca et al., 2014; Vallee et al., 2018), mitochondrial function and regeneration (Corona and Duchen, 2016) and others. Reddy et al., provided evidence that activation of PPARg, which in turn results in increasing levels of GPx3, protects murine lungs from cigarette smoke-induced Chronic Obstructive Pulmonary Diseases (COPD) (Reddy et al., 2018). Another study reported a protective role for PPARg signaling against cigarette smoke induced inflammation via activation of AMP-activated protein kinase (AMPK) (Wang et al., 2018). Furthermore, activation of this signaling cascade protects against LPS-induced acute lung injury (Jiang et al., 2018) as well as Pulmonary Arterial Hypertension (PAH) (Rashid et al., 2018).

1.2.3. PPARg signaling in Idiopathic Pulmonary Fibrosis

PPARg signaling is significantly altered in fibrotic disease of the lung as well as other organs (Burgess et al., 2005; Marra et al., 2000). Treatment of fibroblasts with TGFβ1 results in suppression of PPARg signaling, a process that can be rescued via supplementation with PPARg agonists (Bartram and Speer, 2004; Burgess et al., 2005). Treatment of human lung fibroblasts with recombinant human TGFβ1 leads to increased phosphorylation of SMAD3/SMAD4, shutting of this complex into the nucleus and binding to consensus TGFβ1 inhibitory element (TIE) and also to canonical SMAD-binding elements (SBEs) at PPARg promoter. Occupation of these binding sites with SMAD3/SMAD4 complex results in inhibition of *PPARg* expression (Lakshmi et al., 2017). On the other hand, activation of PPARg-RXR heterodimer leads to suppression of *TGFβ1* expression via dephosphorylation of zinc-finger transcription factor-9. Furthermore, PPARg induces expression of *PTEN* (phosphatase and tensin homologue deleted on chromosome 10) which in turn can suppress *TGFβ1* expression in a p70 ribosomal S6 kinase-1 dependent manner (Lee et al., 2006). Moreover, PPARg is the key link between BMP2 and TGFβ1 signaling which seems to play a major role in the progression of PAH (Calvier et al., 2017). Due to significance of TGFβ1 and BMP2 signaling pathway in IPF pathogenesis, this link is potentially critical in the pathogenesis of IPF as well. Furthermore, PPARg can bind to the PPRE element in the promoter region of PETN which can attenuate differentiation of activated myofibroblasts (Teresi et al., 2006; White et al.,

2006). 15-deoxy-(12,14)-15d-prostaglandin J2, another natural PPARg agonist, can attenuate TGFβ1 induced phosphorylation of AKT at serine 473 which in return blocks differentiation of fibroblasts to activated myofibroblasts (Kulkarni et al., 2011).

1.3. Metformin

Metformin is a small molecule, originally developed to combat type II diabetes, is referred to first line medication to manage this malady. It is revealed that metformin reduces blood sugar level via reduction of gluconeogenesis in the liver in addition to sensitizing the cells to insulin (Dhatariya, 2019). Furthermore, the ability of metformin to manipulate cellular metabolism via deactivation of complex I in the electron transfer chain of mitochondria and activation of AMPK is well established (Andrzejewski et al., 2014; Loubiere et al., 2017). Manipulation of cellular metabolism in targeted manner can bear a significant importance to combat a wide range of diseases such as cancer, infectious diseases, diseases related to function of immune system, fibrosis and etc. Since it's well tolerated with very minimal side-effects, the number of reports regarding efficacy of metformin to efficiently manage other diseases grows rapidly. Metformin reduces ability of hepatocellular carcinoma cells to migrate and eventually conduct metastasis via activation of AMPK (Ferretti et al., 2019). Promotion of survivin degradation via AMPK/PKA/GSK-3β axis in the non-small cell lung cancer results in an increased level of apoptosis and reduced survivability of cancer cells (Luo et al., 2019). Moreover, metformin increases expression of brain derived neurotrophic factor in an AMPK/Tet2 dependent manner which acts as an antidepressant (Wang et al., 2019). Its phenomenal effect on slowing down the aging process and aging related diseases which is mainly modulated via NF-kB can't be ignored either (Kanigur Sultuybek et al., 2019). Interestingly, IPF is associated with metabolic disorders. For example, a recent report has shown that IPF lungs display alterations in several metabolites linked to energy consumption (Rowzee et al., 2008). In addition, there is evidence suggesting that several types of lipid molecules present in blood plasma could be used as biomarkers for IPF (Yan et al., 2017). One study has even suggested that type 2 diabetes might be a risk factor for developing IPF (García-Sancho Figueroa et al., 2010). Although it remains

unclear whether these metabolic abnormalities represent a cause or a consequence of the disease, the link between fibrosis and metabolic alterations in the lung raises the question whether antidiabetic drugs can be good candidates for antifibrotic therapy. Rosiglitazone, initially developed as an antidiabetic agent. Several reports provided by us and other groups' demonstrated potential efficacy of rosiglitazone to ameliorate progression of lung fibrosis (El Agha et al., 2017; Burgess et al., 2005). However, due to increased risk of heart failure in the patients suffering from ischemic heart diseases dramatically decreased the enthusiasm to conduct more research on antifibrotic effects of rosiglitazone (Castilla-Guerra et al., 2018).

Many studies have reported the therapeutic effects of metformin in non-diabetic diseases such as non-small-cell lung cancer (Li et al., 2017), prostate cancer(Yu et al., 2017) and cardiovascular diseases (Castilla-Guerra et al., 2018). Moreover, it has been suggested that intraperitoneal administration of metformin attenuates bleomycin-induced lung fibrosis in mice via NADPH oxidase 4 (NOX4) suppression (Sato et al., 2016a). A more recent report has shown that metformin accelerates resolution of bleomycin-induced pulmonary fibrosis, suggesting activation of AMP-activated protein kinase (AMPK) as key underlying signaling event, leading to downregulation of alpha smooth muscle actin (ACTA2) and collagen, and increasing myofibroblast autophagy and ECM turnover (Rangarajan et al., 2018)

2. Objectives

Despite ever-growing number of research reports regarding potential therapeutic targets, battling IPF is still very hard. The approved medications can only at best slow the disease progression and reduces the severity of the symptoms but don't bear a therapeutic function. Hence, the lethality rate remains very high. To explore novel therapeutic interventions for IPF, the characteristic of activated myofibroblasts must be investigated. Better characterization of activated myofibroblasts and their origin will help to improve current understanding of the disease progression and pathogenesis. An underappreciated population of cells which have been over looked for a long time is pulmonary lipofibroblasts. However, to study potential contribution of lipofibroblasts to the pool of activated myofibroblasts, one must first study and better characterize the lipofibroblasts themselves.

This study provides a better characterization of lipofibroblast in the mouse model, time course of their formation in the murine lung in addition to providing evidence regarding involvement of Fgf10 signaling in their formation. Furthermore, using lineage tracing, their contribution to the pool of activated myofibroblasts has been explored. Last but not least, effect of metformin in reversing pulmonary fibrosis via trans-differentiation of activated myofibroblast to lipofibroblasts due to enforcing the lipogenic metabolomics changes. Has been studied.

This study contains two main goals as described below:

I. **Better characterization of lipofibroblasts and investigating their contribution to pool of activated myofibroblasts.**

Using mouse model, formation of lipofibroblasts during the embryonic development was explored utilizing different readouts such as quantitative-PCR and flow cytometry. Staining of the single cell suspension prepared from mouse lung provided opportunity to investigate formation of lipofibroblasts based on existence of lipid droplets which indicates full differentiation status. Furthermore, cell culture and *Fgfr1b* knock out animals were used to study status of Fgf10 signaling in the formation of these cells. Labeling of lipofibroblasts using *AdrpCre-ERT2; mT/mG* mice before bleomycin injury provided

possibility to study fate of preexisting lipofibroblasts during progression of fibrosis and resolution phase.

II. **Trans-differentiation of activated myofibroblasts to lipofibroblasts can be a novel therapeutic intervention**

TGFβ1 signaling is considered to be the most important signaling cascade in the progression of fibrosis. Treatment of pulmonary fibroblasts with recombinant TGFβ1 results in trans-differentiation of these cells to activated myofibroblasts. Rosiglitazone, an agonist of Pparg, can activate Pparg signaling pathway which will counterbalance activation of TGFβ1 pathway. Since rosiglitazone might not be the ideal therapeutic option for patients who are at risk of developing ischemic heart disease, exploring the applicability of alternative therapeutic compounds is clinically relevant. Thus in search for an alternative antidiabetic drug, it was hypothesized that metformin accelerates fibrosis resolution by inducing lipogenic differentiation in lung fibroblasts, while inhibiting TGFβ1-mediated myogenic differentiation. To test this hypothesis, primary cultures of human IPF-derived lung fibroblasts, cultures of precision-cut lung slices (PCLS) derived from human IPF patients, and genetic lineage tracing in the context of the bleomycin injury model of lung fibrosis in mice were used.

The objectives of this study are summarized below:

- Better characterizations of lipofibroblasts during embryonic development in the murine model
- Exploring importance of FGF10 signaling in the formation of lipofibroblasts
- Studying possible transdifferentiation of lipofibroblasts to activated myofibroblasts during progression of fibrosis.
- Investigating efficacy of metformin to reverse pulmonary fibrosis via enforcing lipogenic phenotype in the activated myofibroblasts

3. Materials and Methods

3.1. Animal experiments

All animals were housed under specific pathogen-free (SPF) conditions with free access to food and water. *Acta2-CreERT2 (STOCK_Tg(Acta2-cre/ERT2)12Pcn)* mice were kindly provided by Dr. Pierre Chambon (University of Strasbourg, France). In this transgenic line, CreERT2 coding sequence was inserted at the initiation codon of *Acta2* in a mouse bacterial artificial chromosome (BAC) (MGI: 3831907). The Cre reporter line *tdTomato^{flox}* (*B6;129S6-Gt(ROSA)26Sor$^{tm9(CAG-tdTomato)Hze}$/J* was purchased from the Jackson laboratory (stock number 007909). *RjOrl:SWISS* also known as CD1 line were purchased from Janvier labs. *AdrpCre-ERT2* knock-in mice (knock in of Cre-ERT2 in Exon 8 of the endogenous Adrp locus) were generated at the Max Planck Institute in Bad Nauheim, Germany (A.N., unpublished data) and the experiments performed in collaboration with Aglaia Ntokou, Friederike Klein and Katrin Ahlbrecht (Morty lab in MPI Bad Nauheim). Tandem dimer Tomato (tdTomatoflox) and membrane-targeted tdTomato/membrane-targeted green fluorescent protein (mT/mG) Cre-reporter mice were purchased from the Jackson laboratory.

3.2. Animal experimentation approval

Animal experiments were approved by the local authorities (Austrian Ministry of Education, Science and Culture; BMWFW-66.010/0043-WF/V/3b/2016), local authorities in Bad Nauheim, Germany (protocol number B2/354) and Justus Liebig University Giessen 405_M and performed in accordance with the EU directive 2010/63/EU.

3.3. Mice Genotyping

Tissues from the distal tip of the tails were digested in 200 µl Viagen including 1 µl proteinase K in 55°C on a shaker overnight, then reaction was stopped in 85°C for 40 min. Genotyping was done by PCR. For protocol and primer sequences please see Table 1. PCR products were analyzed using a 1,5 % agarose gel containing TAE buffer with Sybrsafe (50 µl Sybrsafe + 500 ml 1x TAE buffer). 10 µl of PCR samples was loaded with 2 µl loading dye (Biorad Nucleic Acid Sample loading buffer, 5x), and then gel was run

with 120V for 30-45 min. A molecular ladder (QX Size Marker, 100bp-2.5kb, Qiagen) was used to detect the expected band sizes (Table 1).

Table 2. Primer sequences and protocols for genotyping.

Mouse Line	**Primer sequence**	**PCR Protocol**		
		Step	**Temp. (°C)**	**Time**
Acta2-CreERT2	1) ATT TGC CTG CAT TAC CGG TC 2) ATC AAC GTT TTG TTT TCG GA	1	94	30 sec
		2	94	30 sec
		3	55	30 sec
		4 (repeat Step 2-4 30 times total)	72	1 min
		5	4	hold
tdTomato^{flox}	1) CTG TTC CTG TAC GGC ATG G 2) GGC ATT AAA GCA GCG TAT CC 3) CCG AAA ATC TGT GGG AAG TC 4) AAG GGA GCT GCA GTG GAG TA	1	94	3 min
		2	94	20 sec
		3	61	30 sec
		4 (repeat Step 2-4 30 times total)	72	30 sec
		5	72	2 min
		6	4	hold
AdrpCre-ERT2	1) GGT GCA AGC TGA ACA ACA GG	1	94	3 min
		2	94	30 sec

	2) GGT CCT GCC AAT GTG GAT CA	3	57.3	45 sec
		4 (repeat Step 2-4 40 times total)	72	1 min
		5	72	10 min
		6	4	hold
(mT/mG)	1) CCA GGC GGG CCA TTT ACC GTA AG 2) AAA GTC GCT CTG AGT TGT TAT 3) GGA GCG GGA GAA ATG GAT ATG	1	94	2 min
		2	94	20 sec
		3 -0.5 ◦**C** per cycle decrease	65	15 sec
		4 (repeat Step 2-4 10 times total)	68	10 sec
		5	94	15 sec
		6	60	15 sec
		7 (repeat Step 5-7 28 times total)	72	10 sec
		8	72	2 min
		9	4	hold

Table 3. Expected band size of genotyping products.

Mouse line	Expected band size for WT	Expected band size for mutant
Acta2-CreERT2	-	349 bp
tdTomato^{flox}	297 bp	196 bp
AdrpCre-ERT2	-	463 bp
(mT/mG)	603	320 bp

3.4. Bleomycin injury, tamoxifen administration and metformin treatment

At 11-12 weeks of age, *Acta2-CreERT2; tdTomato^{flox}* males were subjected to intratracheal instillation of saline or bleomycin (0.8 U/kg body weight) (Sigma-Aldrich) using a micro-sprayer (Penn-Century, Inc.) at the Ludwig Boltzmann Institute in Graz, Austria. Five days after bleomycin instillation, mice were fed tamoxifen-containing chow (400 mg/kg food, Envigo) for nine days. Metformin (1.5 mg/mL) or vehicle (PBS) was supplied via drinking water at day 14 after bleomycin instillation. Lungs were harvested on day 28.

AdrpCre-ERT2; mT/mG mice were fed tamoxifen-containing pellets starting day -28 until day -14 followed by 14 dyas of normal food (as chase period). Tamoxifen-containing pellets (0.4 g tamoxifen per Kg of pellets) were purchased from Altromin. At day 0, the animals received an intratracheal instillation of saline or bleomycin (3.5 U/Kg of body weight) at the Max Planck Institute in Bad Nauheim, Germany and were sacrificed at day 14.

3.5. Mouse primary cell culture

Whole lungs were dissected from embryos, minced into small pieces and subjected to 0.5% collagenase IV (Gibco)(45 min at 37°C) digestion to give rise to single cells. In the next step cell suspension passed through 70 and 40 micrometer cell strainers, respectively. Following centrifugation (1000 RPM, 10 minutes), cells were resuspended and plated in 6-well plates for 17 minutes in Dulbecco's Modified Eagle's Medium (DMEM) (Invitrogen) supplemented with 10% bovine calf serum (BCS, Gibco) at 37 °C and 5%

CO_2. Due to difference in adhesion capacity of the epithelial and mesenchymal cells, mesenchymal cells will attach to plate while the epithelial and other cell are mostly floating in the media. After 17 minutes, the plates were washed with pre-warmed PBS. Medium was replaced with fresh Dulbecco's Modified Eagle's Medium (DMEM) (Invitrogen) supplemented with 10% bovine calf serum (BCS, Gibco) and incubated at 37 °C and 5% CO_2 for next 24 hours.

3.6. Human-derived specimens

Fresh human lung explants and primary lung fibroblasts were obtained through the European IPF registry (eurIPFreg) at the Universities of Giessen and Marburg Lung Center, member of the German Center for Lung Research. Written consent was obtained from each patient and the study was approved by the ethics committee of Justus-Liebig University Giessen.

3.7. Human cell culture

Primary lung fibroblasts derived from twelve IPF patients were maintained in Dulbecco's Modified Eagle's Medium (DMEM) (Invitrogen) supplemented with 10% bovine calf serum (BCS, Gibco) at 37 °C and 5% CO_2. Cells between passages 3 and 7 were used for the experiments. Briefly, $3x10^5$ cells were seeded per well in 6-well plates (Greiner Bio-One). The next day, cells were starved (0% serum) for 24 h and then treated with different compounds. For imaging experiments, cells were cultured in 4-well chamber slides (Sarstedt) at a density of 75,000 cells per well and were treated according to the same procedure described above. Cells were treated with metformin (Ratiopharm), pirfenidone (Cayman Chemical Company), nintedanib, selumetinib or GSK621 (all from Selleckchem), recombinant human TGFβ1 (rhTGFβ1) or rhBMP2 (both from R&D Systems). Table 3 summarizes treatment conditions. As controls, the same cells were treated with the corresponding solvents as recommended by the manufacturer (same volumes as treated groups).

Table 4. Treatment conditions of primary human lung fibroblasts.		
Compound	Final concentration	Solvent
GSK621	10 µM*	DMSO
Metformin	1 mM, 5 mM,10 mM	DMEM
Nintedanib	1 µM*	DMSO
Pirfenidone	0.3 mg/mL*	Ethanol
Selumetinib	5 µM*	DMSO
rhTGFβ1	2 ng/mL	rhTGFβ1 reconstitution buffer
rhBMP2	50 ng/mL*	rhBMP2 reconstitution buffer

* Dosage was chosen based on a literature search and the dose showing highest efficacy was selected.

3.8. Precision-cut lung slices

Fresh lung specimens were obtained from 4 IPF patients that underwent lung transplantation. Precision-cut lung slices were prepared in two ways: lung specimens were cut into strips (length: 2-3 cm, thickness: 3-5 mm) and later chopped into 200 µm-thick slices using a McIlwain Tissue Chopper (Campden Instruments Ltd.); or lung tissues were gently injected with 1.5% low-melting agarose (Roth) and cut using a vibratome (Thermo Fisher Scientific) into 400 µm-thick slices. Five to six PCLS were cultured in 5 mL of DMEM supplemented with 10% BCS at 37 °C and 5% CO_2 for five days. Cultures were treated with different agents at the beginning of the culture process (without starvation).

3.9. siRNA transfection

siGENOME PRKAA1 siRNA (D-005027-01-0002), siGENOME PPARg siRNA (D-003436-03-0005), and the corresponding scrambled siRNA (siGENOME Non-Targeting siRNA #2 (D-001210-02-05)) were obtained from Dharmacon. When cells reached 50-60% confluence in 6-well plates, they were transfected using lipofectamine RNAiMAX (Invitrogen) according to manufacturer's instructions (25 pmol per well, 7.5 µL lipofectamine per well). The culture medium was replaced 24 h after transfection.

Seventy-two hours after transfection, the culture medium was replaced by either fresh medium or fresh medium supplemented with 5 mM metformin or BMP2. After 72 h, cells were harvested for protein or RNA extraction.

3.10. RNA extraction and quantitative real-time PCR

Total RNA extraction was performed using RNeasy mini or micro kits (Qiagen) and cDNA synthesis was carried out using Quantitect reverse transcription kit (Qiagen) according to manufacturer's instructions. Quantitative real-time PCR (qPCR) was performed using PowerUp SYBR green master mix (Applied Biosystems) and LightCycler 480 II machine (Roche Applied Science). Porphobilinogen deaminase (*PBGD*) was used as a reference gene. Data are presented as expression levels relative to *PBGD* using the $2^{-\Delta CT}$ method. Primer sequences are shown in Table 4.

Table 5. Primer sequences for qPCR.

Gene name (human)	Forward-primer sequence	Reverse-primer sequence
COL1A1	ATGTTCAGCTTTGTGGACCTC	CTGTACGCAGGTGATTGGTG
PBGD	TGTCTGGTAACGGCAATGCG	CCCACGCGAATCACTCTCAT
PLIN2	TCAGCTCCATTCTACTGTTCACC	CCTGAATTTTCTGATTGGCAC
PPARg	TTGCTGTCATTATTCTCAGTGGA	GAGGACTCAGGGTGGTTCAG
Gene name (mouse)	Forward-primer sequence	Reverse-primer sequence
Fgf10	ATGACTGTTGACATCAGACTCCTT	CACTGTTCAGCCTTTTGAGGA
Pparg	GAAAGACAACGGACAAATCACC	GGGGGTGATATGTTTGAACTTG
Adrp	CCTCAGCTCTCCTGTTAGGC	CACTACTGCTGCTGCCATTT
Fgfr2b	CCCTACCTCAAGGTCCTGAA	CATCCATCTCCGTCACATTG
Fgfr1b	CCACAGGTCTGGTGACAGTGA	CGGGAATTAATAGCTCGGATG
Hprt	GCTGACCTGGATTAC	TTGGGGCTGTACTGCTTA

3.11. Protein extraction and Western blotting

Total protein lysates were prepared using RIPA buffer (Santa Cruz) according to manufacturer's instructions. Proteins were separated by sodium dodecyl sulfate-polyacrylamide gel electrophoresis (SDS-PAGE) followed by blotting on polyvinylidene fluoride (PVDF) membranes (Thermo Fisher Scientific) using Trans-Blot SD semi-dry transfer cell (Bio-Rad Laboratories). Antibodies against AMPK (Abcam, 1:2500), PPARγ (H-100) (Santa Cruz, 1:1000), phospho-(Ser^{112})-PPARγ (Merck Millipore, 1:500), p44/42 mitogen-activated protein kinase (MAPK, a.k.a. extracellular signal-regulated kinases 1 and 2, ERK1/2) (Cell Signaling, 1:1000), phospho-p44/42 MAPK [(ERK1) (Tyr204)/(ERK2) (Tyr187) (D1H6G)] (Cell Signaling, 1:1000) and cleaved poly(ADP-ribose) polymerase 1 (PARP1) (Abcam, 1:2000) were used overnight at 4°C. Beta-actin (ACTB) was used as a loading control (Biolegend, 1:2500). HRP-conjugated anti-rabbit IgG (Promega, 1:5000), HRP-conjugated anti-mouse IgG (H+L) (Promega, 1:5000) and HRP-conjugated anti-rat IgG (Biolegend, 1:5000) were used as secondary antibodies for 1 h at room temperature (RT). Subsequently, membranes were covered with AceGlow chemiluminescence substrate (Peqlab) and imaged immediately using ChemiDoc XRS+ (Bio-Rad Laboratories).

3.12. Staining for lipid-droplet accumulation

For time-lapse imaging, live cells were treated with different agents and HCS LipidTOX red neutral lipid dye (Invitrogen, 1:200) was immediately added. Cells were then placed in the incubation chamber (37 °C and 5% CO_2) of DMI6000 B live imaging microscope (Leica). Images were acquired every 1 h. In other cases, cells were fixed using 2% paraformaldehyde (PFA, Roth) for 20 min followed by washing with PBS (Gibco). A mixture of diluted LipidTOX (1:200) and Hoechst (1:5000) in PBS was then used to stain fixed cells. Subsequently, slides were mounted using ProLong Gold Antifade Reagent (Molecular Probes).

3.13. Hematoxylin and Eosin staining

Human-derived PCLS or mouse lung tissues were fixed using 4% PFA followed by embedding in paraffin. Paraffin blocks were sectioned into 5 µm-thick slices and placed on glass slides. Following deparaffinization, lung sections were stained with hematoxylin (Roth) for 2 min, washed with running tap water for 10 min and then stained with eosin (Thermo Fisher Scientific) for 2 min.

3.13.1. Deparaffinization process

Slides will be placed in the jars with specified reagents in the following orders.

- Xylol (6 minutes)
- Xylol (6 minutes)
- 100% Ethanol (2minutes)
- 100% Ethanol (2 minutes)
- 95% Ethanol (2 minutes)
- 70 % Ethanol (2minutes)
- 50% Ethanol (2minutes)
- 30% Ethanol (2minutes)
- Deionized water (2minutes)

3.14. Masson’s trichrome staining and fibrosis quantification

Collagen staining was performed using Masson’s trichrome staining kit according to the protocol recommended by the manufacturer (Thermo Fisher Scientific). Fibrosis was assessed by semi-automated quantification using VIS Image Analysis Software (Visiopharm). In brief, the algorithm calculates the percentage of the area covered by collagen fibers relative to the area covered by lung tissue (excluding airways and airspaces).

3.15. Total collagen assay

In order to assess total collagen levels, 10 mg of each tissue sample was subjected to the total collagen assay kit according to manufacturer’s instructions (Biovision).

3.16. Immunofluorescence

3.16.1. COL1a1 staining

Following deparaffinization, slides underwent antigen retrieval using citrate buffer (Vector Laboratories) for 15 min followed by cooling on ice for 20 min. Slides were then blocked with 3% bovine serum albumin (BSA, Jackson Immunoresearch Laboratories) in PBS for 1h at RT. Anti-collagen 1 A1 (anti-COL1A1) antibodies (Rockland, 1:200) and goat anti-rabbit antibodies (Life Technologies, 1:500) were used for immunofluorescence. Slides were finally mounted with ProLong Gold Antifade Reagent containing DAPI (Molecular Probes).

3.16.2. Staining for ACTA2 and PLIN2

Following deparaffinization, slides were blocked with 3% BSA solution in PBS with 0.4% Triton-X (Sigma-Aldrich) for 1h at RT. Next, either rabbit anti-ADFP antibody (Abcam, 1:250) (overnight at 4°C) or mouse FITC-conjugated anti-alpha smooth muscle actin antibody (Sigma, 1:200) (overnight at 4°C) and goat anti-rabbit antibodies (Life Technologies, 1:500) (Ih at RT) were used for immunofluorescence. Slides were finally mounted with ProLong Gold Antifade Reagent containing DAPI (Molecular Probes).

3.16.3. Staining PCLSs

Human PCLS were fixed in 4% PFA for 2 h and stored in PBS containing 0.02% sodium azide. Fixed PCLS were blocked with 3% BSA in PBS for 2 h at RT, stained with anti-COL1A1 antibodies (Rockland, 1:200) overnight at 4°C and washed with PBS (three times, 30 min each). A mixture of Alexa Fluor 488-conjugated anti-rabbit antibodies (Invitrogen, 1:200), HCS LipidTOX red neutral lipid dye (Invitrogen, 1:200) and Hoechst (1:5000) was added for 3 h at RT. After washing, PCLS were placed in glass-bottomed 4-well micro slides (Ibidi) containing PBS and imaged by confocal microscopy (Leica TCS SP5).

3.17. Flow Cytometry

Cultured fibroblasts were washed with PBS and resuspended in PBS containing LipidTOX (1:200). Following incubation for 30 min, cells were subjected to flow cytometry using Accuri C6 (BD Biosciences). Cultured PCLS and/or finely minced mouse lung tissues

underwent digestion with 0.5% collagenase (Gibco) in PBS for 45 min at 37 °C while rotating. Cell suspensions were then aspirated through 18, 20, 24 G needles and passed through 70- and 40-µm cell strainers (Greiner Bio-One). Cells were pelleted, resuspended in PBS and stained with anti-CD45 (Biolegend, 1:100), CD31 (Biolegend, 1:100) and CD326 (EpCAM, Biolegend, 1:50) antibodies, as well as LipidTOX (1:200). Stained cell suspensions were then analyzed using LSRFortessa (BD Biosciences). Data were analyzed using FlowJo software (FlowJo, LLC).

3.18. Gene expression microarrays

Total RNA Cy5-labeling was carried out using the LIRAK kit (Agilent Technologies) according to manufacturer's instructions. Per reaction, 200 ng of total RNA was used. Cy-labeled aRNA was hybridized overnight to 8 x 60K 60mer oligonucleotide-spotted microarray slides (Agilent Technologies, design ID 028005). Hybridization and subsequent washing and drying of the slides were performed following the Agilent hybridization protocol. Dried slides were scanned at 2 µm/pixel resolution using the InnoScan is900 (Innopsys). Image analysis was performed using Mapix 6.5.0 software and calculated values for all spots were saved as GenePix results files. Stored data were evaluated using the R software and the limma package from BioConductor. Log mean spot signals were taken for further analysis. Data were quantile-normalized before averaging. Genes were ranked for differential expression using a moderated t-statistic. Pathway analyses were done using gene set tests on the ranks of t-statistics.

3.19. Kinase activity assay

Kinase activity of metformin- or vehicle-treated IPF fibroblasts (n=3 per group) was analyzed by the PamStation (PamGene International BV) that uses a methodology that allows robust analysis of the activity of tyrosine as well as serine/threonine kinases in cells and tissues(Anderson et al., 2015, 2016; Arsenault et al., 2011; Piersma et al., 2010). Hereby, active kinases phosphorylate their distinct peptide substrates presented on a peptide array chip. Phosphorylated peptides are recognized by phospho-specific FITC-labeled antibodies and detection, performed in multiple cycles at different exposure times, is monitored by a CCD camera. Software-based image analysis integrates the

signals obtained within the time course of the incubation of the kinase lysate on the chip into one single value for each peptide for each sample (exposure time scaling). Log transformation of processed signals allows easier graphical presentation of the raw data. Thereby, data with significant differences in intensity are visualized on the log-transformed y-axis in a heat map that shows the degree of phosphorylation for each peptide.

For protein isolation including active kinases, IPF fibroblasts were washed with 5 mL ice-cold PBS and scraped from the dishes in 100 µL of M-PER lysis buffer (Thermo Fisher Scientific) containing protease and phosphatase inhibitor cocktails (Pierce). The lysate was incubated for 1 h at 4°C with constant agitation followed by centrifugation at 16,000 g for 15 min at 4°C. The supernatant was immediately flash-frozen in liquid nitrogen and stored at -80°C. Protein concentration was determined using a bicinchoninic acid (BCA) protein assay kit (Thermo Fisher Scientific) according to manufacturer's instructions.

For tyrosine kinase activity detection, 10 µg of protein lysate was dispensed onto an array of the PamChip PTK (phospho-tyrosine kinase) dissolved in protein kinase buffer and additives (proprietary information) including 1% BSA, 10 mM DTT, 0.6 µL FITC-conjugated antibodies and 400 µM ATP in a final volume of 40 µL (assay master mix). A total of 1 µg of protein lysate was used for serine/threonine kinase activity detection on an array of the PamChip STK (serine/threonine kinase) with protein kinase buffer (proprietary information) supplied with 1% BSA, 0.46 µl primary STK antibody mix and 400 µM ATP (sample mix). After an initial incubation time, secondary FITC-labeled antibodies (0.4 µL) were added. The mixture was dissolved in antibody buffer (proprietary information) and water in a final volume of 30 µL (detection mix).

Upstream kinase prediction on the basis of the different phosphorylation pattern in metformin- and vehicle-treated IPF fibroblasts was conducted using the Bionavigator software v.6.3.67.0 (PamGene International).

3.20. Statistical analyses

Statistical analyses and graph assembly were carried out using GraphPad Prism 6 (GraphPad Prism Software). To assess the normal distribution of data sets, D'Agostino-Pearson normality test was applied. In case of normal distribution, Student's t-test

(unpaired, two-tailed) was utilized to compare the means of two groups, while one-way ANOVA (with post-hoc tests) was used to compare the means of three or more groups. In the cases where data were not normally distributed, respective non-parametric tests were applied (Mann-Whitney test to compare the means of two groups and Kruskal-Wallis test to compare the means of three or more groups). Data are presented as mean ± SEM. The number of biological samples (n) for each group and the utilized statistical tests are stated in the corresponding figure legends. Differences in means were considered statistically significant if $P<0.05$.

4. Results

4.1. PART I. Characterization of murine lipofibroblasts and involvement of fibroblast growth factor 10 in formation of them

4.1.1. Lipofibroblast formation increases progressively during embryonic lung development

Since emergence of LIFs in the embryonic mouse lung was unexplored, first aim was to quantify the relative number of lipid-droplet containing cells between E13.5 and E18.5 using LipidTOX staining followed by flow cytometry. LipidTOX is a dye that labels neutral lipids that are abundantly present in LIFs. Our results represent that LipidTOX+ cells appeared at late pseudoglandular stage, between E15.5 and E16.5, and their count can be as high as 30% of the total cell count in the developing lung (Fig. 1A, B). Next, the expression levels of adipogenic markers such as *Plin2*, *Pparg* and *Fgf10* were assessed in the lung homogenate qPCR (Fig. 1C). Expression level of *Plin2* was very low levels between E11.5 and E15.5 and started to upregulate beginning at E16.5, peaking at E18.5. *Pparg* expression was first detected at E15.5 and increased progressively up to E18.5. Our data revealed Steady increase of *Fgf10* expression from E11.5 to E18.5.

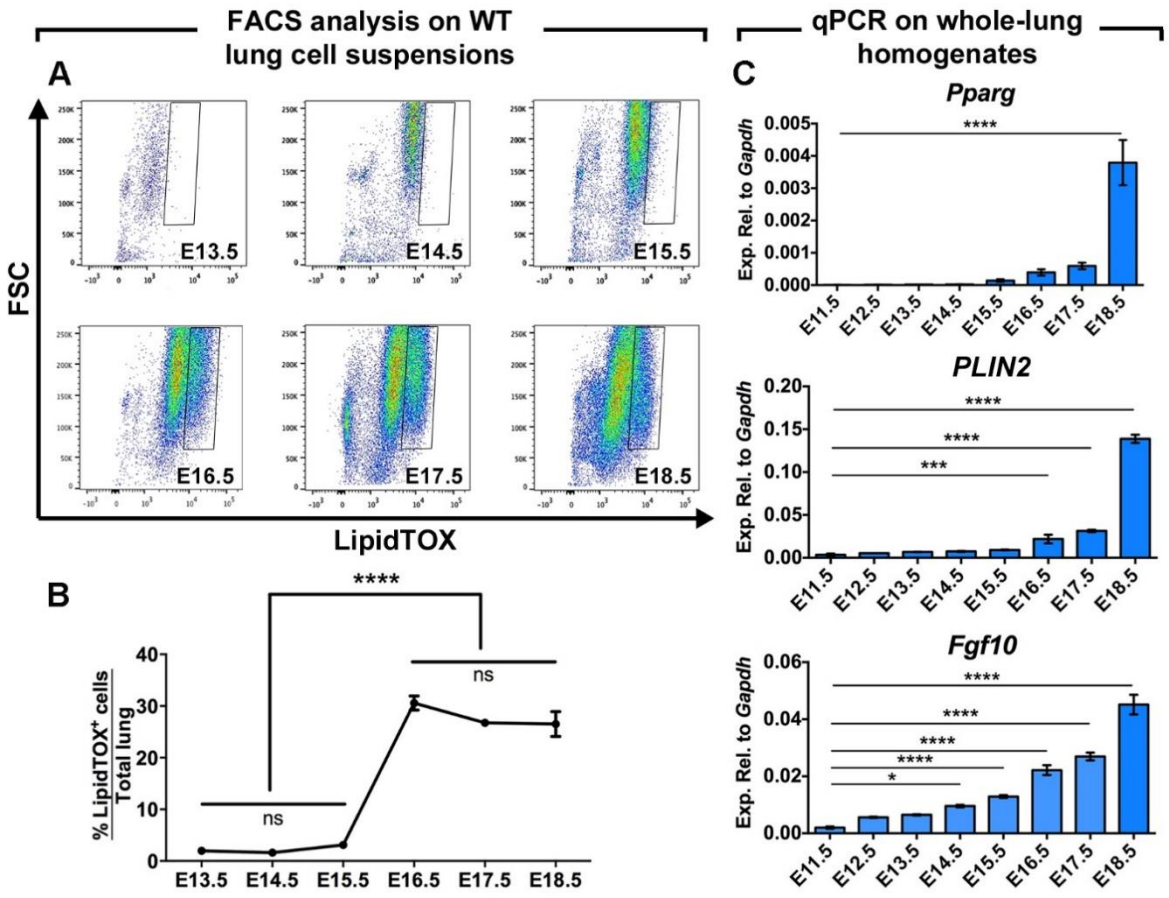

Figure 1. Lipofibroblasts emerge in the mouse lung during the late pseudoglandular stage.

(A) FACS analysis of LipidTOX-stained cell suspensions from embryonic CD1 lungs. **(B)** Quantification of the FACS plots shown in A (n=4 per stage). **(C)** qPCR analysis showing the expression patterns of *Pparg*, *Plin2* and *Fgf10* during embryonic lung development (n=3 per stage).

4.1.2. Increasing level of Fgf10 receptors and lipogenic markers expression in lung fibroblasts

In order to dive deeper in the possible role of Fgf10 in formation of lipofibroblasts and any possible contribution of epithelial cell in formation of LIFs, primary lung mesenchyme was cultured at different embryonic stages (E14.5-E18.5). Following differential adhesion, mesenchymal cells allowed to grow for 24 h before RNA isolation (Fig. 2A). Minimal epithelial contamination of cell culture has been confirmed via Cdh1 IF (Fig. 2B). qPCR revealed low expression levels for *Pparg* (Fig. 2D) and *Plin2* (Fig. 2E) at E14.5 and E15.5 with increased expression levels between E16.5 and E18.5. This is consistent with the data obtained with lung homogenates (Fig. 1C), thus indicating upregulation of *Pparg* and *Plin2* in the lung mesenchyme during late embryonic stages. Parallel to the increase in LIF markers, *Fgf10* expression was also increased in late embryonic stages (Fig. 2C). Strikingly, *Fgfr2b* and *Fgfr1b*, the genes encoding the two Fgf10 receptors, were upregulated in late embryonic lung mesenchyme, with the increase in *Fgfr2b* expression preceding that observed for Fgfr1b (Fig. 2F, G).

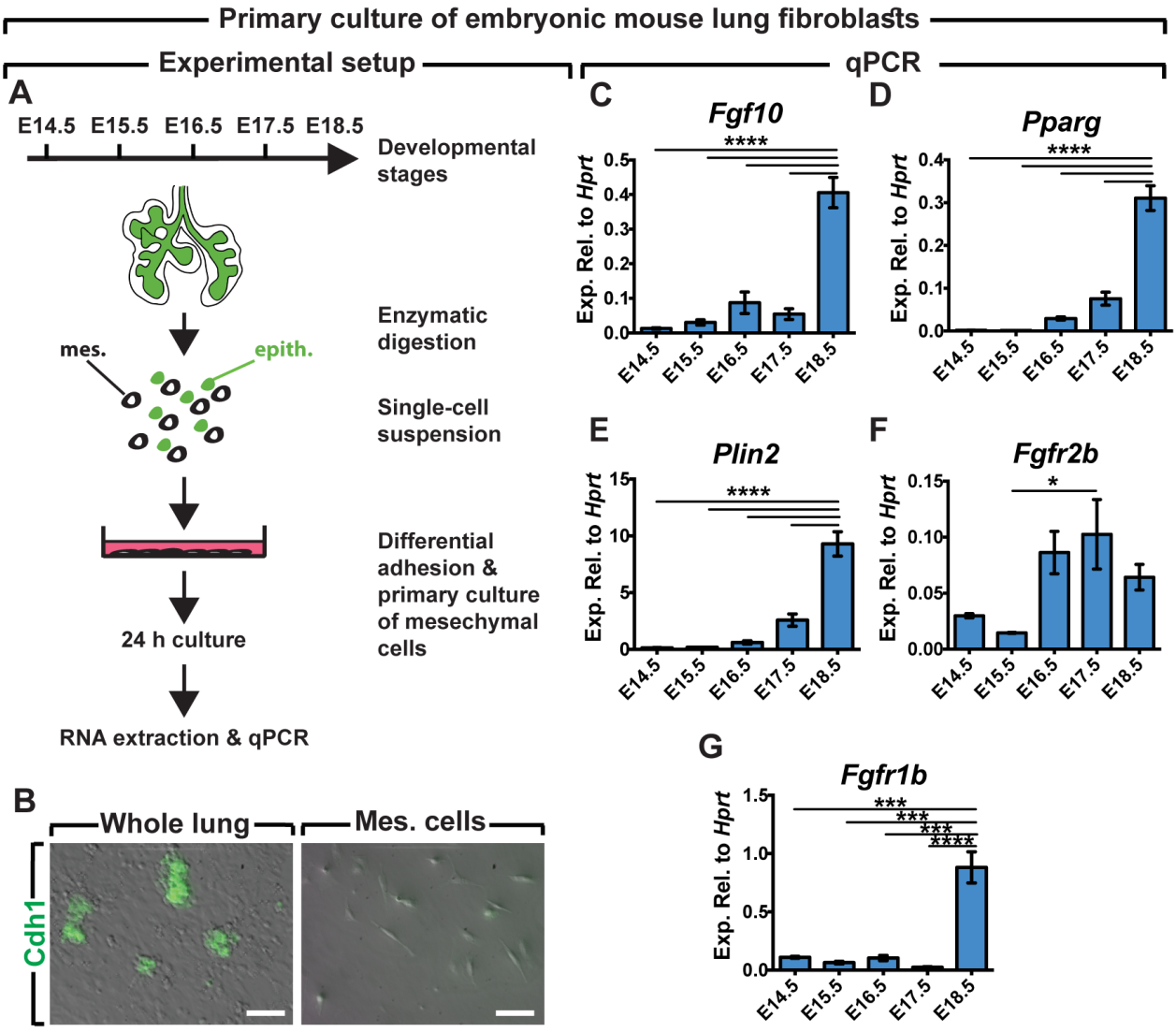

Figure 2. Increasing level of lipogenic markers coincides with increasing level of Fgf receptors in the lung.

(A) Time line for harvesting embryonic lungs and the subsequent cell culture plan. **(B)** IF for Cdh1 showing minimal epithelial contamination in the primary culture of embryonic lung mesenchyme. **(C-G)** qPCR analysis for *Fgf10, Pparg, Plin2, Fgfr2b and Fgfr1b.*

4.1.3. *Fgfr2b* compensates loos of *Fgfr1b* function in formation of lipofibroblasts

Increased mesenchymal expression of *Fgfr1b* and *Fgfr2b* in the late stage of lung development in parallel to formation of lipofibroblasts raised the question whether these two receptors play a functional role in this process. Thus, we investigated the phenotype and status of lipofibroblasts in the Fgfr1b knockout animals. First, the phenotype of E18.5 Fgfr1b knockout lungs was examined, and analysis by qPCR confirmed the absence of *Fgfr1b* expression in knockout lungs (n=4) compared with control lungs (n=7; Fig. 4A). Hematoxylin and Eosin (H&E) staining did not show any apparent phenotype in knockout lungs compared with control lungs (Fig. 3H, I versus F, G). Interestingly, qPCR analysis showed that *Pparg* was significantly increased in the knockouts compared with controls (Fig. 3C), and this was accompanied by a modest increase in *Plin2* expression (Fig. 3D). Surprisingly, *Fgfr2b* expression was increased (Fig. 3E), whereas *Fgf10* expression levels remained unchanged (Fig. 3B).

Investigating the protein levels of Plin2 by IF revealed a slight increase in Plin2 immunoreactivity in the knockouts (Fig. 3L, M) compared with controls (Fig. 3J, K). Quantification of the Plin2 signal using MetaMorph software showed a trend towards an increase in the number (Fig. 3N) and area (Fig. 3O) of Plin2 immunoreactive spots in knockout lungs (n=3) compared with control lungs (n=3). Our results therefore indicate that ubiquitous deletion of *Fgfr1b* in the lung does not compromise LIF formation during embryonic development; instead, there is a trend towards increased LIF formation. Interestingly, the elevated levels of *Fgfr2b* in Fgfr1b knockout lungs suggest that *Fgfr2b* could be compensating for the loss of *Fgfr1b*, thereby allowing normal and even enhanced LIF formation.

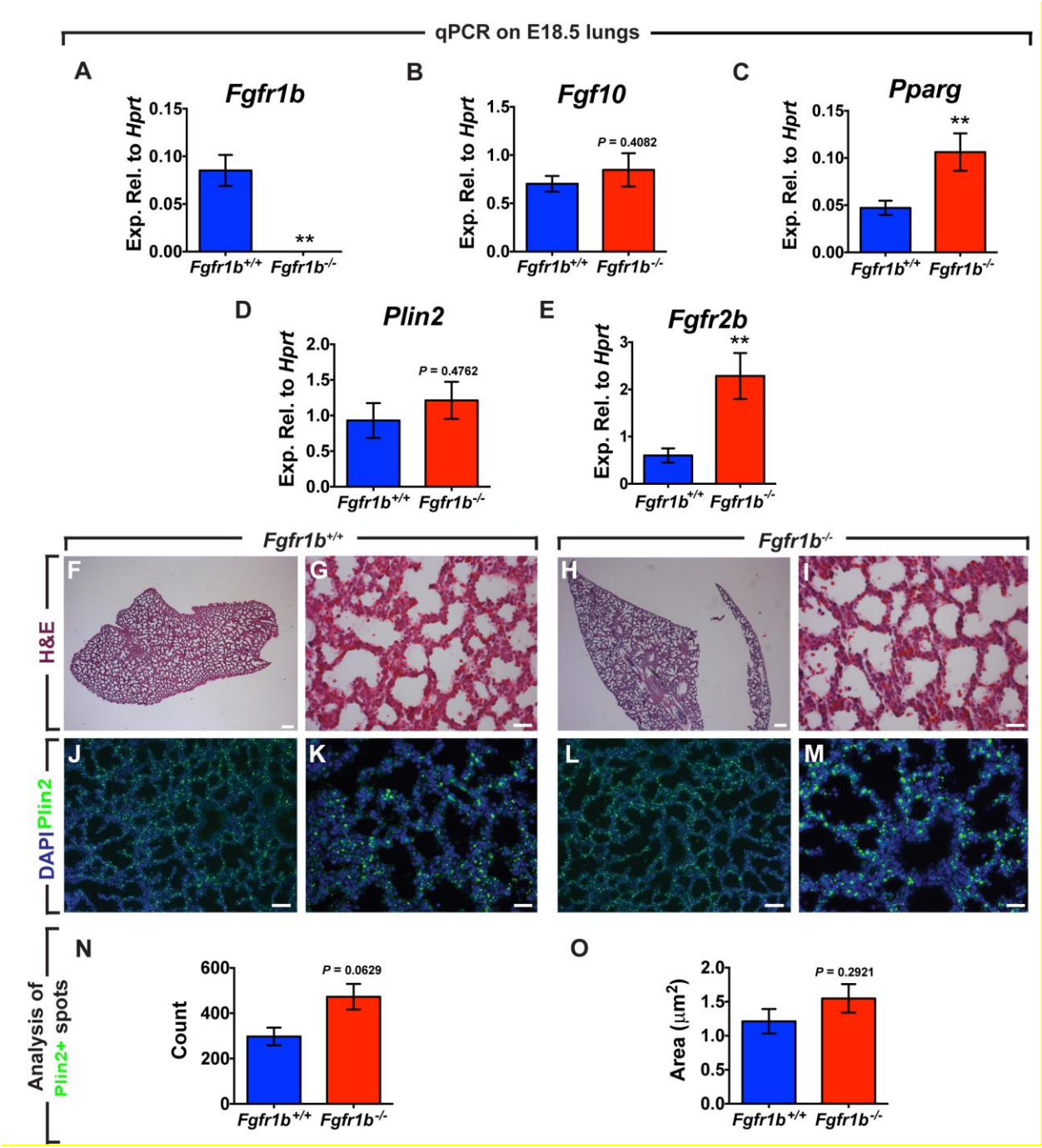

Figure 3. *Fgfr1b* knockouts suggest compensation with Fgfr2b.

(A-E) qPCR analysis of *Fgfr1b*, *Fgf10*, *Pparg*, *Plin2* and *Fgfr2b* in *Fgfr1b*$^{-/-}$ lungs compared with littermate controls. **(F-I)** H&E staining showing no apparent histological differences between control **(F, G)** and Fgfr1b knockout lungs **(H, I)**. **(J-M)** IF for Plin2 showing a slight increase in immunoreactivity in *Fgfr1b* knockout lungs **(L, M)** compared with control lungs **(J,K)**. **(N, O)** Quantification of Adrp immunoreactivity using MetaMorph software. Scale bars: 200 µm in F, H; 25 µm in G, I, K, M; 50 µm in J, L. (A-E) *Fgfr1b*$^{+/+}$, n=7; *Fgfr1b*$^{-/-}$, n=4. (N, O) *Fgfr1b*$^{+/+}$, n=3; *Fgfr1b*$^{-/-}$, n=3.

4.2. Part II. Lipofibroblasts are a source of activated myofibroblasts in lung fibrosis

4.2.1. Lipofibroblasts give rise to activated myofibroblasts during fibrosis formation

To test whether lipofibroblasts contribute to the activated myofibroblast pool during fibrosis formation, pre-existing lipofibroblasts were labeled using a recently generated *AdrpCre-ERT2* knock-in mouse line followed by bleomycin injury (Fig. 4A). *AdrpCre-ERT2 ; mT/mG* mice were fed tamoxifen-containing pellets for 2 weeks followed by 2 weeks of normal pellets before being challenged with either saline or bleomycin (Fig. 4B). Immunofluorescent staining showed minimal co-localization of the lineage label (mGFP) and ACTA2 in saline-treated lungs at 14 d.p.i. (Day Post Instilation) (Fig. 4C-G). In contrast, mGFP^{+} cells were located in dense fibrotic areas where ACTA2^{+} myofibroblasts were also aggregated in bleomycin-treated lungs (Fig. 4H-L). FACS analysis was used to quantify the contribution of lipofibroblasts to activated myofibroblast formation (Fig. 4M-O). To restrict the analysis to resident fibroblasts, hematopoietic, endothelial and epithelial cells were excluded from the analysis. The results showed that our lineage-tracing tool labeled 27.2%–34.8% of LipidTOX^{+} fibroblasts in the lung (Fig. 4V) in parallel to a dramatic decrease in the number of LipidTOX^{+} cells after bleomycin injury (from 9.4% to 1.5%) (Fig. 4T), hinting at a lipofibroblast-to-activated-myofibroblast transdifferentiation. An increase in the number of ACTA2^{+} cells from 2.3% to 5.7% was observed upon bleomycin injury (Fig. 4P),

concomitantly with an increase in the number of $mGFP^+$ cells that co-stained for ACTA2 (Fig. 4R) and a decrease in the number of $mGFP^+$ that co-stained for LipidTOX (Fig. 4U). Interestingly, while the number of lineage-labeled cells remained unchanged (Fig. 4Q), these cells contributed to 19.7% of the total $ACTA2^+$ cells in bleomycin-treated lungs (Fig. 4S). Sorted $mGFP^+$ cells by FACS were subjected to gene expression analysis by qPCR. Activated myofibroblast markers (*Acta2* and *Col1a1*) were drastically upregulated in lineage-labeled cells derived from fibrotic lungs compared to control lungs (7.8-fold and 35.1-fold, respectively) (Fig. 4W, X), indicating that these cells acquired an activated myofibroblast phenotype. *Fgf10* was also significantly upregulated (3-fold) in lineage-labeled cells upon bleomycin treatment (Fig. 4Y).

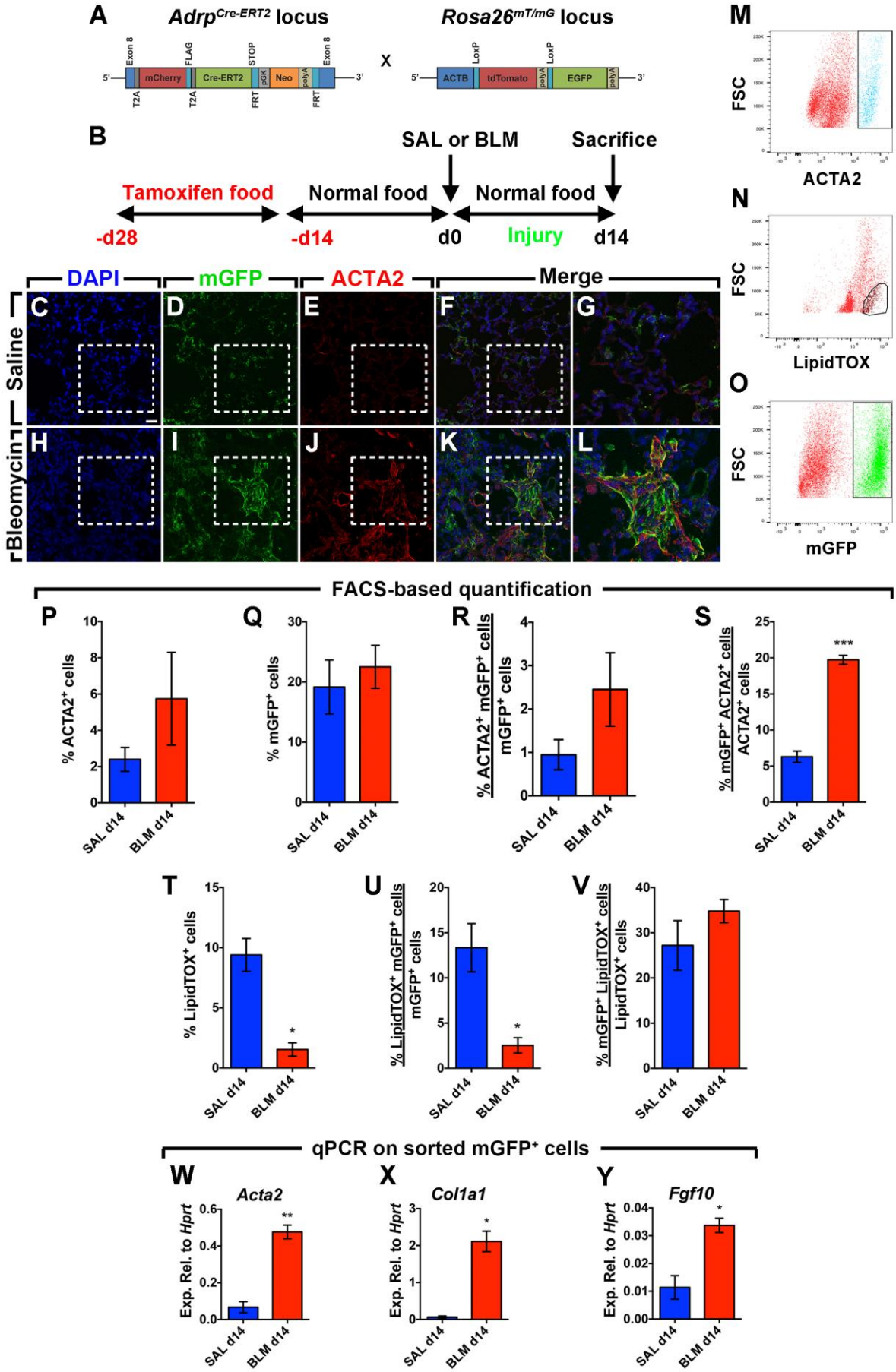
A
Adrp^Cre-ERT2 locus
Rosa26^mT/mG locus
Exon 8
FLAG
STOP
Exon 8
mCherry
Cre-ERT2
Neo
T2A
T2A
FRT
FRT
LoxP
LoxP
ACTB
tdTomato
EGFP
B
SAL or BLM
Sacrifice
Tamoxifen food
Normal food
Normal food
-d28
-d14
d0
Injury
d14
DAPI
mGFP
ACTA2
Merge
Saline
Bleomycin
C
D
E
F
G
H
I
J
K
L
M
FSC
ACTA2
N
FSC
LipidTOX
O
FSC
mGFP
FACS-based quantification
P
% ACTA2+ cells
Q
% mGFP+ cells
R
% ACTA2+ mGFP+ cells / mGFP+ cells
S
% mGFP+ ACTA2+ cells / ACTA2+ cells
***
SAL d14
BLM d14
T
% LipidTOX+ cells
*
U
% LipidTOX+ mGFP+ cells / mGFP+ cells
*
V
% mGFP+ LipidTOX+ cells / LipidTOX+ cells
qPCR on sorted mGFP+ cells
W
Acta2
Exp. Rel. to Hprt
**
X
Col1a1
*
Y
Fgf10
*

Figure 4. Lipofibroblasts contribute to the pool of activated myofibroblasts during fibrosis formation

(A) Schematic representation of the *AdrpCre-ERT2* and *mT/mG* constructs. **(B)** Timeline of tamoxifen and saline or bleomycin treatments. Mice were fed tamoxifen-containing pellets before saline or bleomycin was administered intratracheally. Lungs were harvested at 14 d.p.i. **(C–F)** Immunofluorescent staining of saline-treated lungs showing DAPI, mGFP, and ACTA2 single channels in addition to a merged image. **(G)** A high-magnification image of the region marked by the box in the merged image **(F)**. **(H–K)** Immunofluorescent staining of bleomycin-treated lungs showing DAPI, mGFP, and ACTA2 single channels in addition to a merged image. **(L)** A high-magnification image of the region marked by the box in the merged image **(K)**. **(M–O)** Gating strategy for the detection of ACTA2+, LipidTOX+, and mGFP+ cell populations by FACS. **(P–V)** FACS-based quantification of ACTA2+, mGFP+, and LipidTOX+ cell populations at 14 d.p.i. **(W–Y)** qPCR for *Acta2, Col1a1*, and *Fgf10* on mGFP+ cells sorted from saline- and bleomycin-treated lungs at 14 d.p.i. Scale bar: 25 μm. SAL d14, n = 3; BLM d14, n = 3–4; n represents biological replicates

4.2.2. Activation of Pparg signaling antagonizes TGFβ1-mediated fibrogenic response

In order to investigate whether TGFβ1 activity in IPF fibroblasts can be suppressed via activation of PPARg signaling and reinforcing the lipogenic phenotype, human lung fibroblasts were cultured in the presence of the PPARg agonist rosiglitazone (20 μM) and/or recombinant TGFβ1 (1 ng/mL), and cells were harvested after 72 hr for qPCR analysis (Fig. 5). TGFβ1 treatment strongly inhibited *PPARg* (Fig. 5A) and *PLIN2* expression (Fig. 5B) (18.6-fold and 6.8-fold downregulation, respectively) and upregulated *ACTA2* (Fig. 5C) and *COL1A1* expression (Fig. 5D) (7-fold and 9.5-fold, respectively) compared to the control group. Interestingly, rosiglitazone treatment significantly upregulated *PLIN2* expression (3.3-fold compared to the control group) and attenuated its downregulation by TGFβ1 (Fig. 5B) (with 2.9-fold upregulation in the TGFβ1+Rosi group compared to the TGFβ1-treated group). In parallel to the inhibition of TGFβ1-mediated downregulation of lipogenic markers, rosiglitazone treatment

significantly attenuated TGFβ1-mediated upregulation of myogenic markers *ACTA2* and *COL1A1* (Fig. 5C, D) (with 2.2-fold and 1.25-fold downregulation, respectively, in the TGFβ1+Rosi group compared to the TGFβ1-treated group).

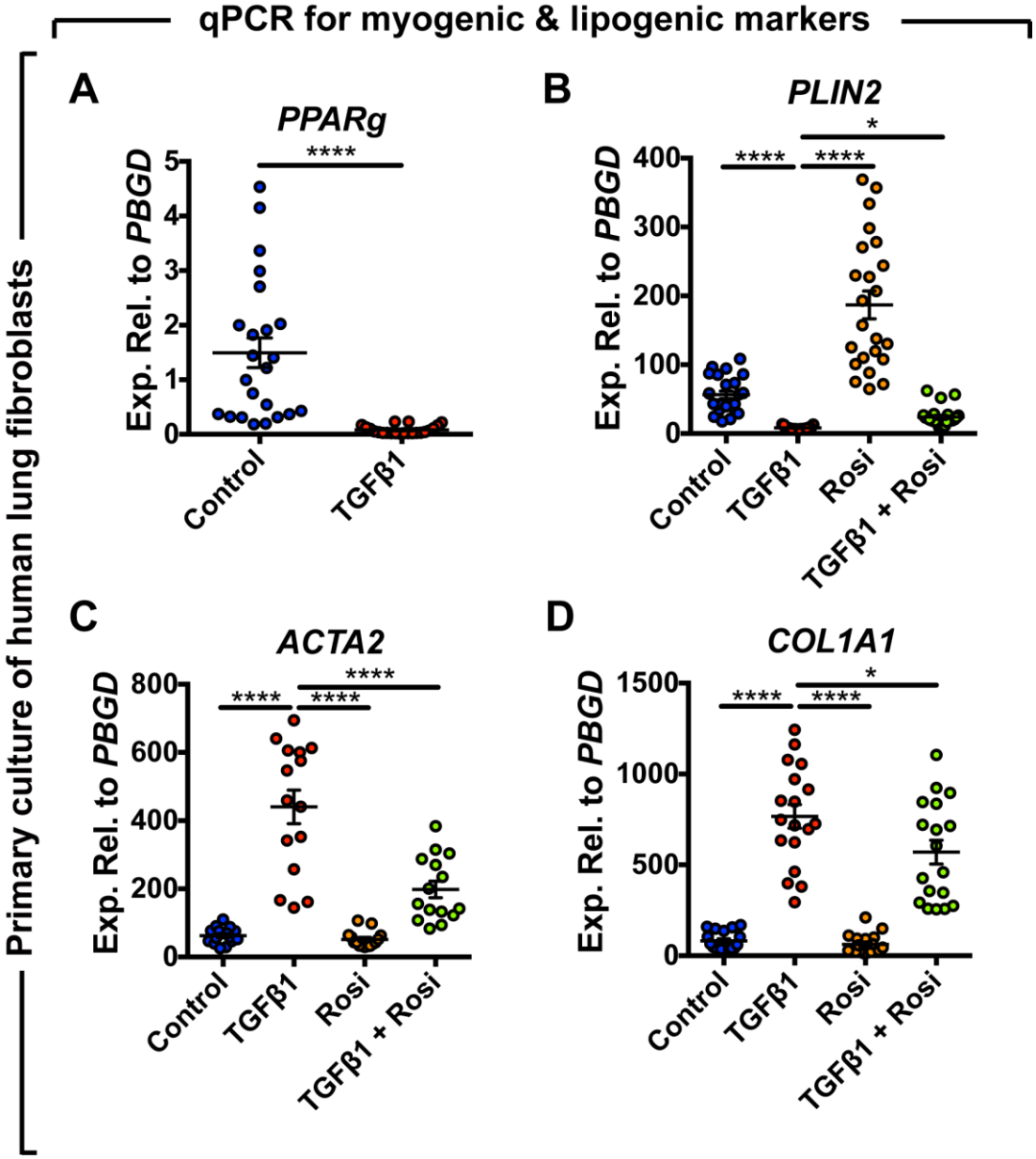

Figure 5. Rosiglitazone attenuates TGFβ1-mediated fibrogenesis via reinforcement of the lipogenic phenotype in human lung fibroblasts.
following starvation for 24 hours cells were treated with 1 ng/mL recombinant TGFβ1 and/or 20 μM rosiglitazone. After 72 hours, cells were harvested and gene expression

was analyzed by qPCR. **(A)** TGFβ1 strongly inhibits *PPARg* expression. **(B)** Rosiglitazone induces the expression of *PLIN2* and attenuates TGFβ1-mediated downregulation. **(C and D)** TGFβ1 significantly upregulates *ACTA2* and *COL1A1* and rosiglitazone attenuates this effect. Rosi, rosiglitazone. Control, n = 18–23; TGFβ1, n = 15–22; Rosi, n = 15–23; TGFβ1+Rosi, n = 15–24; n represents biological replicates.

4.3. Part III. Metformin induces lipogenic differentiation in myofibroblasts to reverse mouse and human lung fibrosis

4.3.1. Metformin induces lipid-droplet accumulation in human IPF lung fibroblasts

In order to investigate whether metformin impacts lipogenic versus myogenic fibroblastic phenotypes in the lung, we carried out a dose-finding study. Human lung fibroblasts isolated from 7 IPF patients were starved for 24 h before being treated with 1, 5 or 10 mM metformin for 72 h (Fig. 6). Treatment of cells with 5 mM metformin resulted in significant upregulation of the lipogenic markers adipose differentiation-related protein (a.k.a. perilipin 2, *PLIN2,* 18.3 folds, Fig. 6A) and *PPARg* (6.6 folds, Fig. 6B) in parallel to a significant 9.7-fold downregulation of *COL1A1* (Fig. S1C). Treatment with 10 mM metformin led to comparable results (Fig. 6A-C). No induction of apoptosis (Fig. 6D) or massive cell death were observed in response to metformin treatment (5 mM). Therefore, we decided to use the 5 mM concentration for the rest of the study.

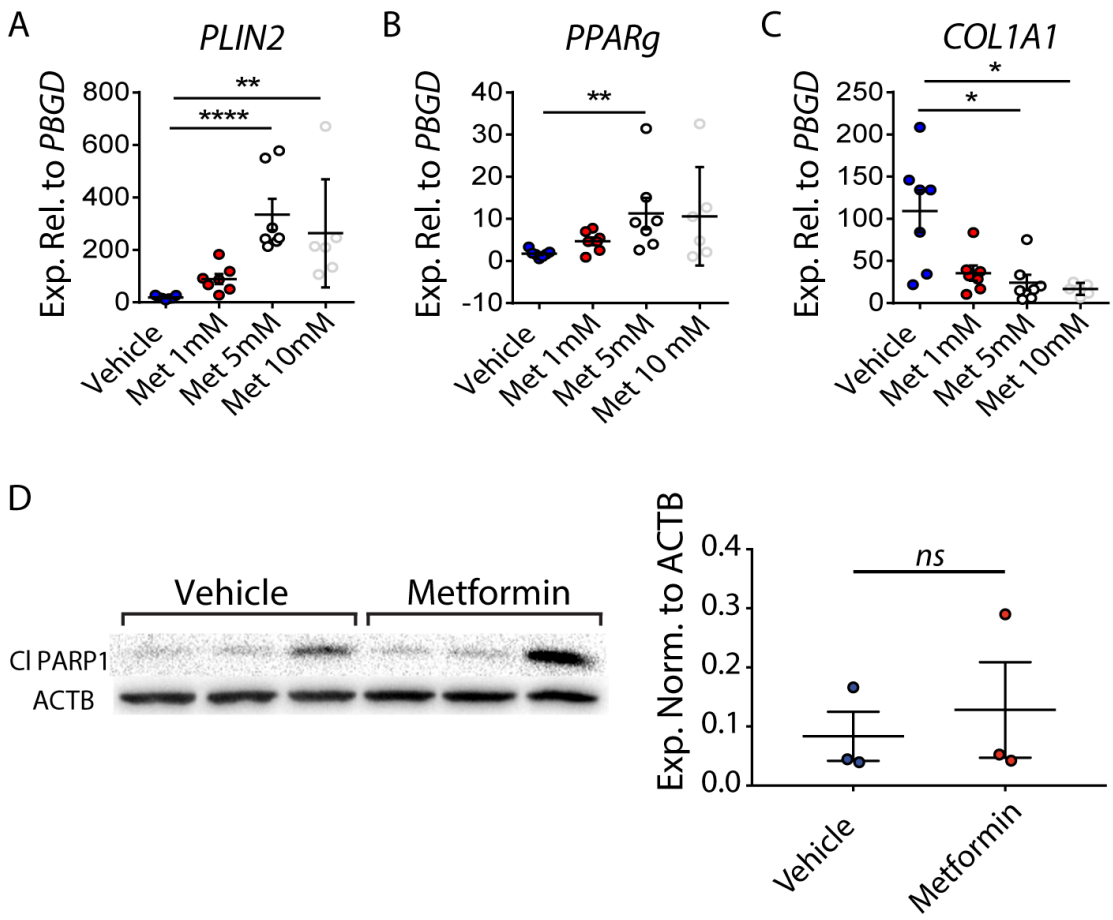

Figure 6. Dose-finding study for treating human IPF lung fibroblasts with metformin.

(A-C) qPCR analysis of *PLIN2, PPARg* and *COL1A1* in IPF fibroblasts treated with 1 mM, 5 mM or 10 mM metformin or vehicle. **(D)** Western blot showing the expression of the apoptotic marker PARP1 in fibroblasts treated with vehicle or 5 mM metformin. Quantification of the immunoblot is shown in the right panel. Each data point corresponds to one patient. (A-C) n=6-7 per group, (D): n=3 per group. Kruskal-Wallis test was used in (A-C) and Mann-Whitney test was used in (D).

In order to gain further insights into the dynamics of this process, human lung fibroblasts isolated from 5 IPF patients were treated with 5 mM metformin and analyzed after 48, 72 and 96 h (Fig. 7A). Analysis at 48 h showed a significant 3.4-fold downregulation of *COL1A1* expression (Fig. 7D) but without affecting lipogenic marker expression (Fig. 7B,

C) or lipid-droplet accumulation (as shown by staining with the neutral lipid dye LipidTOX) (Fig. 7K, L, Q). At 72 h, a significant 9.6-fold downregulation of *COL1A1* (Fig. 7G) was accompanied by significant upregulation of *PLIN2* (33.5 folds, Fig. 7E) and *PPARg* (12.4 folds, Fig. 7F) and a 4.3-fold increase in lipid-droplet accumulation (Fig. 7M, N, R). The effect of metformin was comparable at 96 h (Fig. 7H-J, O, P, S). These data indicate that metformin first leads to *COL1A1* downregulation and then induces lipogenic marker expression in primary human IPF lung fibroblasts. The 72 h time point was chosen for subsequent analyses.

Following the establishment of an optimal dose and time point for metformin treatment, pulmonary fibroblasts isolated from 12 IPF patients were treated with 5 mM metformin and analyzed after 72 h (Fig. 8A). The results showed significant upregulation of *PLIN2* (22.1 folds, Fig. 8B) and *PPARg* (8.3 folds, Fig. 8C), and a robust 8.1-fold downregulation of *COL1A1* (Fig. 8D). Despite the variation in the response of fibroblasts isolated from different patients, the pattern of response was highly significant and clearly consistent among all samples (i.e. induction of lipogenic marker expression and suppression of *COL1A1* expression). As a final readout for lipogenic differentiation, the neutral lipid stain LipidTOX was used and the increase in lipid-droplet accumulation in fibroblasts was demonstrated by fluorescence microscopy (Fig. 8E, F). Flow cytometry-based quantification of LipidTOX$^+$ cells displayed a significant 2.1-fold increase in metformin-treated cells compared to vehicle-treated cells (Fig. 8G-I).

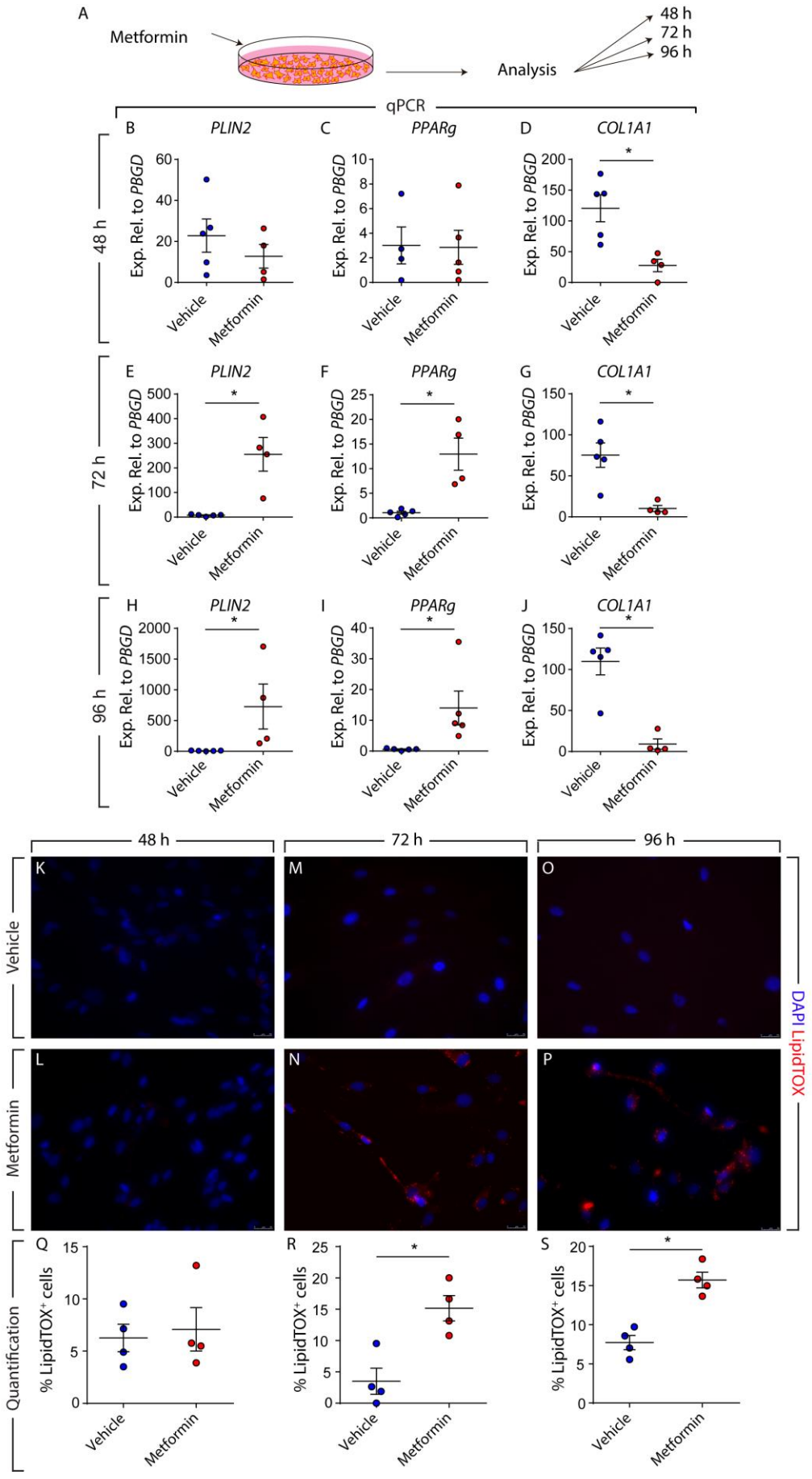
A
Metformin
Analysis
48 h
72 h
96 h
qPCR
B PLIN2
C PPARg
D COL1A1
E PLIN2
F PPARg
G COL1A1
H PLIN2
I PPARg
J COL1A1
48 h
72 h
96 h
Exp. Rel. to PBGD
Vehicle
Metformin
*
48 h
72 h
96 h
Vehicle
Metformin
K
L
M
N
O
P
DAPI LipidTOX
Quantification
Q
R
S
% LipidTOX+ cells
Vehicle
Metformin
*

Figure 7. Metformin induces lipogenic differentiation in IPF fibroblasts starting at 72 h after treatment.

(A) Schematic representation of the experimental setup. **(B-D)** qPCR analysis of *PLIN2, PPARg* and *COL1A1* in IPF fibroblasts treated with 5 mM metformin for 48 h. A Similar analysis is shown after 72 **(E-G)** and 96 h **(H-J). (K-P)** Staining of metformin- and vehicle-treated cells with LipidTOX (red) and DAPI (blue) at 48, 72 and 96 h. **(Q-S)** Quantification of lipid-droplet accumulation shown in (K-P). Scale bars: (K-P) 25 µm. Each data point corresponds to one patient. (B-J) n=4-5 per group. (Q-S) n=4 per group. Mann-Whitney test was used in (B-J, Q-S).

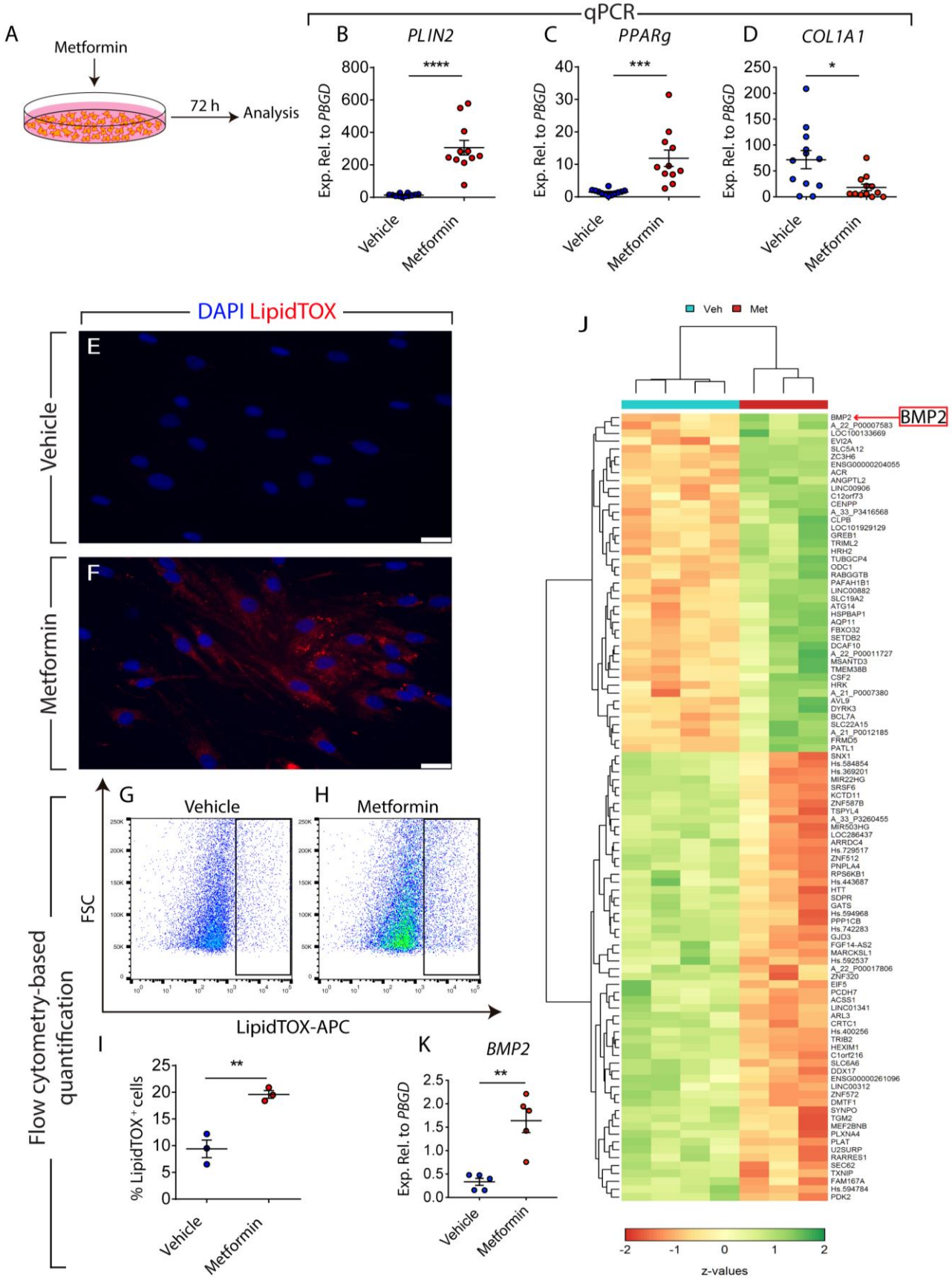
A
Metformin
72 h
Analysis
qPCR
B
PLIN2
C
PPARg
D
COL1A1
Exp. Rel. to PBGD
****
***
*
Vehicle
Metformin
DAPI LipidTOX
E
F
Vehicle
Metformin
G
H
FSC
LipidTOX-APC
Flow cytometry-based quantification
I
% LipidTOX+ cells
**
K
BMP2
J
Veh
Met
BMP2
z-values

Figure 8. Metformin induces lipogenic marker expression in human IPF lung fibroblasts. (A) Schematic representation of the experimental setup. **(B-D)** qPCR analysis for the lipogenic marker genes *PLIN2* and *PPARg,* as well as the myofibroblast marker *COL1A1* in human IPF lung fibroblasts treated with metformin or vehicle. **(E, F)** Staining of lipid droplets in fibroblasts using LipidTOX (red). Nuclei were counterstained with DAPI (blue). **(G-H)** Gating strategy for detecting LipidTOX$^+$ cells by flow cytometry. **(I)** Quantification of LipidTOX$^+$ cell abundance in response to metformin treatment. **(J)** Heatmap representation of the top 100 differentially expressed genes in fibroblasts following metformin treatment. **(K)** qPCR analysis for *BMP2* in metformin- and vehicle-treated cells. Scale bars: (E, F) 25 µm. Each data point within a given group corresponds to one patient. (B-D) Vehicle-treated group: n=12, Metformin-treated group: n=11. (I) n=3 per group. (K): n=5 per group. Student's t-test was used in (B-D) and Mann-Whitney test was used in (I, K).

In order to explore global patterns of gene expression regulation induced by metformin and to generate further hypotheses, gene expression microarrays were carried out for 4 vehicle-treated and 3 metformin-treated human IPF lung fibroblasts. A heatmap depicting the top 100 differentially regulated genes (based on z-values) are shown in Fig. 8J. Interestingly, KEGG pathway analysis revealed that metformin treatment led to the modulation of several metabolic pathways, few of which have previously been implemented in IPF such as glycosaminoglycan biosynthesis - heparan sulfate / heparin (P=0.003), sphingolipid metabolism(Zhao et al., 2017) (trend) and arginine/proline metabolism (trend) (Fig. 9). The latter pathway is relevant to collagen synthesis. In agreement with our observation that metformin induces lipogenic differentiation in human IPF lung fibroblasts, pathway analysis also showed statistically significant modulations of fatty acid metabolism (P=0.006), biosynthesis of unsaturated fatty acids (P=0.02), glycerolipid metabolism (P=0.03) and fatty acid elongation (P=0.04) (Fig. 9). Although not statistically significant, there were also trends for modulations of other relevant pathways such as linoleic acid metabolism, insulin signaling pathway, fatty acid degradation and fatty acid biosynthesis (Fig. 9). We also inspected selected markers of lipogenic differentiation to validate the microarray data and we observed upregulation of *PLIN2*

(P=0.001)*, PPARg* (trend) *and CEBPB* (P=0.003) coupled to significant downregulation of the myofibroblast marker *COL1A1* (P=0.002). Other significantly modulated metabolic pathways included steroid biosynthesis ($P=7.9x10^{-5}$), vitamin B6 metabolism (P=0.001), drug metabolism – cytochrome P450 (P=0.004), terpenoid backbone biosynthesis (P=0.006), retinol metabolism (P=0.006), N-Glycan biosynthesis (P=0.007), glycolysis / gluconeogenesis (P=0.01) and metabolism of xenobiotics by cytochrome 450 (P=0.02) (Fig. 9). The microarray data also showed significant modulation of the TGFβ signaling pathway (P=0.01). Intriguingly, the top upregulated gene in metformin-treated fibroblasts was *BMP2* (red arrow in Fig. 8J). This finding was validated by qPCR and the result indeed showed significant upregulation of *BMP2* in metformin-treated cells compared to vehicle-treated controls (Fig. 8K).

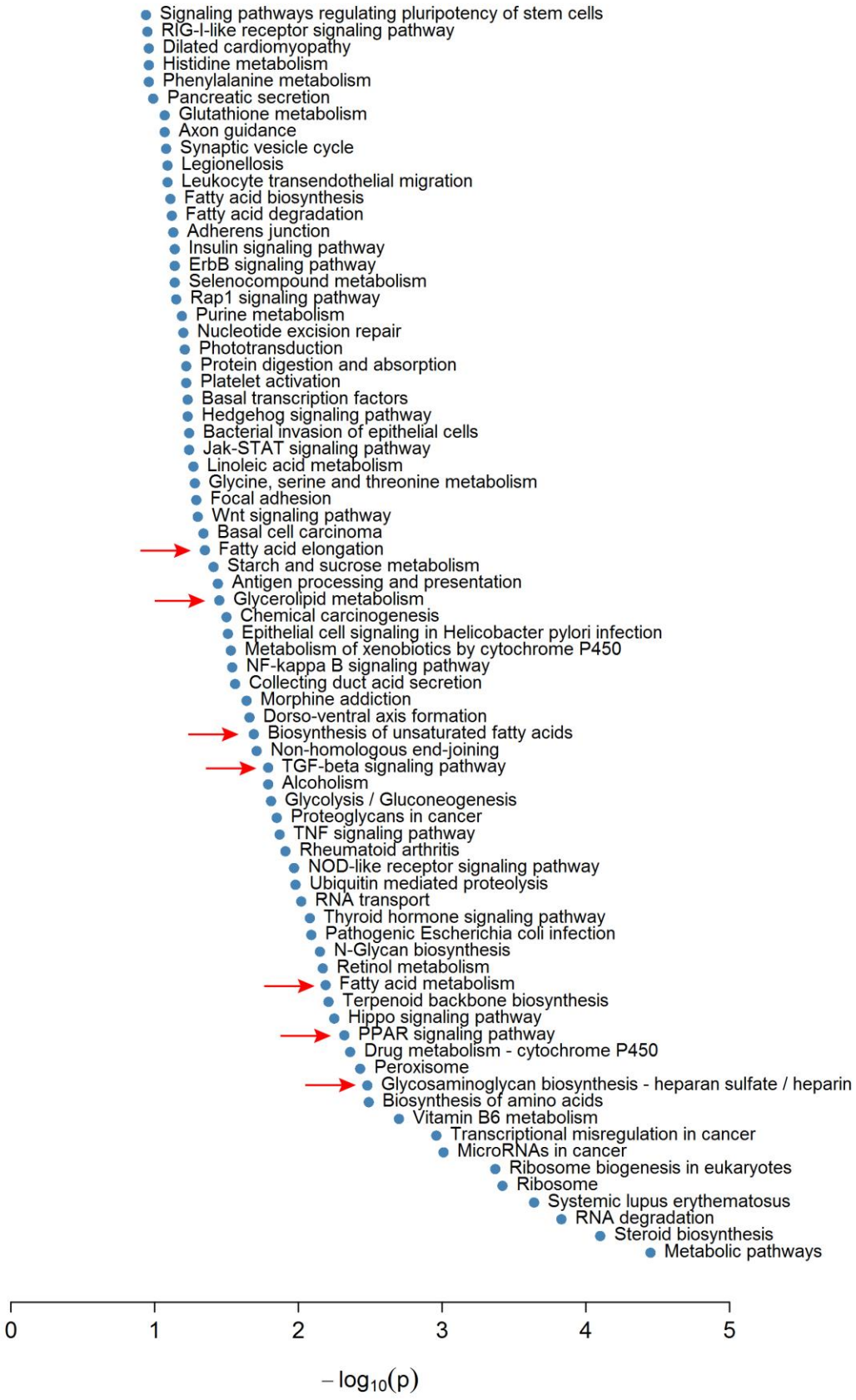
Signaling pathways regulating pluripotency of stem cells
RIG-I-like receptor signaling pathway
Dilated cardiomyopathy
Histidine metabolism
Phenylalanine metabolism
Pancreatic secretion
Glutathione metabolism
Axon guidance
Synaptic vesicle cycle
Legionellosis
Leukocyte transendothelial migration
Fatty acid biosynthesis
Fatty acid degradation
Adherens junction
Insulin signaling pathway
ErbB signaling pathway
Selenocompound metabolism
Rap1 signaling pathway
Purine metabolism
Nucleotide excision repair
Phototransduction
Protein digestion and absorption
Platelet activation
Basal transcription factors
Hedgehog signaling pathway
Bacterial invasion of epithelial cells
Jak-STAT signaling pathway
Linoleic acid metabolism
Glycine, serine and threonine metabolism
Focal adhesion
Wnt signaling pathway
Basal cell carcinoma
Fatty acid elongation
Starch and sucrose metabolism
Antigen processing and presentation
Glycerolipid metabolism
Chemical carcinogenesis
Epithelial cell signaling in Helicobacter pylori infection
Metabolism of xenobiotics by cytochrome P450
NF-kappa B signaling pathway
Collecting duct acid secretion
Morphine addiction
Dorso-ventral axis formation
Biosynthesis of unsaturated fatty acids
Non-homologous end-joining
TGF-beta signaling pathway
Alcoholism
Glycolysis / Gluconeogenesis
Proteoglycans in cancer
TNF signaling pathway
Rheumatoid arthritis
NOD-like receptor signaling pathway
Ubiquitin mediated proteolysis
RNA transport
Thyroid hormone signaling pathway
Pathogenic Escherichia coli infection
N-Glycan biosynthesis
Retinol metabolism
Fatty acid metabolism
Terpenoid backbone biosynthesis
Hippo signaling pathway
PPAR signaling pathway
Drug metabolism - cytochrome P450
Peroxisome
Glycosaminoglycan biosynthesis - heparan sulfate / heparin
Biosynthesis of amino acids
Vitamin B6 metabolism
Transcriptional misregulation in cancer
MicroRNAs in cancer
Ribosome biogenesis in eukaryotes
Ribosome
Systemic lupus erythematosus
RNA degradation
Steroid biosynthesis
Metabolic pathways
0
1
2
3
4
5
$-\log_{10}(p)$

Figure 9. KEGG significance plot showing signaling pathway alterations in metformin- and vehicle-treated human IPF lung fibroblasts.
The top 75 candidate pathways are shown. Note the statistically significant modulations observed for metabolic pathways related to glycosaminoglycan biosynthesis – heparan sulfate / heparin, fatty acid metabolism, glycerolipid metabolism and fatty acid elongation. PPAR and TGFβ signaling pathways are also among the top candidates. The dashed red line represents the cut-off value of P=0.05. Vehicle-treated group: n=4, metformin-treated group: n=3.

4.3.2. Metformin inhibits TGFβ1-mediated fibrogenesis in vitro

The TGFβ1 signaling pathway is widely regarded as the master regulator of fibrogenesis in vitro and in vivo. In order to investigate whether metformin inhibits the profibrotic effect of TGFβ1 in vitro, primary lung fibroblasts isolated from 10 IPF patients were starved for 24 h and then treated with 2 ng/mL rhTGFβ1 (or vehicle) for 72 h and then treated with 5 mM metformin (or vehicle) for 72 h (Fig. 10A). This experimental setup allows examining the ability of metformin to change the phenotype of myofibroblasts that arise from TGFβ1 treatment. The effect of TGFβ1 treatment was validated after 72 h by qPCR and the results showed significant downregulation of the lipogenic markers *PLIN2* (Fig. 10B) and *PPARg* (Fig. 10C) in parallel to significant upregulation of *COL1A1* (Fig. 10D) as we previously described(El Agha et al., 2017). We also expected that activation of TGFβ1 signaling would result in disappearance of lipid droplets at the expense of *ACTA2* and *COL1A1* upregulation. To test this hypothesis, cells were stained with LipidTOX and anti-ACTA2 antibodies. Fluorescent microscopy showed increased abundance of ACTA2 filaments (Fig. 10H) and absence of lipid droplets (Fig. 2F) in TGFβ1-treated cells compared to vehicle-treated cells (Fig. 10E, G) after 72 h. Time-lapse microscopy of vehicle- (supplementary movie 1), rhTGFβ1- (supplementary movie 2) or metformin-treated cells (supplementary movie 3) in the presence of LipidTOX was also carried out for 68 h. Metformin led to an increase in lipid-droplet accumulation after 48 h while vehicle or rhTGFβ1 treatment led to cell elongation and disappearance of lipid droplets.

Next, the response to metformin treatment was analyzed. At the end of day 6 (144 h), qPCR showed significant upregulation of *PLIN2* (4.6 folds, Fig. 10I) and *PPARg* (1.3 folds, Fig. 2J), and a significant 7.1-fold downregulation of *COL1A1* expression (Fig. 10K) in the [TGFβ1 plus metformin] group compared to the [TGFβ1 plus vehicle] group. Interestingly, lipid-droplet accumulation was regained in fibroblasts treated with [TGFβ1 plus metformin] compared to the [TGFβ1 plus vehicle] group (Fig. 10L, M). These results suggest that metformin affects the phenotype of myofibroblasts arising from TGFβ1 treatment by downregulating myogenic markers and inducing lipogenic differentiation.

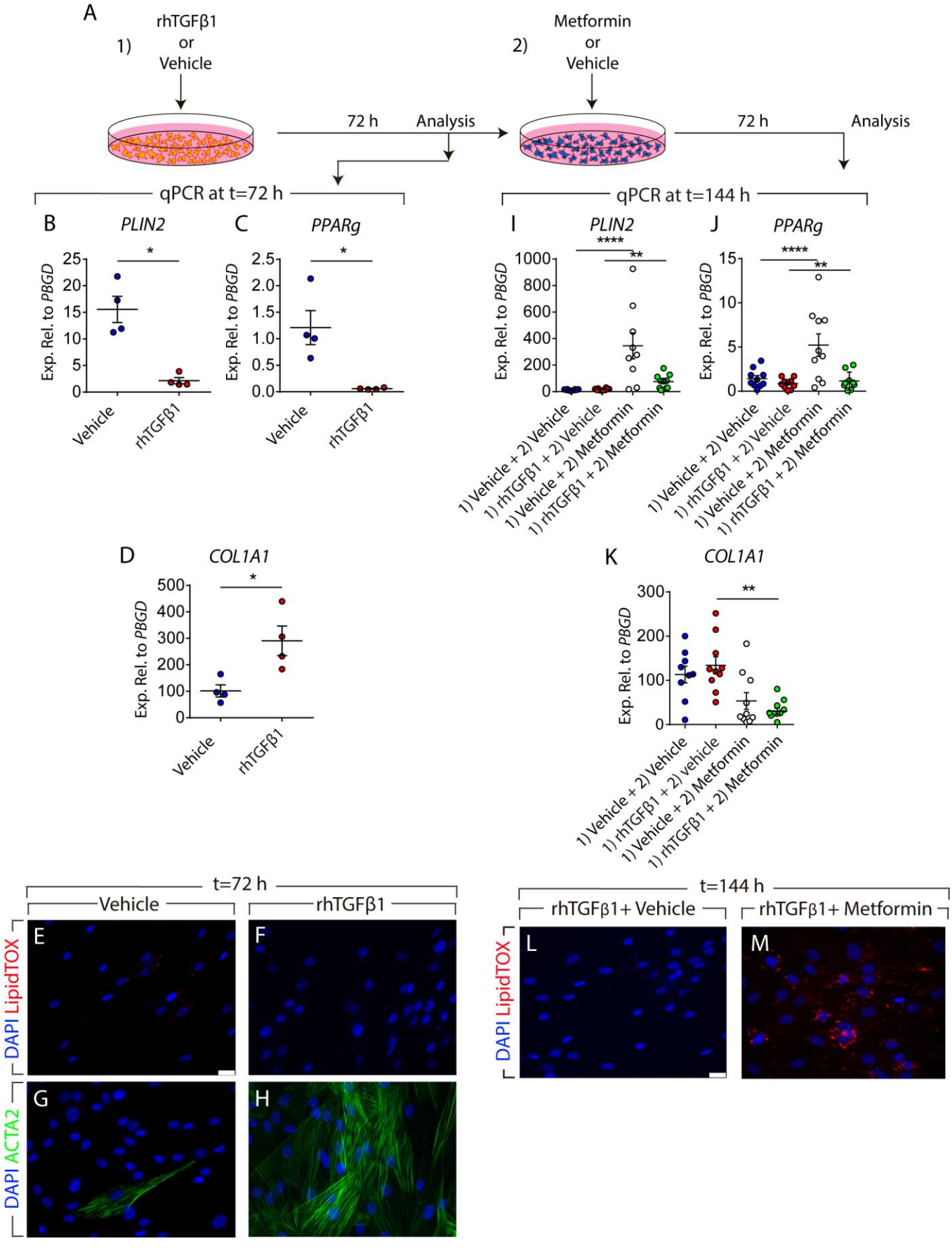
A
1)
rhTGFβ1
or
Vehicle
72 h
Analysis
2)
Metformin
or
Vehicle
72 h
Analysis
qPCR at t=72 h
qPCR at t=144 h
B
PLIN2
C
PPARg
I
PLIN2
J
PPARg
Exp. Rel. to PBGD
Vehicle
rhTGFβ1
1) Vehicle + 2) Vehicle
1) rhTGFβ1 + 2) Vehicle
1) Vehicle + 2) Metformin
1) rhTGFβ1 + 2) Metformin
D
COL1A1
K
COL1A1
t=72 h
t=144 h
Vehicle
rhTGFβ1
rhTGFβ1+ Vehicle
rhTGFβ1+ Metformin
DAPI LipidTOX
DAPI ACTA2
E
F
G
H
L
M

Figure 10. Metformin attenuates TGFβ1-mediated fibrogenesis in vitro.
(A) Schematic representation of the experimental setup. **(B-D)** qPCR analysis for *PLIN2, PPARg* and *COL1A1* in human lung fibroblasts treated with TGFβ1 or vehicle for 72 h. **(E-H)** Staining of TGFβ1- and vehicle-treated cells with LipidTOX (red), anti-ACTA2 antibodies (green) and DAPI (blue). **(I-K)** qPCR analysis for *PLIN2, PPARg* and *COL1A1* in human lung fibroblasts treated with TGFβ1 or vehicle for 72 h, followed by treatment with metformin or vehicle for 72 h. **(L-M)** Staining of TGFβ1- and vehicle-treated cells with LipidTOX (red) and DAPI (blue) at the end of treatment (t=144 h). Scale bars: (E-H) and (L-M) 25 µm. Each data point within a given group corresponds to one patient. (B-D) n=4 per group. (I-K) n=9-10 per group. Mann-Whitney test was used in (B-D), one-way ANOVA was used in (I, J) and Kruskal-Wallis test was used in (K).

4.3.3. Metformin improves lung structure in an ex vivo system

One drawback of using cell-culture systems is that cells growing in vitro are deprived of their microenvironmental cues and their behavior might not resemble that of an in vivo context. We therefore set out to test whether metformin exerts similar beneficial effects in a more complex system that better mimics the in vivo setting. Therefore, we used precision-cut lung slices (PCLS), an ex vivo culture system which allows maintenance of viable, metabolically active lung tissue with preserved structure for five days. Two hundred micrometer-thick PCLS were prepared from fibrotic regions of fresh IPF lung tissues and were cultured in DMEM supplemented with 10% BCS in the presence or absence of 5 mM metformin for five days (Fig. 11A). Bright-field imaging showed that metformin-treated PCLS displayed a more relaxed structure with open airspaces (Fig. 11E) compared to their vehicle-treated counterparts (Fig. 11D). PCLS were then embedded in paraffin, sectioned into 5 µm-thick slices, and processed for histological analysis. Hematoxylin and eosin staining (Fig. 11H, I), Masson's trichrome staining (Fig. 11J, K) and COL1A1 immunostaining (Fig. 11L, M) showed improved lung structure and decreased collagen deposition in metformin-treated samples compared to controls. Another set of PCLS was not sectioned but was subjected to whole-mount staining using

anti-COL1A1 antibodies and LipidTOX followed by confocal microscopy. Three-dimensional (3D) reconstruction using z-stacks acquired from these samples revealed decreased COL1A1 expression and increased lipid-droplet accumulation (Fig. 11N, O). Flow cytometry-based quantification confirmed the histological observations and showed a significant increase in the abundance of lipid-droplet-containing cells (following depletion of $CD45^+$ bone marrow-derived cells, $CD31^+$ endothelial cells and $EpCAM^+$ epithelial cells) in metformin-treated PCLS (12 ± 0.6%) compared to controls (7.2 ± 1.1%) (Fig. 11P, Q). Finally, total collagen assay showed a significant reduction in collagen content from 26.9 ± 0.9 µg/µL to 20.8 ± 0.9 µg/µL in response to metformin treatment (Fig. 11R).

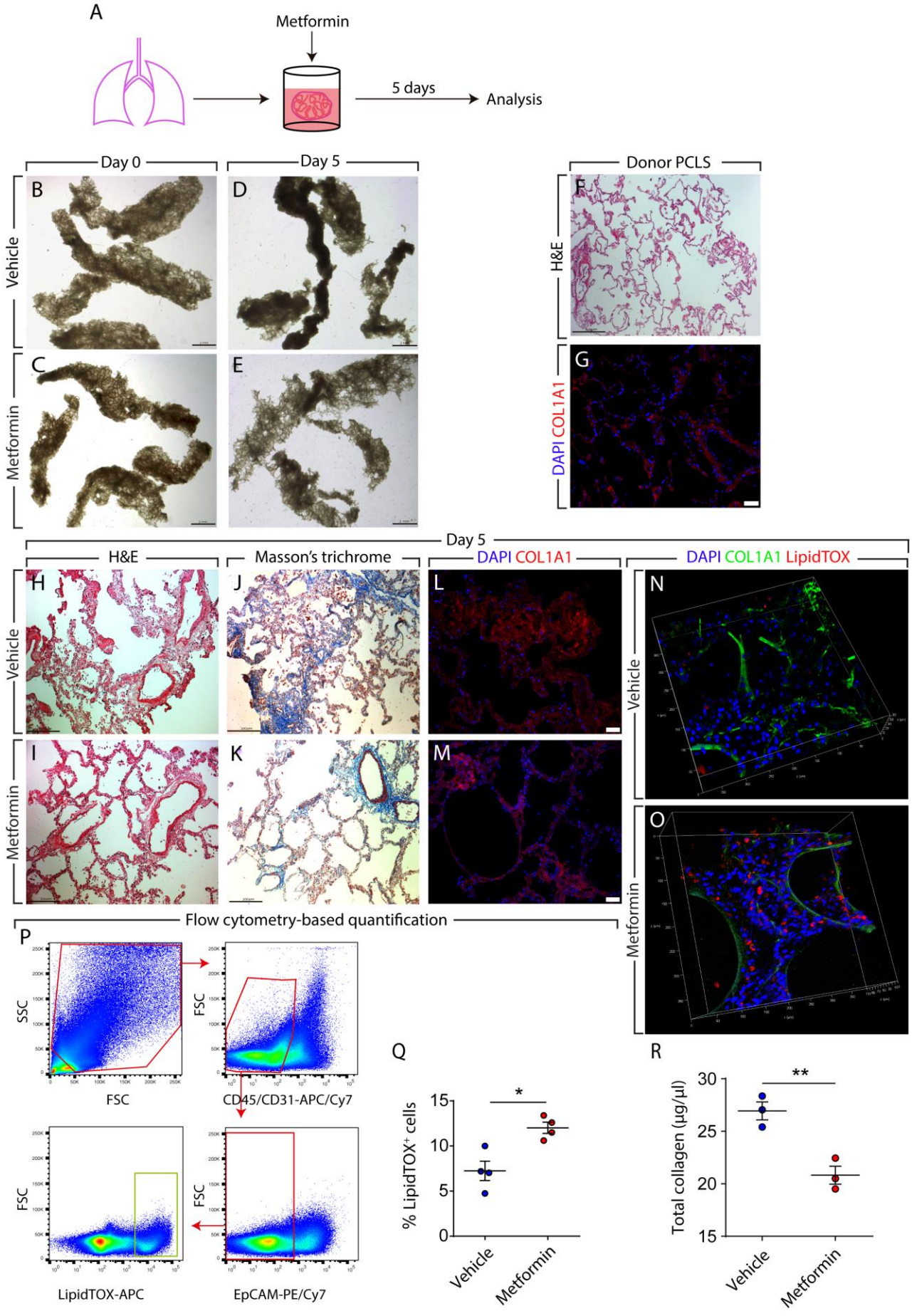
A
Metformin
5 days
Analysis
Day 0
Day 5
Donor PCLS
Vehicle
Metformin
B
C
D
E
F
G
H&E
DAPI COL1A1
Day 5
H&E
Masson's trichrome
DAPI COL1A1
DAPI COL1A1 LipidTOX
H
I
J
K
L
M
N
O
Flow cytometry-based quantification
P
SSC
FSC
CD45/CD31-APC/Cy7
LipidTOX-APC
EpCAM-PE/Cy7
Q
% LipidTOX+ cells
R
Total collagen (µg/µl)

Figure 11. Metformin improves IPF lung structure ex vivo.
(A) Schematic representation of the experimental setup. **(B-E)** Bright-field imaging of PCLS treated with metformin or vehicle for five days. **(F, G)** Hematoxylin and eosin staining and COL1A1 immunostaining of PCLS prepared from a non-IPF donor lung. **(H-M)** Hematoxylin and eosin staining, Masson's trichrome staining and COL1A1 immunostaining of PCLS prepared from an IPF lung and treated with metformin or vehicle for five days. **(N, O)** 3D-reconstruction of z-stacks of metformin- and vehicle-treated PCLS stained for COL1A1 (green) and lipid droplets (red). **(P)** Gating strategy for flow cytometry-based quantification of LipidTOX$^+$ cells that are negative for hematopoietic (CD45), endothelial (CD31) and epithelial (EpCAM) cell markers. **(Q)** Quantification of flow cytometry measurements on metformin- and vehicle-treated cells. **(R)** Total collagen assay for metformin- and vehicle-treated cells. Scale bars: (B-E) 2 mm, (F) 500 µm, (G, L, M) 50 µm, (H-K) 200 µm. Each data point within a given group corresponds to one patient. (Q) n=4 per group. (R) n=3 per group. Mann-Whitney test was used in (Q, R).

4.3.4. Metformin accelerates resolution of bleomycin-induced pulmonary fibrosis in mice

We next sought to test whether the ability of metformin to alter the myofibroblast fate also applies to the in vivo context of lung fibrosis. In order to address this question, we employed a lineage-tracing approach in the context of bleomycin-induced pulmonary fibrosis (Fig. 12). This model of injury is reversible and animals start to spontaneously recover from lung fibrosis after day 14. Moreover, we previously reported that the *Acta2-Cre-ERT2; tdTomato^{flox}* lineage-tracing tool allows genetic labeling of ACTA2$^+$ myofibroblasts as they accumulate during the buildup of lung fibrosis when tamoxifen is introduced between days 5 and 14 after bleomycin injury (El Agha et al., 2017). Therefore, double transgenic animals were treated with bleomycin, fed tamoxifen-containing pellets between days 5 and 14, treated with metformin (or vehicle) starting at day 14 after bleomycin instillation, and were sacrificed at day 28 (Fig. 12A, B). This experimental setup

allows labeling myofibroblasts that form during fibrosis formation and tracing their fate during resolution in the presence or absence of metformin. Already upon gross optical inspection, hematoxylin and eosin as well as masson's trichrome stained lungs explanted at day 28 showed enhanced recovery from fibrosis upon metformin treatment (Fig. 12C-F). Correspondingly, quantification of lung fibrosis showed a significant decrease in the extent of fibrosis from 12 ± 1.5% in the vehicle-treated group to 8 ± 0.6% in the metformin-treated group (Fig. 12G). Immunofluorescent staining allowed visualization of lineage-traced myofibroblast-derived cells (tdTomato$^+$) and also confirmed the decrease in COL1A1 deposition upon metformin treatment (Fig. 12H, I). Interestingly, LipidTOX staining carried out on frozen sections revealed the presence of lipid droplets in tdTomato$^+$ cells at day 28 (Fig. 12J, K). In order to quantify the impact of metformin on altering the myofibroblast fate, flow cytometry was carried out. The results showed similar proportions of tdTomato$^+$ cells in both groups (Fig. 12Q), while the proportion of LipidTOX$^+$ mesenchymal cells increased from 13.5 ± 2.5% to 18.8 ± 1.8% upon metformin treatment (Fig. 12S). More importantly, the proportion of myofibroblast descendants (tdTomato$^+$) that also contained lipid droplets increased from 6.8 ± 0.1% in the control group to 12.2 ± 0.5% in the metformin-treated group (Fig. 12R). Collectively, these data clearly demonstrate that metformin accelerates fibrosis resolution and this is accompanied by the induction of myogenic-to-lipogenic conversion in lung fibroblasts in vivo.

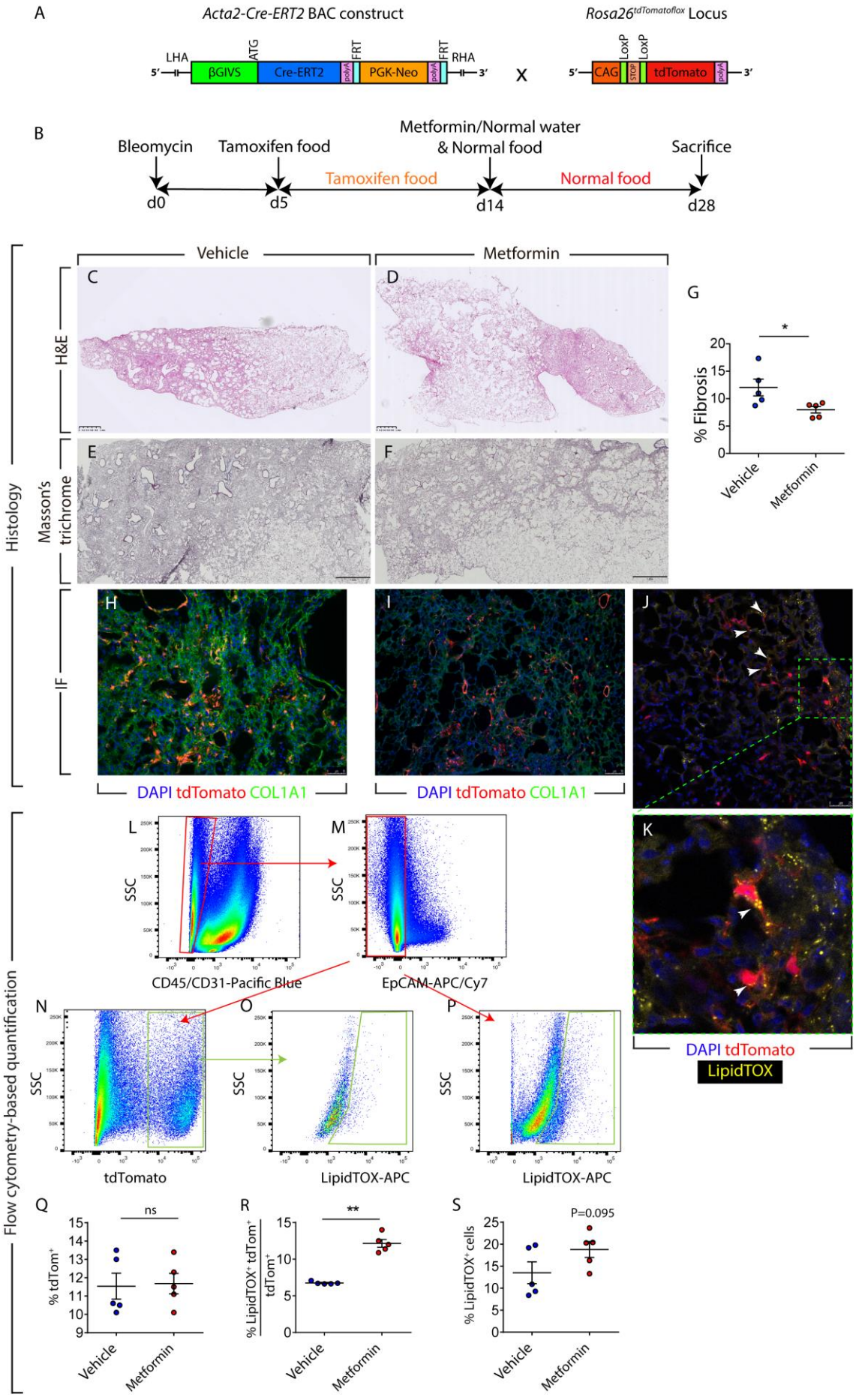
A
Acta2-Cre-ERT2 BAC construct
LHA
ATG
FRT
FRT
RHA
βGIVS
Cre-ERT2
polyA
PGK-Neo
polyA
5′
3′
X
Rosa26tdTomatoflox Locus
LoxP
LoxP
CAG
STOP
tdTomato
polyA
B
Bleomycin
Tamoxifen food
Metformin/Normal water & Normal food
Sacrifice
Tamoxifen food
Normal food
d0
d5
d14
d28
Vehicle
Metformin
Histology
H&E
Masson's trichrome
IF
C
D
E
F
G
% Fibrosis
Vehicle
Metformin
H
I
J
K
DAPI tdTomato COL1A1
DAPI tdTomato COL1A1
DAPI tdTomato
LipidTOX
Flow cytometry-based quantification
L
M
SSC
CD45/CD31-Pacific Blue
EpCAM-APC/Cy7
N
O
P
tdTomato
LipidTOX-APC
LipidTOX-APC
Q
R
S
% tdTom+
% LipidTOX+ tdTom+ / tdTom+
% LipidTOX+ cells
ns
**
P=0.095
Vehicle
Metformin

Figure 12. Metformin accelerates fibrosis resolution in the bleomycin model in mice.

(A) Schematic representation of the *Acta2-Cre-ERT2* and *tdTomato^{flox}* construct. **(B)** Schematic representation of the timeline of the experiment. Bleomycin was administered intratracheally at day 0. Between days 5 and 14, mice were fed tamoxifen-containing pellets and starting at day 14, metformin (1.5 mg/mL) or vehicle was administered through drinking water. Mice were sacrificed at day 28. **(C-F)** Hematoxylin and eosin and Masson's trichrome staining of metformin- and vehicle-treated lungs. **(G)** Quantification of fibrosis in metformin- and vehicle-treated lungs. **(H, I)** Immunofluorescence for COL1A1 (green). Endogenous tdTomato signal (red) and DAPI (blue) are also shown. **(J)** LipidTOX staining (green) and tdTomato$^+$ cells (red) are shown. The box in (J) is magnified in **(K).** Arrowheads indicate LipidTOX$^+$ tdTomato$^+$ cells. **(L-S)** Gating strategy (to detect CD45$^-$ CD31$^-$ EpCAM$^-$ tdTomato$^+$ and/or LipidTOX$^+$ cells) and quantification of various cell populations based on tdTomato and LipidTOX detection. Scale bars: (C-F) 1 mm, (H, I) 50 µm, (J) 25 µm. Each data point within a given group corresponds to one animal. n=5 per group. Mann-Whitney test was used in (G, Q-S).

4.3.5. The mechanism of action of metformin in human lung fibroblasts is only partially dependent on AMPK signaling

Activation of the AMPK signaling cascade is one of the major molecular mechanisms that have been proposed for metformin. In order to investigate whether metformin-mediated lipogenic differentiation is AMPK-dependent, gain and loss-of-function approaches were carried out. In a first set of experiments, primary human lung fibroblasts isolated from 8 IPF patients were cultured and treated with GSK621 (a selective activator of AMPK signaling pathway) for 72 h (Fig. 13A). The results showed a trend for mild downregulation of the lipogenic markers *PLIN2* (Fig. 13B) and *PPARg* (Fig. 13C) in parallel to a robust, significant downregulation of *COL1A1* (Fig. 13D). Accordingly, GSK621 treatment failed to promote lipid-droplet accumulation in these cells (Fig. 13L-N).

In another set of experiments, primary human lung fibroblasts isolated from 5 IPF patients were transfected with siRNAs targeting *AMPK*. After 72 h, cells were treated with metformin and were analyzed after 72 h (Fig. 13F). Western blotting revealed a 90% knockdown of *AMPK* in these cells compared to scramble-transfected cells at the time of analysis (Fig. 13J, K). Interestingly, metformin treatment led to upregulation of *PLIN2* and *PPARg* regardless of *AMPK* knockdown (Fig. 13G, H). Metformin-mediated *COL1A1* downregulation, however, was attenuated upon *AMPK* knockdown (Fig. 13I). Altogether, these data demonstrate that the mechanism of action of metformin in promoting lipogenic differentiation in human lung fibroblasts is largely independent of AMPK signaling while inhibition of COL1A1 production is mainly AMPK-dependent.

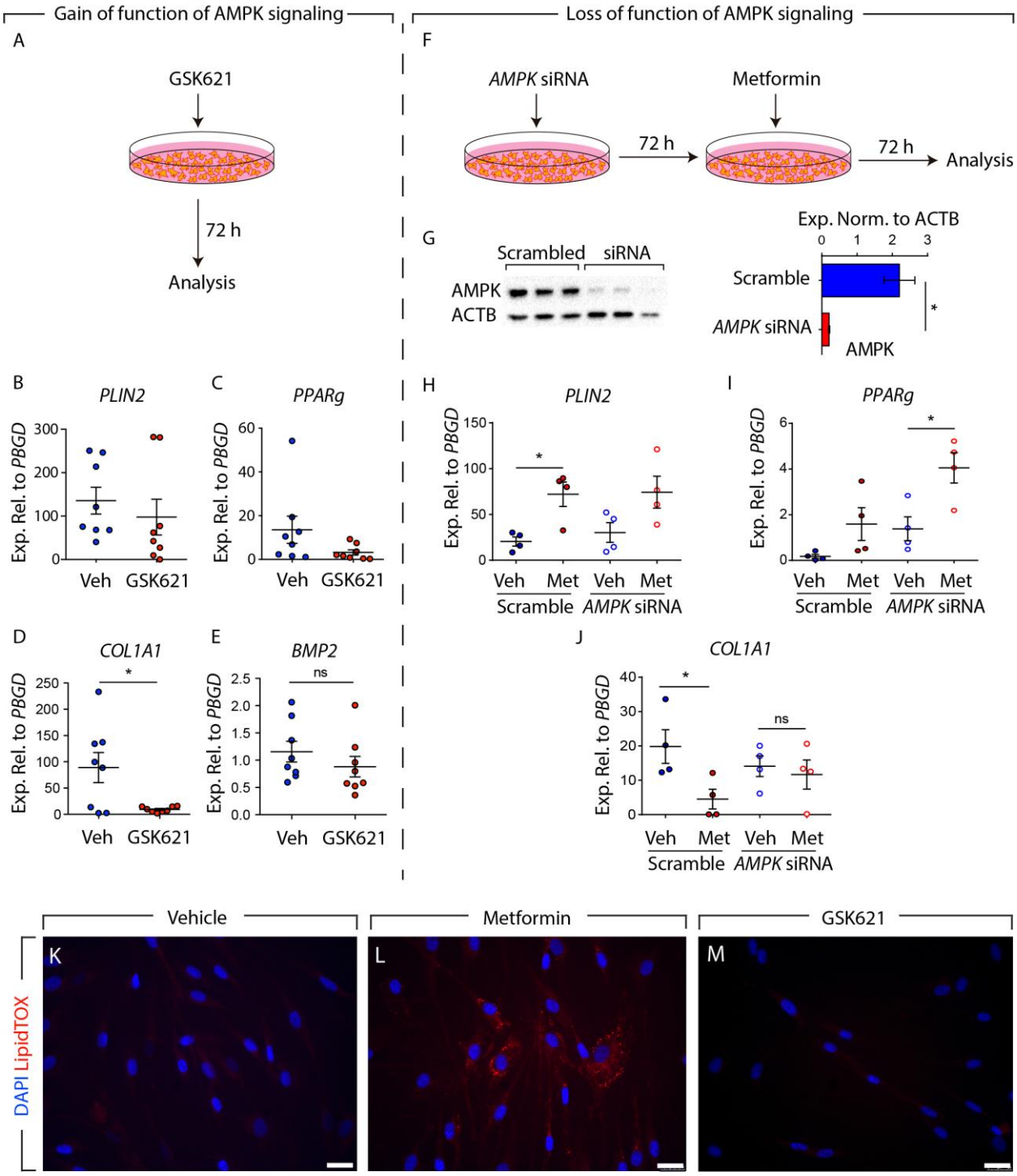

Figure 13. Mode of action of metformin is partially independent of AMPK signaling.

(A) Schematic representation of the gain-of-function experimental setup for AMPK signaling. **(B-E)** qPCR analysis of *PLIN2, PPARg*, *COL1A1* and *BMP2* in human IPF lung fibroblasts treated with the AMPK agonist GSK621 or vehicle. **(F)** Schematic representation of the loss-of-function experimental setup for AMPK signaling. **(G-I)** qPCR analysis of *PLIN2, PPARg* and *COL1A1* in IPF fibroblasts treated with *AMPK* siRNA or scramble siRNA. The decrease of AMPK protein levels at the time of analysis is shown in **(J, K). (L-N)** Staining of GSK621- and vehicle-treated cells with LipidTOX (red) and DAPI (blue). Metformin-treated cells were used as a positive control for lipid-droplet accumulation (M). Scale bars: (L-N) 25 µm. Each data point corresponds to one patient. (B-E) Vehicle-treated group: n=8, GSK621-treated group: n=8. (G-I) n=4 per group. (K) n=3 per group. Mann-Whitney test was used in (B-E, K) and Kruskal-Wallis test was used in (G-I).

4.3.6. Metformin induces the expression of lipogenic markers via induction of *BMP2* expression and phosphorylation of PPARγ

The next step was to better define the molecular mechanism by which metformin induces lipogenic differentiation in human lung fibroblasts. Our gene expression microarrays showed that *BMP2* was the top upregulated gene in fibroblasts upon metformin treatment (Fig. 8J). BMP2 is known to inhibit smooth muscle cell growth in a mechanism involving PPARγ activation. Calvier et al. also reported that BMP2 inhibits TGFβ1 signaling via PPARγ in vascular smooth muscle cells in the lung(Calvier et al., 2017). Therefore, we treated 11 human IPF lung fibroblasts with rhBMP2 and gene expression was analyzed after 72 h (Fig. 14A). Intriguingly, rhBMP2 treatment resulted in significant upregulation of *PLIN2* (1.9 folds, Fig. 14B) and *PPARg* (2.5 folds, Fig. 14C), while *COL1A1* expression levels remained unchanged (Fig. 14D). LipidTOX staining confirmed the increase in lipid-droplet accumulation in these cells (Fig. 14E, F). We then performed siRNA-mediated knockdown of *PPARg* in human IPF lung fibroblasts (Fig. 14G) and tested the effect of rhBMP2 treatment on lipogenic differentiation. The results showed that *PPARg* knockdown abolished rhBMP2-induced lipogenic differentiation in these cells (Fig. 14H, I). As expected, *COL1A1* levels were not modulated by this intervention (Fig. 14J). Thus, BMP2 is a positive regulator of lipogenic differentiation in human IPF lung fibroblasts. The

activation of PPARγ signaling pathway can also be induced post-translationally via PPARγ phosphorylation at serine residue 112 (Ser^{112})(Compe et al., 2005; Iankova et al., 2006; Zhang et al., 1996a). Therefore, we set out to determine whether BMP2 (and metformin) induce lipogenic differentiation in human lung fibroblasts by inducing PPARγ phosphorylation. Cells were treated with rhBMP2 (or vehicle) and protein lysates were collected after 72 h. PPARγ phosphorylation was induced 7.6 folds in rhBMP2-treated fibroblasts while PPARγ protein levels remained unchanged (Fig. 14K).

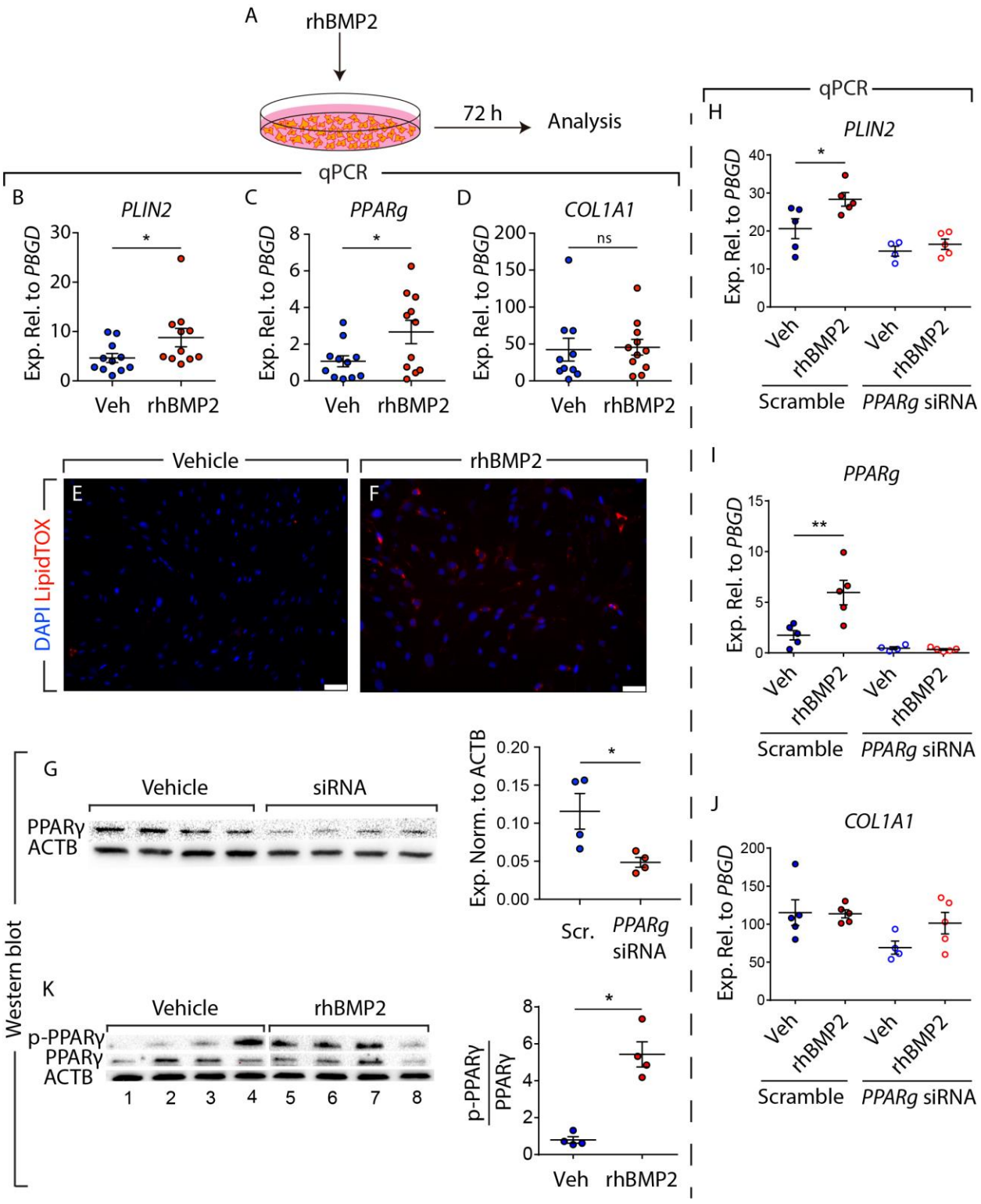

Figure 14. rhBMP2 induces PPARγ phosphorylation and lipogenic differentiation in human IPF lung fibroblasts.

(A) Schematic representation of the experimental setup. **(B-D)** qPCR analysis of *PLIN2, PPARg* and *COL1A1* in IPF fibroblasts treated with rhBMP2 or vehicle. **(E, F)** Staining of rhBMP2- and vehicle-treated cells with LipidTOX (red) and DAPI (blue). **(G)** Western blot validating the knockdown of PPARγ levels 72 h after siRNA treatment. Quantification of the immunoblot is shown in the right panel. **(H-J)** qPCR analysis of *PLIN2, PPARg* and *COL1A1* in IPF fibroblasts transfected with siRNA against *PPARg* (for 72 h) and then treated with vehicle or rhBMP2 for 72 h. **(K)** Western blot showing the induction of PPARγ phosphorylation in response to rhBMP2 treatment. Lanes 1-4 and lanes 5-8 were run in parallel on different gels under the same conditions. Quantification of the immunoblot is shown in the right panel. Scale bars: (E-F) 50 µm. Each data point corresponds to one patient. (B-D) n=11 per group except for *COL1A1* vehicle-treated group (n=10). (G) n=4 per group. (K) Scramble/vehicle-, scramble/rhBMP2- and siRNA/rhBMP2-treated groups: n=5 per group, siRNA/vehicle-treated group: n= 4. Mann-Whitney test was used in (B, D, G, K) and Student's t-test was used in (C). Kruskal-Wallis test was used in (H-J).

In another set of experiments, treatment of cells with TGFβ1 led to a 24.4-fold reduction in p-PPARγ levels (Fig. 7A, lanes 4-6 and Fig. 15B) while treatment with metformin led to a 3.3-fold increase in p-PPARγ levels (Fig. 7A, lanes 7-9 and Fig. 15B) compared to vehicle-treated cells (Fig. 15A, lanes 1-3 and Fig. 15B). In order to investigate whether metformin counteracts the profibrotic effects of TGFβ1 in fibroblasts by modulating the phosphorylation status of PPARγ, cells were first starved for 24 h and then treated with rhTGFβ1 for 72 h, followed by vehicle, rhTGFβ1 or metformin treatment for another 72 h. The results showed that in comparison to transient (Fig. 15A, lanes 10-12) or continuous treatment with rhTGFβ1 (Fig. 15A, lanes 13-15), treatment with metformin after rhTGFβ1 treatment rescued p-PPARγ levels (Fig. 15A, lanes 16-18 and Fig. 15C). Of note, qPCR analysis revealed that activation of AMPK signaling via GSK621 treatment did not induce *BMP2* expression in IPF fibroblasts (Fig. 15E), indicating that the metformin-BMP2-p-PPARγ axis is independent of AMPK signaling.

In order to demonstrate that metformin-induced lipogenic differentiation is mediated by BMP2 signaling, cells were treated with metformin in the presence or absence of the BMP inhibitor noggin. The levels of p-SMAD1/5/8 were used as readout for BMP2 signaling. Treatment with metformin led to significant phosphorylation of SMAD1/5/8 (Fig. 15D, lanes 11-14 and Fig. 15E), indicating that metformin treatment indeed activates BMP2 signaling. As expected, treatment with vehicle (Fig. 15D, lanes 1-3 and Fig. 15E), noggin (Fig. 15D, lanes 4-6 and Fig. 15E) or metformin + noggin (Fig. 15D, lanes 7-10 and Fig. 15E) did not yield significant SMAD1/5/8 phosphorylation. In line with these data, qPCR analysis revealed that noggin treatment abolished metformin-mediated upregulation of *PLIN2* (Fig. 15F) and *PPARg* (Fig. 15G) without affecting metformin-mediated downregulation of *COL1A1* (Fig. 15H). These results indicate that metformin-induced lipogenic differentiation, but not collagen reduction, is mediated by BMP2 signaling.

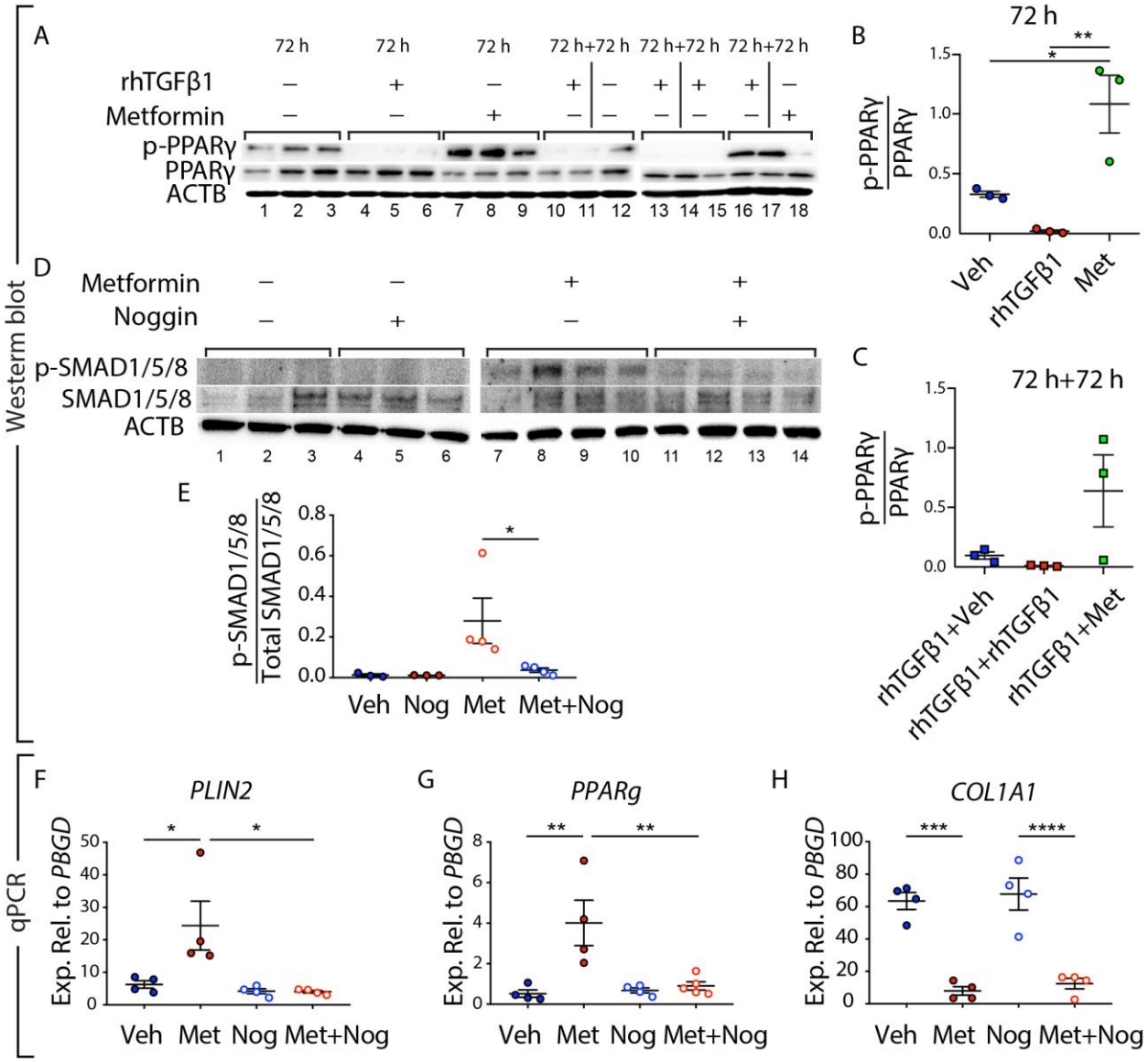

Figure 15. Metformin-mediated lipogenic differentiation in human IPF lung fibroblasts is mediated by BMP2 signaling.

(A-C) Western blot showing the opposing effects of metformin and rhTGFβ1 on PPARγ phosphorylation, and the ability of metformin to partially restore PPARγ phosphorylation in rhTGFβ1-treated IPF fibroblasts. Lanes 1-12 and lanes 13-18 were run in parallel on different gels under the same conditions. **(D)** Western blot showing the phosphorylation status of SMAD1/5/8 in the presence of metformin and/or the BMP signaling inhibitor noggin. Quantification of the immunoblot is shown in **(E). (F-H)** qPCR analysis of *PLIN2, PPARg* and *COL1A1* in IPF fibroblasts treated with vehicle, metformin, noggin and

noggin+metformin. Each data point corresponds to one patient. (A-C) n=3 per group. (D) Vehicle- and noggin-treated groups: n=3 per group, metformin- and metformin/noggin-treated groups: n=4. (F) n=4 per group. (G) n=4 per group except for Nog+Metformin (n=5). (H) n=4 per group. Kruskal-Wallis test was used in (B, C, E-H).

4.3.7. Pirfenidone and nintedanib do not induce lipogenic differentiation in human lung fibroblasts

Currently, there are two FDA-approved drugs for treating IPF; pirfenidone, which is believed to act as a TGFβ1 inhibitor, and nintedanib, which is a multi-receptor tyrosine kinase inhibitor. Therefore, we set out to determine whether these two drugs alter lung fibroblast fate in a similar fashion to metformin. Firstly, primary human lung fibroblasts were treated with either nintedanib (1 µM) or pirfenidone (0.3 mg/ml) for 72 h (Fig. 16A). Quantitative real-time PCR analysis showed that neither nintedanib nor pirfenidone enhanced the expression of the lipogenic markers *PLIN2 and PPARg* (Fig. 16B, C, E, F). Nintedanib and pirfenidone did, however, lead to a 1.9- and 2.3-fold downregulation of *COL1A1*, respectively (Fig. 16D, G). In line with these data, LipidTOX staining did not reveal any change in lipid-droplet accumulation following nintedanib or pirfenidone treatment (Fig. 16H-J). Finally, whole-mount staining followed by confocal imaging and 3D reconstruction of IPF-derived PCLS (cultured for five days in the presence or absence of nintedanib or pirfenidone) revealed a slight decrease in COL1A1 deposition without an evident change in the abundance of LipidTOX$^+$ cells (Fig. 16K-O).

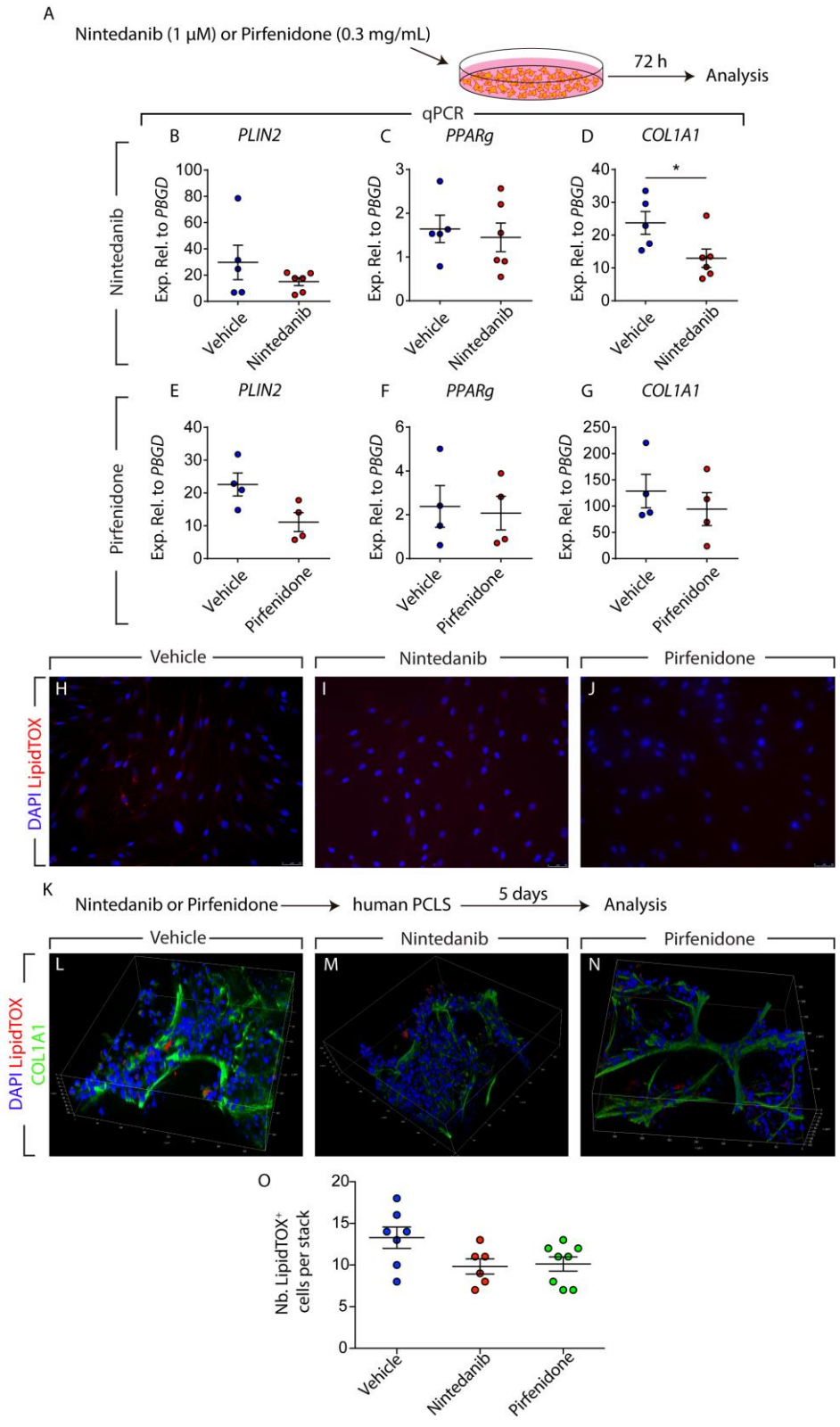

Figure 16. Nintedanib and pirfenidone do not induce lipogenic differentiation in IPF lung fibroblasts.

(A) Schematic representation of the experimental setup. **(B-D)** qPCR analysis of *PLIN2, PPARg* and *COL1A1* in human IPF lung fibroblasts treated with nintedanib. A similar analysis for pirfenidone-treated cells is shown in **(E-G). (H-J)** Staining of nintedanib-, pirfenidone- and vehicle-treated cells with LipidTOX (red) and DAPI (blue). **(K)** Schematic representation of the experimental setup using PCLS. **(L-N)** 3D-reconstruction of z-stacks of nintedanib-, pirfenidone- and vehicle-treated PCLS stained for COL1A1 (green) and lipid droplets (red). **(O)** Quantification of LipidTOX$^+$ cells as determined by manual counting across z-stacks. Scale bars: (H-J) 50 µm. (B-G) Each data point within a given group corresponds to one patient. (B-D) Vehicle-treated group: n=5, nintedanib-treated group: n=6. (E-G) n=4 per group. (O) Each data point within a given group corresponds to one z-stack. Vehicle-treated group: n=7, nintedanib-treated group: n=6, pirfenidone-treated group: n=8. Mann-Whitney test was used in (B-G) and Kruskal-Wallis test was used in (O).

In an attempt to explore modulations in serine/threonine protein kinase activities upon metformin treatment, human IPF lung fibroblasts were subjected to a protein kinase activity assay (PamStation). The results showed significantly reduced kinase activities for CDK1, CDK3, MAPK11/14 and ERK1/2 (Fig. 17A). Given the relevance of ERK1/2 in lung fibrosis(Madala et al., 2012) and the fact that PPARγ can serve as a substrate for MAPK(Hosooka et al., 2008; Zhang et al., 1996a), the effect of metformin in inhibiting the activity of ERK1/2 was validated by Western blotting and the results showed robust inhibition of p-ERK1/2 levels in IPF lung fibroblasts in response to metformin treatment (Fig. 17B). Treatment of human IPF lung fibroblasts with Selumetinib (a potent and selective inhibitor of MEK that is directly upstream of ERK) did not yield significant changes in the expression levels of lipogenic or myogenic marker genes (Fig. 17C-F). Therefore, we conclude that the ERK pathway is not involved in metformin-mediated myo- to lipofibroblast transdifferentiation and collagen reduction.

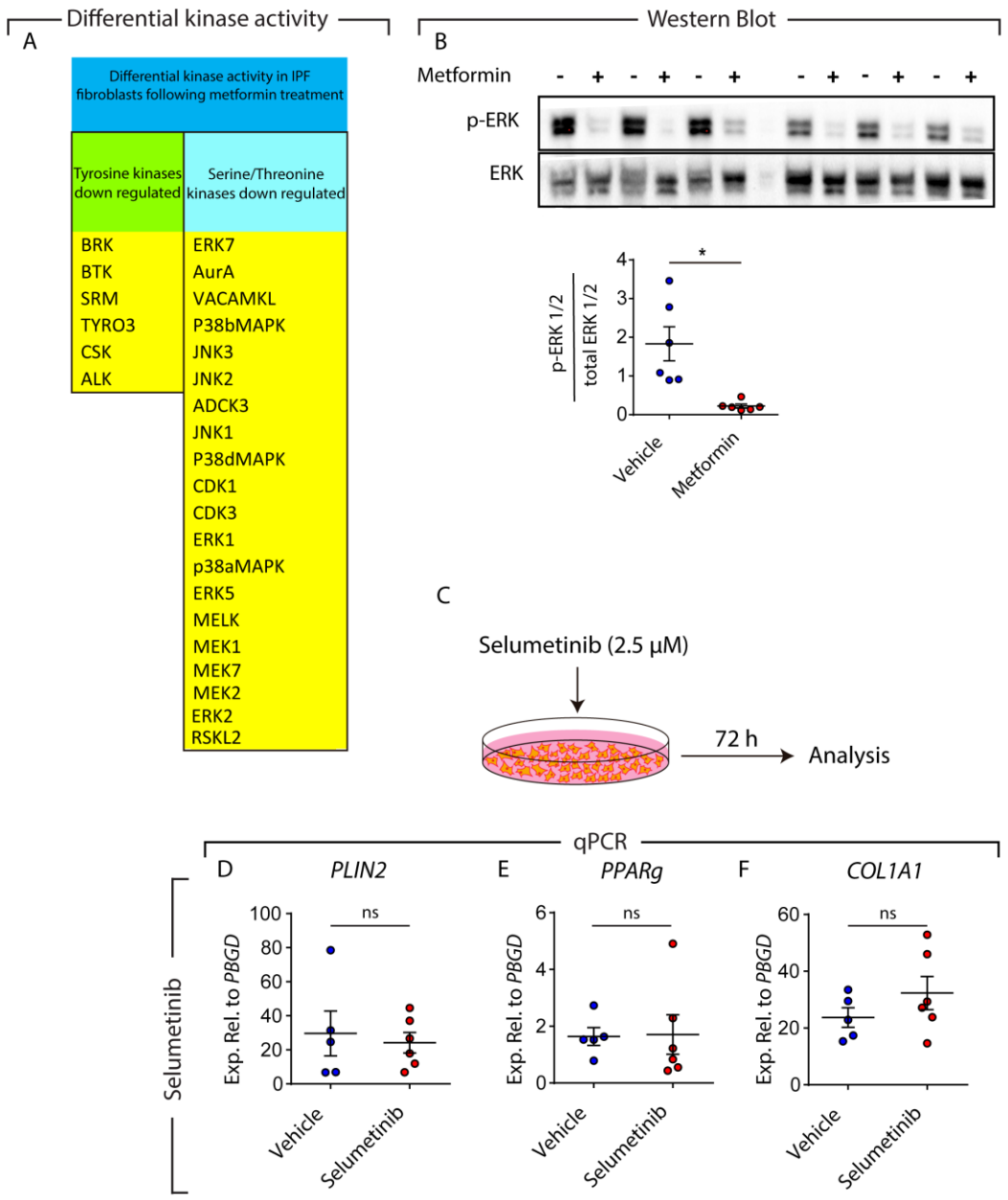

Figure 17. Inhibition of ERK phosphorylation does not mediate the antifibrotic effect of metformin in human IPF lung fibroblasts.

(A) Kinase activity assay as determined by PamStation analysis. **(B)** Western blot showing decreased p-ERK levels in response to metformin treatment. Quantification of

p-ERK levels is shown in the lower panel. **(C)** Schematic representation of the experimental setup. **(D-F)** qPCR analysis of *PLIN2, PPARg* and *COL1A1* in IPF fibroblasts treated with selumetinib or vehicle for 72 h. Each data point corresponds to one patient. (B) n=6 per group. (D-F) Vehicle-treated group: n=5, Selumetinib-treated group: n=6. Mann-Whitney test was used

5. Discussion

5.1. Formation of the lipofibroblasts during development

Despite being described in 1970, lipofibroblasts remained one of the least studied cell populations in the lung until recently. During this study, we have attempted to better characterize these cells. Using flow cytometry, the data showed that lipofibroblast start to appear at late pseudoglandular stage which coincides with the start of the differentiation process of AECIIs (Beers and Moodley, 2017). Due to being located in close proximity of AECII, lipofibroblasts are believed to assist these cells in the process of surfactant production via shuttling of stored lipids to AECIIs (Tordet et al., 1981).

The signaling pathways which are important for the formation of lipofibroblasts remain ill understood as well. Previously, our group provided evidence that a subpopulation of $Fgf10^{+}$ mesenchymal cells gives rise to lipofibroblasts (El Agha et al., 2014). Furthermore, induction of *Fgf10* expression in the lipofibroblasts can be one of the major sources of this growth factor which is crucial for the expansion and differentiation of epithelial cells (Ramasamy et al., 2007; Yuan et al., 2018). In addition to paracrine function, our data also suggests an autocrine function of Fgf10 on lipofibroblasts as well which it seems mainly conducted through Fgfr2b. Fgfr1b knockdown animals manifested a slight increase in the expression of lipofibroblastic markers and also Plin2 immunostaining which is most likely due to compensatory role of Fgfr2b.

In the early developing mouse lung, it is well accepted that mesenchymal Fgf10 acts on the epithelium through its receptor Fgfr2b, whereas a direct action on the mesenchyme does not occur until E14.5 (De Langhe et al., 2006). Our results suggest that during late lung development, Fgf10 signals to the mesenchyme through both Fgfr2b and Fgfr1b and that the two receptors play redundant roles in terms of LIF formation. The expression of *Fgfr2b* in the lung mesenchyme is a novel finding that suggests a mechanism of alternative splicing to allow the expression of this receptor. In the future, it will be interesting to investigate what controls *Fgfr2b* expression in the mesenchyme. The generation of double conditional knockout of Fgfr1b/2b in the mesenchyme will also be important to clarify whether these two receptors are the only mediators of Fgf10 signaling in the lung mesenchyme.

5.2. Contribution of preexisting lipofibroblasts to the pool of activated myofibroblasts during progression of fibrosis

The next question in the line was whether preexisting lipofibroblasts play a role in the progression of fibrosis. Our lineage tracing data using *AdrpCre-ERT2; mT/mG* mice showed that lipofibroblasts transdifferentiate to activated myofibroblasts at the peak of fibrosis (14 d.p.i.). Following observing this phenomenon another question rose whether pre-existing lipofibroblasts that transdifferentiate to activated myofibroblasts during fibrosis formation are the same cells that revert to a lipofibroblast-like phenotype following fibrosis resolution. Other possibility would be that the latter event is a general phenomenon of activated myofibroblast dedifferentiation after recovery. Unfortunately, due to the patchy and heterogeneous pattern of lung fibrosis, it cannot be concluded with certainty that either of these two scenarios is true.

PPARg, the main conductor of lipogenic differentiation in preadipocytes as well as mesenchymal stem cells, is also involved in lipofibroblast formation (Rehan and Torday, 2012) and PPARg agonists have been shown to protect mice from developing fibrosis (Fang et al., 2012; Genovese et al., 2005). Furthermore, adiponectin, which is a direct transcriptional target for PPARg, has shown a similar effect in primary culture of skin fibroblasts isolated from scleroderma patients (Fang et al., 2012). Here, we show that PPARg signaling is inhibited in IPF, likely due to hyperactive TGFb1 signaling. We also provide further mechanistic insights into the mode of action of rosiglitazone. We show that TGFb1 represses the lipogenic program by inhibiting PPARg expression in favor of the activation of the myogenic program in primary human lung fibroblasts. Conversely, rosiglitazone reinforces the lipogenic phenotype and inhibits TGFb1-mediated fibrogenesis. Thus, it is likely that in IPF, endogenous PPARg signaling is unable to counteract TGFb1 signaling without an exogenous stimulus. Our data emphasize the phenotypic

A recent study has reported the absence of lipid-droplet-containing cells in the human lung (Tahedl et al., 2014), although a previous study clearly demonstrated the presence of Oil Red O+ cells in both infant and adult human lungs (Rehan et al., 2006). In this study, we used the neutral lipid fluorescent stain LipidTOX and we clearly demonstrate

the presence of resident lipogenic cells that are located adjacent to AEC2 in human lungs. The discrepancy between the aforementioned findings might be related to the unsaturated fatty acid composition of lipid droplets in the human lung and the differences in detection methods (Ahlbrecht and McGowan, 2014). The process of spontaneous myofibroblast dedifferentiation observed in the mouse model of lung fibrosis is yet to be investigated in human IPF lungs. However, the data attained with human lung fibroblasts indicate that this process can be induced through intervention with PPARg agonists. Whether myofibroblasts are able to dedifferentiate to cell types other than lipofibroblasts is yet to be established. To date, there is a gap in the knowledge regarding cellular heterogeneity of human lung mesenchyme, apart from the classification of lung fibroblasts into lipogenic and myogenic populations. Thus, there is an urgent need to employ emerging new technologies such as single-cell RNA-seq to assess mesenchymal heterogeneity in the human lung and identify new cell types based on unique surface markers and molecular signatures. Such an approach might uncover novel fibroblastic populations and open new avenues to cure, or at least attenuate, IPF.

5.3. Metformin enforces lipogenic phenotype in activated myofibroblasts and accelerates resolution of fibrosis

There is emerging literature about the association between metabolic disorders and IPF incidence. Our group and others have already shown that the PPARγ agonist rosiglitazone, which is an antidiabetic agent, counteracts TGFβ1-mediated fibrogenesis in vitro and in vivo (El Agha et al., 2017; Burgess et al., 2005; Genovese et al., 2005). In this study, we demonstrate that the first-line antidiabetic drug, metformin, inhibits collagen production in primary human lung fibroblasts and in ex vivo cultured human IPF PCLS and strongly enhances myo- to lipofibroblast transdifferentiation linked with phenotypic recovery from fibrosis (Fig.18).

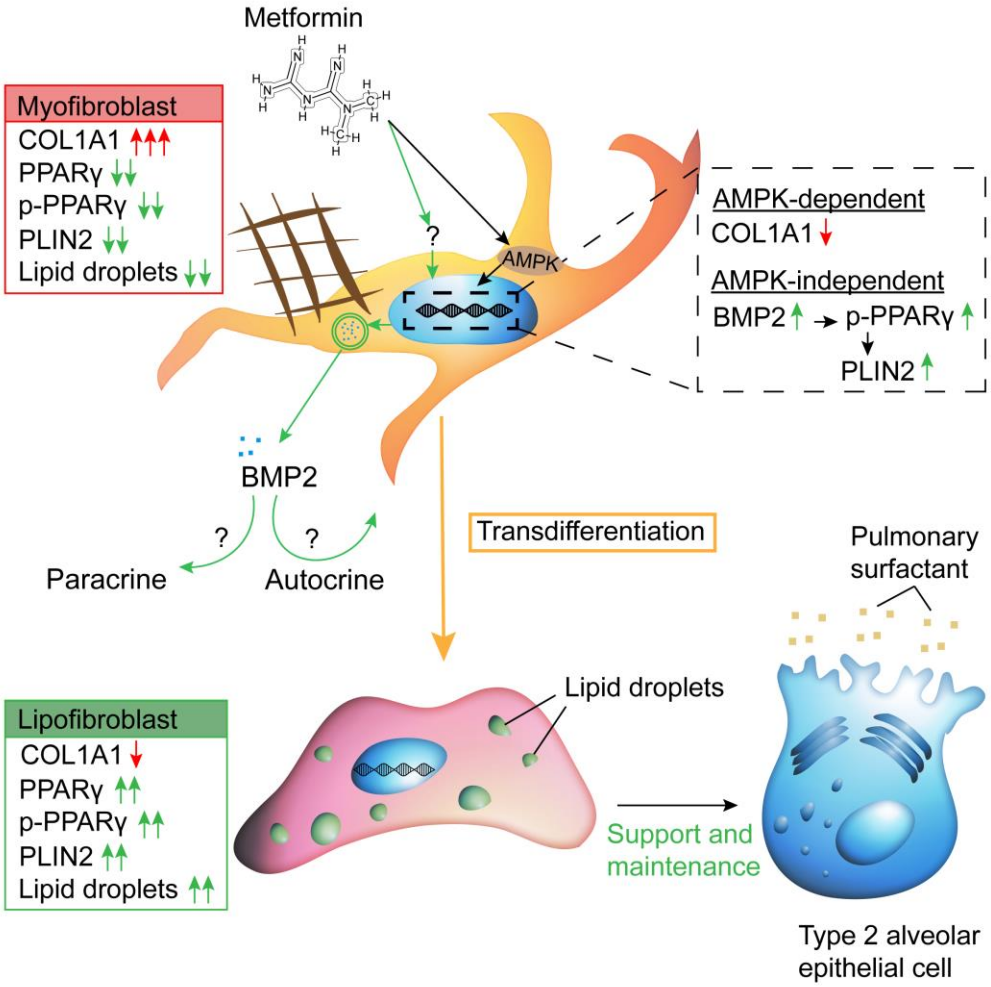

Figure 18. Model for the antifibrotic mechanism of action of metformin in human lung fibrosis.

Metformin activates AMPK signaling in myofibroblasts, leading to suppression of collagen production, and induces lipogenic differentiation via an AMPK-independent mechanism involving BMP2 release and PPARγ phosphorylation. Arising lipofibroblasts are known to support type 2 alveolar epithelial stem cells in the lung.

Although the PCLS culture system does not fully recapitulate the in vivo situation, it adds cellular, molecular and matrix complexity compared to standard cell culture techniques and – in our opinion – offers a valuable preclinical analytical tool. Accordingly, therapeutic application of metformin in bleomycin-injured mice resulted in accelerated resolution of fibrosis by altering the fate of fibrosis-associated myofibroblasts and inducing their

lipogenic differentiation. In our in vivo experiments, metformin was introduced through drinking water and the effects on lung repair were evident based on fibrosis assessment and myofibroblast fate switching. No adverse, systemic side effects of such treatment were observed. Although metformin is safe and well tolerated in humans, it confers the risk of hypoglycemia in case of long-term use, although this risk is still lower than that associated with other antidiabetic agents (Leonard et al., 2018). Notably, detailed pathway analysis showed that the reduction of collagen synthesis was largely AMPK-dependent, whereas the transdifferentiation of myo- to lipofibroblasts occurred in a BMP2-PPARγ-dependent fashion and was largely AMPK-independent.

As mentioned above PPARγ is the master regulator of adipogenesis and it is expressed in various cell types in the human body. Its functions include – in addition to differentiation and maintenance of adipocytes (Siersbaek et al., 2010) - regulation of inflammatory responses in macrophages (Malur et al., 2009), regulation of osteogenesis (Sun et al., 2013) and cell metabolism (Lodhi and Semenkovich, 2014). Therefore, its role in homeostasis and disease is strictly context-dependent. PPARγ phosphorylation has been shown to act as an activation or inhibitory signal depending on the protein kinase involved and the cell type being studied. For example, an earlier study has shown that phosphorylation of Ser^{112} in the N-terminal transactivation domain of PPARγ by MAPK acts as an activation signal in Chinese hamster ovary (CHO) cells (Zhang et al., 1996a). On the other hand, a later study has shown that the same phosphorylation event of PPARγ by MAPK is an inhibitory signal in white adipose tissue (WAT) (Hosooka et al., 2008). Moreover, phosphorylation of the same serine residue in WAT by cyclin-dependent kinase 7 (CDK7) acts as an activation signal (Compe et al., 2005), and so does phosphorylation by CDK9 in the embryonic mouse preadipocyte cell line 3T3-L1 (Iankova et al., 2006). Therefore, it is clear that the outcome of phosphorylation in terms of PPARγ activation and consequently lipogenic differentiation is context-dependent. In this study, we found that metformin significantly upregulates *BMP2* and *PPARg* (at the mRNA level), increases the phosphorylation of PPARγ protein at Ser^{112}, upregulates the downstream target *PLIN2* (Rehan and Torday, 2012; Varisco et al., 2012) and induces lipid-droplet acumulation in human IPF lung fibroblasts. Interestingly, it has been reported that metformin inhibits the upregulation of *PPARg* and *PLIN2* in mouse hepatocytes in

response to fructose diet (Karise et al., 2017). Metformin, however, does not alter *PPARg* and *PLIN2* expression levels in animals that receive normal diet (Karise et al., 2017). Moreover, it has been shown that metformin inhibits adipogenesis in mesenchymal stem cells (Chen et al., 2017) and 3T3-L1 preadipocytes (Alexandre et al., 2008). Therefore, the biological and physiological outcome of metformin treatment is clearly context-and cell type-specific.

In an attempt to explore modulations in serine/threonine protein kinase activities upon metformin treatment, human IPF lung fibroblasts were subjected to a protein kinase activity assay (PamStation). The results showed significantly reduced kinase activities for CDK1, CDK3, MAPK11/14 and ERK1/2. It is worth mentioning that CDK7 and CDK9 did not show a conclusive activity profile (data not shown). Considering the relevance of ERK1/2 in lung fibrosis (Madala et al., 2012) and the fact that PPARγ can serve as a substrate for MAPK (Hosooka et al., 2008; Zhang et al., 1996a), we validated the effect of metformin in inhibiting the activity of ERK1/2 by Western blotting and the results showed robust inhibition of p-ERK1/2 levels in IPF lung fibroblasts in response to metformin treatment. Treatment of human IPF lung fibroblasts with Selumetinib (a potent and selective inhibitor of MEK that is directly upstream of ERK) did not yield significant changes in the expression levels of lipogenic or myogenic marker genes (Fig. S5C-F). Therefore, we conclude that the ERK pathway is not involved in metformin-mediated myo- to lipofibroblast transdifferentiation and collagen reduction. Our finding that loss of function of *AMPK* did not affect lipogenic differentiation in response to metformin treatment suggests that AMPK is not the major kinase responsible for PPARγ phosphorylation and lipogenic differentiation. The identity of the protein kinase(s) responsible for PPARγ phosphorylation at Ser^{112}, including members of the CDK family, and induction of lipogenic differentiation in response to metformin or BMP2 treatment warrants further investigations. Recently, two independent groups have shown that metformin inhibits the profibrotic effect of TGFβ1 in lung fibroblasts via AMKP activation (Rangarajan et al., 2018; Sato et al., 2016b). Our data are in line with these reports, but additionally reveal a novel mechanism by which metformin acts on lung fibroblasts to attenuate fibrosis. We show a central role for BMP2-PPARγ-induced myofibroblast-to-lipofibroblast transdifferentiation in the process of fibrosis resolution in response to

metformin. Our gain-of-function experiments showed that while AMPK activation significantly downregulated *COL1A1*, it did not induce *BMP2* and lipogenic marker expression or lipid-droplet accumulation, which indicates that activation of the AMPK pathway alone is not enough to trigger the transdifferentiation of myofibroblasts into lipofibroblasts. Correspondingly, knockdown of *AMPK* did not abolish metformin-mediated induction of lipogenic markers but attenuated the suppression of *COL1A1* expression. These data suggest that alternative signaling mechanisms also contribute to the antifibrotic effects of metformin. Our data strongly suggest that *BMP2* upregulation and PPARγ phosphorylation are centrally involved in these mechanisms. Interestingly, although treatment of primary human IPF lung fibroblasts with rhBMP2 was sufficient to phosphorylate PPARγ and induce lipogenic marker expression, rhBMP2 treatment did not result in *COL1A1* downregulation. Additionally, inhibition of BMP2 signaling suppressed metformin-induced lipogenic differentiation without affecting the ability of metformin to inhibit collagen production, and knockdown of *PPARg* abolished the ability of BMP2 to induce lipogenic differentiation. Therefore, we propose a model in which metformin firstly activates AMPK signaling, which downregulates *COL1A1*, and secondly activates an alternative pathway involving *BMP2* upregulation and PPARγ phosphorylation, which induces lipogenic differentiation.

Myofibroblast-to-lipofibroblast trans- or redifferentiation is a central hitherto largely underappreciated route for resolution of lung fibrosis. Side-by-side comparison of metformin with pirfenidone and nintedanib showed that the latter agents did not converge on this resolution route. It is worth mentioning that cells and tissues used for pirfenidone, nintedanib or metformin treatment were derived from the same patients. Metformin, like rosiglitazone and maybe other antidiabetic medications, may add a unique antifibrotic profile by inducing transdifferentiation of myo- to lipofibroblasts. Another likely possibility is that since IPF lung tissues are derived from end-stage patients that underwent lung transplantation, it might be that these samples had developed resistance to pirfenidone and nintedanib. Nevertheless, the robust response of these samples to metformin treatment in terms of *COL1A1* downregulation and lipogenic differentiation highlights the therapeutic potential of metformin in IPF.

Many reports have described the involvement of metformin in manipulating various metabolic pathways (Gonzalez-Barroso et al., 2012; Phielix et al., 2011; Viollet et al., 2012). In fact, metformin is known to disrupt mitochondrial complex I, thus inhibiting cellular respiration. Recently, Zhao et al. published an extensive analysis of metabolic alterations in IPF lungs compared to donors (Zhao et al., 2017). They concluded that several types of long- and medium-chain fatty acids are enriched in IPF lungs (Zhao et al., 2017). Sphingolipid metabolism was found to be suppressed while arginine metabolism was found to be enhanced in the IPF lungs (Zhao et al., 2017) Our KEGG analysis on metformin-treated human lung fibroblasts suggests that metformin might be able to correct such metabolic dysregulations. Better understanding of the metabolic switch in lung fibroblasts in response to metformin and the mechanisms leading to accumulation of lipid droplets warrants further research. Additionally, we cannot exclude that the beneficial effect of metformin in the context of lung fibrosis could also be attributed to direct effects on AT2, rather than solely mediated by effects on mesenchymal cells. In the future, it would be extremely important to establish a mesenchyme-free AT2 culture model (derived from IPF lungs) and test the effect of metformin, as well as other therapeutic candidates, in this context. Last but not least, the therapeutic role of metformin described in this study might also apply to other fibrotic diseases such as liver fibrosis and scleroderma, characterized by an imbalance between myofibroblasts and adipocyte-like cells (hepatic stellate cells) (Mederacke et al., 2013) and subcutaneous adipocytes (Marangoni et al., 2015; Plikus et al., 2017), respectively.

In a recent report, post-hoc analysis was performed on IPF patients derived from the placebo arms of three phase 3, double-blind, controlled trials of pirfenidone(Spagnolo et al., 2018). In that study, 71 metformin users did not present improvements in clinical outcomes compared to 553 non-metformin users (Spagnolo et al., 2018). As pointed out by Tzouvelekis and colleagues, these data cannot be generalized into the global IPF population due to many caveats in the study design including the post-hoc nature of the study, the low number of metformin users, lack of stringent criteria for diagnosis and assessment of diabetes control, inability to link metformin mechanisms to IPF pathogenesis or to delineate drug-drug interactions (Tzouvelekis et al., 2018). Given its low cost and the fact that it is well tolerated in humans, it will be useful to test the curative

effect of metformin, either alone or in combination with other antifibrotic agents, in non-diabetic IPF patients. A key aspect will be to identify biomarkers that predict drug responsiveness in the heterogeneous population of IPF patients. Given the high financial burden of developing novel medicines, drug repositioning might help accelerate the process of discovering a cure for IPF patients.

6. Conclusion

This study provides a better characterization of lipofibroblasts during lung development and their contribution to progression of pulmonary fibrosis. Furthermore, it gives more insight regarding potential therapeutic efficacy of the first line antidiabetic drug, metformin, in reversing pulmonary fibrosis via enforcing lipogenic phenotype in activated myofibroblasts.

In the first part of this study, dynamics of lipofibroblast formation and involvement of FGF10 signaling in this procedure were explored. Lipofibroblasts start to appear at late pseudoglandular stage in the lung development.

Next, the hypothesis that whether lipofibroblasts can contribute to the pool of activated myofibroblasts and revert back to their original status were examined. Lineage tracing experiments, showed that preexisting lipofibroblasts indeed transdifferentiate to activated myofibroblasts due to hyperactive TGFβ1 signaling and revert to their lipogenic form during resolution phase. Suppression of PPARg signaling pathway, as the master switch of lipogenesis, via TGFβ1 can be rescued by forced activation of this signaling pathway using PPARg agonists such as rosiglitazone.

Later, the potential therapeutic effect of metformin on reversing pulmonary fibrosis was investigated. The data revealed that metformin can effectively attenuate TGFβ1 induced trans-differentiation to activated myofibroblasts and enforce activation of lipogenic pathways in the fibroblasts. In addition to primary culture of fibroblasts, this phenomenon was confirmed in ex-vivo model of lung organ culture, also known as Precision Cut Lung Slices (PCLS) and in-vivo model of bleomycin induced fibrosis. Furthermore, data demonstrated activation of a novel BMP2-PPARg axis following metformin treatment. Metformin induces production of BMP2 which in a potentially auto and paracrine manner results in activation of BMP2 signaling. This results in increasing level of PPARg phosphorylation which results in lipogenic differentiation.

7. Summary

As of today, lipofibroblasts remain as one of the most ill-defined cell populations is the lung. They are part of the lung mesenchyme and contain lipid droplets. Since they are located near alveolar epithelial type II cells, they shuttle the accumulated lipid droplets into AECII cells and support them with surfactant production. Our data revealed that lipofibroblasts start to emerge at E16.5 which is around the time that AECIIs start to appear. FGF10 acts in an autocrine and paracrine fashion on mesenchymal and epithelial cells which are crucial for the formation of LIFs and AECIIs. In the next step we have provided evidence regarding the contribution of lipofibroblasts to the pool of activated myofibroblasts during progression of fibrosis. In brief LIFs transdifferentiate to activated myofibroblasts due to hyperactivity of TGFβ1 signaling. Following the fate of these cells, our lineage tracing using *AdrpCre-ERT2*; *tdTomato^{flox}* mouse line, confirmed that during resolution phase, activated myofibroblasts, which were resulted from transdifferentiation of lipofibroblasts, revert back to their original status. Activation of PPARg signaling via treatment of cells with rosiglitazone negated the effects of TGFβ1 treatment and enforced the lipogenic phenotype in the pulmonary fibroblasts.

Following this concept, we hypothesized that treatment of the fibrotic lungs with reagents which activate PPARg signaling and enforce lipogenic phenotype in the activated myofibroblasts would yield beneficial effects for the patients. However, since rosiglitazone might not be the best choice due to increased risk of ischemic heart failure in the patients, we set the journey to find other antidiabetic drugs which would manipulate the cellular metabolism of activated myofibroblasts in the favor of lipofibroblasts. Thus, we decided to investigate the potential of metformin in conducting such effects. Treatment of pulmonary fibroblasts with TGFβ1 (forcefully transdifferentiating them to activated myofibroblasts) followed by metformin resulted in efficient suppression of TGFβ1 signaling and transdifferentiation to lipofibroblasts. To better mimic the in vivo situation, we cultured fresh PCLSs from human IPF patients and treated them with metformin. The results showed obvious improvement of tissue architecture, reduction of COL1A1 and increasing number of lipofibroblasts. The same readouts were also confirmed via treatment of bleomycin injured *ACTA2-CreERT2, tdTomato^{flox}* mice starting at 14 d.p.i. for the next 14 days. Metformin is a well-known agonist of AMPK. While, our data showed

that metformin reduces expression of *COL1A1* in an AMPK-dependent manner, induction of lipogenic markers such as *PLIN2* and *PPARg* via metformin treatment were independent of AMPK. To explore the molecular mechanism behind this event, the transcriptome of fibroblasts treated with metformin for 72 h was analyzed. KEGG analysis revealed that in addition to alteration of many of the metabolic pathways in favor of inducing lipid droplets, *BMP2* was expressed in much higher levels compared to control group. Treatment of fibroblasts with BMP2 induced expression of lipogenic markers and accumulation of lipid droplets. However, BMP2 treatment was not enough to reduce expression of COL1A1. Post translational modification analysis of PPARg following BMP2 or metformin treatment, illustrated a significant increase in PPARg phosphorylation at Ser-112. Hence, metformin suppresses expression of COL1A1 through activation of AMPK, in parallel to induction of lipogenic markers via BMP2-PPARg axis.

8. Zusammenfassung

Nach dem heutigen Stand der Wissenschaft, gehören die Lipofibroblasten (LIF) zu den wenig untersuchten Zellpopulationen der Lunge. Sie sind ein Bestandteil des Mesenchyms und enthalten lipidhaltige Vesikel. Aufgrund ihrer Nähe zu den Alveolareptihelzellen Typ II (AECII), transferieren sie die akkumulierten lipidhaltigen Vesikel zu den AECII Zellen und unterstützen diese damit in der Surfactantproduktion. Unsere Daten zeigten, dass die terminale Differenzierung der Lipofibroblasten am Embryonaltag 16.5 (E16.5) stattfindet, zu dem Zeitpunkt, wo die AECII erstmals in Erscheinung treten. FGF10 wirkt in einer autokrinen und parakrinen Weise auf die mesenchymalen und epithelialen Zellen, die für die Entstehung von LIFs und AECs II essentiell sind. Im nächsten Schritt, haben wir Beweise dafür, dass die Lipofibroblasten während der Fibroseenstehung einen entscheidenden Anteil an der Population der aktivierten Myofibroblasten beitragen. Kurz gefasst, transdifferenzieren die LIFs aufgrund einer Hyperaktivität von TGFß1 Signalweg zu aktivierten Myofibroblasten. Mit Hilfe der *AdrpCre-ERT2*; *tdTomato^{flox}* Mauslinie verfolgten wir die Veränderungen der LIFs während der Fibroserückbildung. Wir konnten feststellen, dass die aktivierten Myofibroblasten, die durch Transdifferenzierung der LIFs entstanden sind, sich wieder in ihren Urpsrungsstatus des LIFs zurückbildeten. Die Aktivierung des PPARg Signalweges durch Behandlung der Zellen mit Rosiglitazone hebt den Effekt der TGFß1 Behandlung auf und verstärkt den lipogenen Phänotyp der pulmonalen Fibroblasten.

Wir verfolgten dieses Konzept und stellten die Hypothese, dass eine Behandlung der fibrotischen Lunge mit Reagenzien, die den PPARg Signalweg aktivieren und den lipogenen Phänotyp in aktivierten Myofibroblasten forcieren, zu einem positiven Effekt für die Patienten führen könnten. Da Rosiglitazone jedoch ein erhöhtes Risiko für ischämisches Herzversagen darstellt, suchten wir nach anderen antidiabetischen Arzneimitteln, die den Zellmetabolismus der aktivierten Myofibroblasten zugunsten der Lipofibroblasten verändern. Infolgedessen, untersuchten wir Metformin im Hinblick auf diese Effekte. Die Behandlung von pulmonalen Fibroblasten mit TGFß1 führt zwingend zur Transdifferenzierung dieser zu aktivierten Myofibroblasten. Eine anschließende Behandlung mit Metformin resultiert in einer effizienten Suppression des TGFß1 Signalweges und eine Transdifferenzierung der aktivierten Myofibroblasten zu

Lipofibroblasten. Um die Situation in humanen Lungen zu simulieren, wurden frisch kultivierte Lungenschnitte (precision cut lung slices = PCLS) von Patienten mit idiopathische Pulmonalfibrose (IPF) mit Metformin behandelt. Dies führte zu einer Verbesserung der pumonalen Mikrostruktur, Reduktion von COL1A1 und Zunahme der Lipofibroblasten. Dieselben Ergebnisse erzielten wir, als wir mit Bleomycin behandelte Mäuse der Linie *ACTA2Cre-ERT2; tdTomato^{flox}*, 14 Tage nach Bleomycin Gabe für 14 Tage mit Metformin behandelten. Metformin ist ein bekannter Agonist von AMPK. Unsere Ergebnisse zeigten, dass Metformin über einen AMPK-abhängigen Mechanismus die Expression von COL1A1 reduziert. Andererseits ist die Induktion von lipogenen Marker wie PLIN2 und PPARg durch Metformin unabhängig von AMPK. Um den zu Grunde liegenden Mechanismus zu verstehen, wurden die Transkriptome der Fibroblasten 72 h nach Behandlung mit Metformin untersucht. KEGG Analysen zeigten neben der Aktivierung von vielen metabolischen “Pathways” zur Induktion von lipidhaltigen Vesikeln, eine deutlich erhöhte Expression von BMP2 im Vergleich zur Kontrollgruppe. Eine Behandlung von Fibroblasten mit BMP2 induziert Expression von lipogenen Markern und führt zur Akkumulation von lipighaltigen Vesikeln. Jedoch führte BMP2 nicht zur reduzierten Expression von *COL1A1*. Eine posttranslationale Analyse von PPARg nach Behandlung mit BMP2 oder Metformin, zeigte einen drastischen Anstieg von Ser-112 in PPARg, die zu einer höheren Aktivierung des Proteins führt. Infolgedessen schlußfolgern wir, dass Metformin über die Aktivierung von AMPK die Expression von *COL1A1* unterdrückt, während sie parallel die lipogenen Marker über die BMP2-PPARg Achse induziert.

9. References

El Agha, E., Herold, S., Al Alam, D., Quantius, J., MacKenzie, B., Carraro, G., Moiseenko, A., Chao, C.-M., Minoo, P., Seeger, W., et al. (2014). Fgf10-positive cells represent a progenitor cell population during lung development and postnatally. Development *141*, 296–306.

El Agha, E., Moiseenko, A., Kheirollahi, V., De Langhe, S., Crnkovic, S., Kwapiszewska, G., Szibor, M., Kosanovic, D., Schwind, F., Schermuly, R.T., et al. (2017). Two-Way Conversion between Lipogenic and Myogenic Fibroblastic Phenotypes Marks the Progression and Resolution of Lung Fibrosis. Cell Stem Cell *20*, 261–273.e3.

Ahlbrecht, K., and McGowan, S.E. (2014). In search of the elusive lipofibroblast in human lungs. Am. J. Physiol. Cell. Mol. Physiol. *307*, L605–L608.

Alexandre, K.B., Smit, A.M., Gray, I.P., and Crowther, N.J. (2008). Metformin inhibits intracellular lipid accumulation in the murine pre-adipocyte cell line, 3T3-L1. Diabetes, Obes. Metab. *10*, 688–690.

Anderson, J.C., Willey, C.D., Mehta, A., Welaya, K., Chen, D., Duarte, C.W., Ghatalia, P., Arafat, W., Madan, A., Sudarshan, S., et al. (2015). High Throughput Kinomic Profiling of Human Clear Cell Renal Cell Carcinoma Identifies Kinase Activity Dependent Molecular Subtypes. PLoS One *10*, e0139267.

Anderson, J.C., Minnich, D.J., Dobelbower, M.C., Denton, A.J., Dussaq, A.M., Gilbert, A.N., Rohrbach, T.D., Arafat, W., Welaya, K., Bonner, J.A., et al. (2016). Correction: Kinomic Profiling of Electromagnetic Navigational Bronchoscopy Specimens: A New Approach for Personalized Medicine. PLoS One *11*, e0161986.

Andrzejewski, S., Gravel, S.-P., Pollak, M., and St-Pierre, J. (2014). Metformin directly acts on mitochondria to alter cellular bioenergetics. Cancer Metab. *2*, 12.

Arsenault, R., Griebel, P., and Napper, S. (2011). Peptide arrays for kinome analysis: new opportunities and remaining challenges. Proteomics *11*, 4595–4609.

Averill, F., Albertson, T.E., Baratz, D.M., Chaudhary, S., Mobin, S., O'Brien, T., Scholand, M.B., Whelan, T.P.M., Poyurovsky, M., Schueller, O., et al. (2018). A Phase 2 Trial of

KD025 to Assess Efficacy, Safety and Tolerability in Patients with Idiopathic Pulmonary Fibrosis. In C97. DIFFUSE PARENCHYMAL LUNG DISEASES: EVALUATION, OUTCOMES, AND TRIALS, (American Thoracic Society), pp. A5927–A5927.

Barron, L., Gharib, S.A., and Duffield, J.S. (2016). Lung Pericytes and Resident Fibroblasts: Busy Multitaskers. Am. J. Pathol. *186*, 2519–2531.

Barry-Hamilton, V., Spangler, R., Marshall, D., McCauley, S., Rodriguez, H.M., Oyasu, M., Mikels, A., Vaysberg, M., Ghermazien, H., Wai, C., et al. (2010). Allosteric inhibition of lysyl oxidase-like-2 impedes the development of a pathologic microenvironment. Nat. Med. *16*, 1009–1017.

Bartram, U., and Speer, C.P. (2004). The role of transforming growth factor beta in lung development and disease. Chest *125*, 754–765.

Beers, M.F., and Moodley, Y. (2017). When Is an Alveolar Type 2 Cell an Alveolar Type 2 Cell? A Conundrum for Lung Stem Cell Biology and Regenerative Medicine. Am. J. Respir. Cell Mol. Biol. *57*, 18–27.

Brody, J.S., and Kaplan, N.B. (1983). Proliferation of alveolar interstitial cells during postnatal lung growth. Evidence for two distinct populations of pulmonary fibroblasts. Am. Rev. Respir. Dis. *127*, 763–770.

Burgess, H.A., Daugherty, L.E., Thatcher, T.H., Lakatos, H.F., Ray, D.M., Redonnet, M., Phipps, R.P., and Sime, P.J. (2005). PPARgamma agonists inhibit TGF-beta induced pulmonary myofibroblast differentiation and collagen production: implications for therapy of lung fibrosis. Am. J. Physiol. Lung Cell. Mol. Physiol. *288*, L1146-53.

Calvier, L., Chouvarine, P., Legchenko, E., Hoffmann, N., Geldner, J., Borchert, P., Jonigk, D., Mozes, M.M., and Hansmann, G. (2017). PPARgamma Links BMP2 and TGFbeta1 Pathways in Vascular Smooth Muscle Cells, Regulating Cell Proliferation and Glucose Metabolism. Cell Metab. *25*, 1118–1134.e7.

Castilla-Guerra, L., Fernandez-Moreno, M.D.C., Leon-Jimenez, D., and Carmona-Nimo, E. (2018). Antidiabetic drugs and stroke risk. Current evidence. Eur J Intern Med *48*, 1–5.

Chen, S.C., Brooks, R., Houskeeper, J., Bremner, S.K., Dunlop, J., Viollet, B., Logan, P.J., Salt, I.P., Ahmed, S.F., and Yarwood, S.J. (2017). Metformin suppresses adipogenesis through both AMP-activated protein kinase (AMPK)-dependent and AMPK-independent mechanisms. Mol. Cell. Endocrinol. *440*, 57–68.

Compe, E., Drane, P., Laurent, C., Diderich, K., Braun, C., Hoeijmakers, J.H.J., and Egly, J.-M. (2005). Dysregulation of the Peroxisome Proliferator-Activated Receptor Target Genes by XPD Mutations. Mol. Cell. Biol. *25*, 6065–6076.

Corona, J.C., and Duchen, M.R. (2016). PPARgamma as a therapeutic target to rescue mitochondrial function in neurological disease. Free Radic. Biol. Med. *100*, 153–163.

Dhatariya, K. (2019). Diabetes: the place of new therapies. Ther. Adv. Endocrinol. Metab. *10*, 2042018818807599.

Fang, F., Liu, L., Yang, Y., Tamaki, Z., Wei, J., Marangoni, R.G., Bhattacharyya, S., Summer, R.S., Ye, B., and Varga, J. (2012). The adipokine adiponectin has potent anti-fibrotic effects mediated via adenosine monophosphate-activated protein kinase: novel target for fibrosis therapy. Arthritis Res. Ther. *14*, R229.

Ferretti, A.C., Hidalgo, F., Tonucci, F.M., Almada, E., Pariani, A., Larocca, M.C., and Favre, C. (2019). Metformin and glucose starvation decrease the migratory ability of hepatocellular carcinoma cells: targeting AMPK activation to control migration. Sci. Rep. *9*, 2815.

Friedmacher, F., Hofmann, A.D., Takahashi, H., Takahashi, T., Gosemann, J.-H., and Puri, P. (2014). Disruption of THY-1 signaling in alveolar lipofibroblasts in experimentally induced congenital diaphragmatic hernia. Pediatr. Surg. Int. *30*, 129–135.

García-Sancho Figueroa, M.C., Carrillo, G., Pérez-Padilla, R., Fernández-Plata, M.R., Buendía-Roldán, I., Vargas, M.H., and Selman, M. (2010). Risk factors for idiopathic pulmonary fibrosis in a Mexican population. A case-control study. Respir. Med. *104*, 305–309.

Genovese, T., Cuzzocrea, S., Di Paola, R., Mazzon, E., Mastruzzo, C., Catalano, P., Sortino, M., Crimi, N., Caputi, A.P., Thiemermann, C., et al. (2005). Effect of rosiglitazone

and 15-deoxy-Delta12,14-prostaglandin J2 on bleomycin-induced lung injury. Eur. Respir. J. Off. J. Eur. Soc. Clin. Respir. Physiol. *25*, 225–234.

Gonzalez-Barroso, M.M., Anedda, A., Gallardo-Vara, E., Redondo-Horcajo, M., Rodriguez-Sanchez, L., and Rial, E. (2012). Fatty acids revert the inhibition of respiration caused by the antidiabetic drug metformin to facilitate their mitochondrial beta-oxidation. Biochim. Biophys. Acta *1817*, 1768–1775.

Günther, A., Korfei, M., Mahavadi, P., von der Beck, D., Ruppert, C., and Markart, P. (2012). Unravelling the progressive pathophysiology of idiopathic pulmonary fibrosis. Eur. Respir. Rev. *21*, 152–160.

Hosooka, T., Noguchi, T., Kotani, K., Nakamura, T., Sakaue, H., Inoue, H., Ogawa, W., Tobimatsu, K., Takazawa, K., Sakai, M., et al. (2008). Dok1 mediates high-fat diet–induced adipocyte hypertrophy and obesity through modulation of PPAR-γ phosphorylation. Nat. Med. *14*, 188–193.

Hung, C., Linn, G., Chow, Y.-H., Kobayashi, A., Mittelsteadt, K., Altemeier, W.A., Gharib, S.A., Schnapp, L.M., and Duffield, J.S. (2013). Role of lung pericytes and resident fibroblasts in the pathogenesis of pulmonary fibrosis. Am. J. Respir. Crit. Care Med. *188*, 820–830.

Iankova, I., Petersen, R.K., Annicotte, J.-S., Chavey, C., Hansen, J.B., Kratchmarova, I., Sarruf, D., Benkirane, M., Kristiansen, K., and Fajas, L. (2006). Peroxisome Proliferator-Activated Receptor γ Recruits the Positive Transcription Elongation Factor b Complex to Activate Transcription and Promote Adipogenesis. Mol. Endocrinol. *20*, 1494–1505.

Jiang, X., Chen, L., Zhang, Z., Sun, Y., Wang, X., and Wei, J. (2018). Protective and Therapeutic Effects of Engeletin on LPS-Induced Acute Lung Injury. Inflammation *41*, 1259–1265.

Kanigur Sultuybek, G., Soydas, T., and Yenmis, G. (2019). NF-kappaB as the mediator of metformin's effect on aging and age-related diseases. Clin. Exp. Pharmacol. Physiol.

Karise, I., Ornellas, F., Barbosa-da-Silva, S., Matsuura, C., del Sol, M., Aguila, M.B., and Mandarim-de-Lacerda, C.A. (2017). Liver and Metformin: Lessons of a fructose diet in

mice. Biochim. Open *4*, 19–30.

Kendall, R.T., and Feghali-Bostwick, C.A. (2014). Fibroblasts in fibrosis: novel roles and mediators. Front. Pharmacol. *5*, 123.

Kim, K.K., Kugler, M.C., Wolters, P.J., Robillard, L., Galvez, M.G., Brumwell, A.N., Sheppard, D., and Chapman, H.A. (2006). Alveolar epithelial cell mesenchymal transition develops in vivo during pulmonary fibrosis and is regulated by the extracellular matrix. Proc. Natl. Acad. Sci. U. S. A. *103*, 13180–13185.

King, T.E.J., Bradford, W.Z., Castro-Bernardini, S., Fagan, E.A., Glaspole, I., Glassberg, M.K., Gorina, E., Hopkins, P.M., Kardatzke, D., Lancaster, L., et al. (2014). A phase 3 trial of pirfenidone in patients with idiopathic pulmonary fibrosis. N. Engl. J. Med. *370*, 2083–2092.

Kolb, M., Raghu, G., Wells, A.U., Behr, J., Richeldi, L., Schinzel, B., Quaresma, M., Stowasser, S., and Martinez, F.J. (2018). Nintedanib plus Sildenafil in Patients with Idiopathic Pulmonary Fibrosis. N. Engl. J. Med. *379*, 1722–1731.

Kulkarni, A.A., Thatcher, T.H., Olsen, K.C., Maggirwar, S.B., Phipps, R.P., and Sime, P.J. (2011). PPAR-gamma ligands repress TGFbeta-induced myofibroblast differentiation by targeting the PI3K/Akt pathway: implications for therapy of fibrosis. PLoS One *6*, e15909.

Lakshmi, S.P., Reddy, A.T., and Reddy, R.C. (2017). Transforming growth factor beta suppresses peroxisome proliferator-activated receptor gamma expression via both SMAD binding and novel TGF-beta inhibitory elements. Biochem. J. *474*, 1531–1546.

De Langhe, S.P., Carraro, G., Warburton, D., Hajihosseini, M.K., and Bellusci, S. (2006). Levels of mesenchymal FGFR2 signaling modulate smooth muscle progenitor cell commitment in the lung. Dev. Biol. *299*, 52–62.

Lee, S.J., Yang, E.K., and Kim, S.G. (2006). Peroxisome Proliferator-Activated Receptor-γ and Retinoic Acid X Receptor α Represses the TGFβ1 Gene via PTEN-Mediated p70 Ribosomal S6 Kinase-1 Inhibition: Role for Zf9 Dephosphorylation. Mol. Pharmacol. *70*, 415 LP-425.

Leonard, C.E., Han, X., Brensinger, C.M., Bilker, W.B., Cardillo, S., Flory, J.H., and Hennessy, S. (2018). Comparative risk of serious hypoglycemia with oral antidiabetic monotherapy: A retrospective cohort study. Pharmacoepidemiol. Drug Saf. *27*, 9–18.

Li, C., Xue, Y., Xi, Y.R., and Xie, K. (2017). Progress in the application and mechanism of metformin in treating non-small cell lung cancer. Oncol Lett *13*, 2873–2880.

Lodhi, I.J., and Semenkovich, C.F. (2014). Peroxisomes: a nexus for lipid metabolism and cellular signaling. Cell Metab. *19*, 380–392.

Loubiere, C., Clavel, S., Gilleron, J., Harisseh, R., Fauconnier, J., Ben-Sahra, I., Kaminski, L., Laurent, K., Herkenne, S., Lacas-Gervais, S., et al. (2017). The energy disruptor metformin targets mitochondrial integrity via modification of calcium flux in cancer cells. Sci. Rep. *7*, 5040.

Luo, Z., Chen, W., Wu, W., Luo, W., Zhu, T., Guo, G., Zhang, L., Wang, C., Li, M., and Shi, S. (2019). Metformin promotes survivin degradation through AMPK/PKA/GSK-3beta-axis in non-small cell lung cancer. J. Cell. Biochem.

Madala, S.K., Schmidt, S., Davidson, C., Ikegami, M., Wert, S., and Hardie, W.D. (2012). MEK-ERK pathway modulation ameliorates pulmonary fibrosis associated with epidermal growth factor receptor activation. Am. J. Respir. Cell Mol. Biol. *46*, 380–388.

Madala, S.K., Korfhagen, T.R., Schmidt, S., Davidson, C., Edukulla, R., Ikegami, M., Violette, S.M., Weinreb, P.H., Sheppard, D., and Hardie, W.D. (2014). Inhibition of the alphavbeta6 integrin leads to limited alteration of TGF-alpha-induced pulmonary fibrosis. Am. J. Physiol. Lung Cell. Mol. Physiol. *306*, L726-35.

Maharaj, S., Shimbori, C., and Kolb, M. (2013). Fibrocytes in pulmonary fibrosis: a brief synopsis. Eur. Respir. Rev. *22*, 552–557.

Maher, T.M., Bareille, P., Costa, M.J., Fahy, W.A., Harrison, S.A., Holman, B.F., Lukey, P., Man, Y., Saunders, P., Simpson, J.K., et al. (2017). A Randomised, Placebo-Controlled, Double-Blind, Repeat Dose Escalation Study with Omipalisib (GSK2126458) in Patients with Idiopathic Pulmonary Fibrosis (IPF). In D14. IPF: MOVING FORWARD, (American Thoracic Society), pp. A7010–A7010.

Maher, T.M., van der Aar, E.M., Van de Steen, O., Allamassey, L., Desrivot, J., Dupont, S., Fagard, L., Ford, P., Fieuw, A., and Wuyts, W. (2018). Safety, tolerability, pharmacokinetics, and pharmacodynamics of GLPG1690, a novel autotaxin inhibitor, to treat idiopathic pulmonary fibrosis (FLORA): a phase 2a randomised placebo-controlled trial. Lancet. Respir. Med. *6*, 627–635.

Maksvytis, H.J., Vaccaro, C., and Brody, J.S. (1981). Isolation and characterization of the lipid-containing interstitial cell from the developing rat lung. Lab. Invest. *45*, 248–259.

Malur, A., Mccoy, A.J., Arce, S., Barna, B.P., Kavuru, M.S., Malur, A.G., and Thomassen, M.J. (2009). Deletion of PPAR gamma in alveolar macrophages is associated with a Th-1 pulmonary inflammatory response. J. Immunol. *182*, 5816–5822.

Marangoni, R.G., Korman, B.D., Wei, J., Wood, T.A., Graham, L. V, Whitfield, M.L., Scherer, P.E., Tourtellotte, W.G., and Varga, J. (2015). Myofibroblasts in murine cutaneous fibrosis originate from adiponectin-positive intradermal progenitors. Arthritis Rheumatol. (Hoboken, N.J.) *67*, 1062–1073.

Marginean, C.O.C., Marginean, C.O.C., and Melit, L.E. (2018). New Insights Regarding Genetic Aspects of Childhood Obesity: A Minireview. Front. Pediatr. *6*, 271.

Marra, F., Efsen, E., Romanelli, R.G., Caligiuri, A., Pastacaldi, S., Batignani, G., Bonacchi, A., Caporale, R., Laffi, G., Pinzani, M., et al. (2000). Ligands of peroxisome proliferator-activated receptor gamma modulate profibrogenic and proinflammatory actions in hepatic stellate cells. Gastroenterology *119*, 466–478.

Martin, H. (2010). Role of PPAR-gamma in inflammation. Prospects for therapeutic intervention by food components. Mutat. Res. *690*, 57–63.

McGowan, S.E., Jackson, S.K., Doro, M.M., and Olson, P.J. (1997). Peroxisome proliferators alter lipid acquisition and elastin gene expression in neonatal rat lung fibroblasts. Am. J. Physiol. *273*, L1249-57.

Mederacke, I., Hsu, C.C., Troeger, J.S., Huebener, P., Mu, X., Dapito, D.H., Pradere, J.-P., and Schwabe, R.F. (2013). Fate tracing reveals hepatic stellate cells as dominant contributors to liver fibrosis independent of its aetiology. Nat. Commun. *4*, 2823.

Medina-Gomez, G., Gray, S.L., Yetukuri, L., Shimomura, K., Virtue, S., Campbell, M., Curtis, R.K., Jimenez-Linan, M., Blount, M., Yeo, G.S.H., et al. (2007). PPAR gamma 2 prevents lipotoxicity by controlling adipose tissue expandability and peripheral lipid metabolism. PLoS Genet. *3*, e64.

Moore, B.B., Murray, L., Das, A., Wilke, C.A., Herrygers, A.B., and Toews, G.B. (2006). The role of CCL12 in the recruitment of fibrocytes and lung fibrosis. Am. J. Respir. Cell Mol. Biol. *35*, 175–181.

Nathan, S.D., Albera, C., Bradford, W.Z., Costabel, U., du Bois, R.M., Fagan, E.A., Fishman, R.S., Glaspole, I., Glassberg, M.K., Glasscock, K.F., et al. (2016). Effect of continued treatment with pirfenidone following clinically meaningful declines in forced vital capacity: analysis of data from three phase 3 trials in patients with idiopathic pulmonary fibrosis. Thorax *71*, 429–435.

O'Hare, K.H., and Sheridan, M.N. (1970). Electron microscopic observations on the morphogenesis of the albino rat lung, with special reference to pulmonary epithelial cells. Am. J. Anat. *127*, 181–205.

Palmer, S.M., Snyder, L., Todd, J.L., Soule, B., Christian, R., Anstrom, K., Luo, Y., Gagnon, R., and Rosen, G. (2018). Randomized, Double-Blind, Placebo-Controlled, Phase 2 Trial of BMS-986020, a Lysophosphatidic Acid Receptor Antagonist for the Treatment of Idiopathic Pulmonary Fibrosis. Chest *154*, 1061–1069.

Park, J., Ivey, M.J., Deana, Y., Riggsbee, K., Sorensen, E., Schwabl, V., Sjoberg, C., Hjertberg, T., Park, G.Y., Swonger, J.M., et al. (2019). The Tcf21 lineage constitutes the lung lipofibroblast population. Am. J. Physiol. Lung Cell. Mol. Physiol.

Parker, J.M., Glaspole, I.N., Lancaster, L.H., Haddad, T.J., She, D., Roseti, S.L., Fiening, J.P., Grant, E.P., Kell, C.M., and Flaherty, K.R. (2018). A Phase 2 Randomized Controlled Study of Tralokinumab in Subjects with Idiopathic Pulmonary Fibrosis. Am. J. Respir. Crit. Care Med. *197*, 94–103.

Penna, G.C., Vaisman, F., Vaisman, M., Sobrinho-Simoes, M., and Soares, P. (2016). Molecular Markers Involved in Tumorigenesis of Thyroid Carcinoma: Focus on

Aggressive Histotypes. Cytogenet. Genome Res. *150*, 194–207.

Phielix, E., Szendroedi, J., and Roden, M. (2011). The role of metformin and thiazolidinediones in the regulation of hepatic glucose metabolism and its clinical impact. Trends Pharmacol. Sci. *32*, 607–616.

Piersma, S.R., Labots, M., Verheul, H.M.W., and Jiménez, C.R. (2010). Strategies for kinome profiling in cancer and potential clinical applications: chemical proteomics and array-based methods. Anal. Bioanal. Chem. *397*, 3163–3171.

Plikus, M. V, Guerrero-Juarez, C.F., Ito, M., Li, Y.R., Dedhia, P.H., Zheng, Y., Shao, M., Gay, D.L., Ramos, R., Hsi, T.-C., et al. (2017). Regeneration of fat cells from myofibroblasts during wound healing. Science *355*, 748–752.

Poulsen, L. la C., Siersbaek, M., and Mandrup, S. (2012). PPARs: fatty acid sensors controlling metabolism. Semin. Cell Dev. Biol. *23*, 631–639.

Raghu, G., Scholand, M.B., de Andrade, J., Lancaster, L., Mageto, Y., Goldin, J., Brown, K.K., Flaherty, K.R., Wencel, M., Wanger, J., et al. (2016). FG-3019 anti-connective tissue growth factor monoclonal antibody: results of an open-label clinical trial in idiopathic pulmonary fibrosis. Eur. Respir. J. *47*, 1481–1491.

Raghu, G., Mouded, M., Culver, D.A., Hamblin, M.J., Golden, J.A., Veeraraghavan, S., Enelow, R.I., Lancaster, L.H., Goldberg, H.J., Frost, A.E., et al. (2018a). Randomized, Double-Blind, Placebo-Controlled, Multiple Dose, Dose-Escalation Study of BG00011 (Formerly STX-100) in Patients with Idiopathic Pulmonary Fibrosis (IPF). In D14. ILD: CLINICAL RESEARCH, (American Thoracic Society), pp. A7785–A7785.

Raghu, G., Richeldi, L., Crestani, B., Wung, P., Bejuit, R., Esperet, C., and Soubrane, C. (2018b). Safety and Efficacy of SAR156597 in Idiopathic Pulmonary Fibrosis (IPF): A Phase 2, Randomized, Double-Blind, Placebo-Controlled Study. In A93. ILD: CLINICAL TRIALS, (American Thoracic Society), pp. A2441–A2441.

Ramasamy, S.K., Mailleux, A.A., Gupte, V. V, Mata, F., Sala, F.G., Veltmaat, J.M., Del Moral, P.M., De Langhe, S., Parsa, S., Kelly, L.K., et al. (2007). Fgf10 dosage is critical for the amplification of epithelial cell progenitors and for the formation of multiple

mesenchymal lineages during lung development. Dev. Biol. *307*, 237–247.

Rangarajan, S., Bone, N.B., Zmijewska, A.A., Jiang, S., Park, D.W., Bernard, K., Locy, M.L., Ravi, S., Deshane, J., Mannon, R.B., et al. (2018). Metformin reverses established lung fibrosis in a bleomycin model. Nat. Med. *24*, 1121–1127.

Rashid, J., Alobaida, A., Al-Hilal, T.A., Hammouda, S., McMurtry, I.F., Nozik-Grayck, E., Stenmark, K.R., and Ahsan, F. (2018). Repurposing rosiglitazone, a PPAR-gamma agonist and oral antidiabetic, as an inhaled formulation, for the treatment of PAH. J. Control. Release *280*, 113–123.

Reddy, A.T., Lakshmi, S.P., Banno, A., and Reddy, R.C. (2018). Role of GPx3 in PPARgamma-induced protection against COPD-associated oxidative stress. Free Radic. Biol. Med. *126*, 350–357.

Rehan, V.K., and Torday, J.S. (2012). PPARγ signaling mediates the evolution, development, homeostasis, and repair of the lung. PPAR Res. *2012*, 289867.

Rehan, V.K., and Torday, J.S. (2014). The lung alveolar lipofibroblast: an evolutionary strategy against neonatal hyperoxic lung injury. Antioxid. Redox Signal. *21*, 1893–1904.

Rehan, V.K., Sugano, S., Wang, Y., Santos, J., Romero, S., Dasgupta, C., Keane, M.P., Stahlman, M.T., and Torday, J.S. (2006). EVIDENCE FOR THE PRESENCE OF LIPOFIBROBLASTS IN HUMAN LUNG. Exp. Lung Res. *32*, 379–393.

Richeldi, L., du Bois, R.M., Raghu, G., Azuma, A., Brown, K.K., Costabel, U., Cottin, V., Flaherty, K.R., Hansell, D.M., Inoue, Y., et al. (2014). Efficacy and safety of nintedanib in idiopathic pulmonary fibrosis. N. Engl. J. Med. *370*, 2071–2082.

Rock, J.R., Barkauskas, C.E., Cronce, M.J., Xue, Y., Harris, J.R., Liang, J., Noble, P.W., and Hogan, B.L.M. (2011). Multiple stromal populations contribute to pulmonary fibrosis without evidence for epithelial to mesenchymal transition. Proc. Natl. Acad. Sci. U. S. A. *108*, E1475-83.

Rowzee, A.M., Lazzarino, D.A., Rota, L., Sun, Z., and Wood, T.L. (2008). IGF Ligand and Receptor Regulation of Mammary Development. J. Mammary Gland Biol. Neoplasia *13*, 361–370.

Sato, N., Takasaka, N., Yoshida, M., Tsubouchi, K., Minagawa, S., Araya, J., Saito, N., Fujita, Y., Kurita, Y., Kobayashi, K., et al. (2016a). Metformin attenuates lung fibrosis development via NOX4 suppression. Respir. Res. *17*, 107.

Sato, N., Takasaka, N., Yoshida, M., Tsubouchi, K., Minagawa, S., Araya, J., Saito, N., Fujita, Y., Kurita, Y., Kobayashi, K., et al. (2016b). Metformin attenuates lung fibrosis development via NOX4 suppression. Respir. Res. *17*, 107.

Schafer, M.J., White, T.A., Iijima, K., Haak, A.J., Ligresti, G., Atkinson, E.J., Oberg, A.L., Birch, J., Salmonowicz, H., Zhu, Y., et al. (2017). Cellular senescence mediates fibrotic pulmonary disease. Nat. Commun. *8*, 14532.

Schultz, C.J., Torres, E., Londos, C., and Torday, J.S. (2002). Role of adipocyte differentiation-related protein in surfactant phospholipid synthesis by type II cells. Am. J. Physiol. Lung Cell. Mol. Physiol. *283*, L288-96.

Sgalla, G., Biffi, A., and Richeldi, L. (2016). Idiopathic pulmonary fibrosis: Diagnosis, epidemiology and natural history. Respirology *21*, 427–437.

Sgalla, G., Iovene, B., Calvello, M., Ori, M., Varone, F., and Richeldi, L. (2018). Idiopathic pulmonary fibrosis: pathogenesis and management. Respir. Res. *19*, 32.

Siersbaek, R., Nielsen, R., and Mandrup, S. (2010). PPARgamma in adipocyte differentiation and metabolism--novel insights from genome-wide studies. FEBS Lett. *584*, 3242–3249.

Sjodahl, G., Jackson Chelsea, L., Bartlett, J., Robert, S.D., and Berman David, M. (2019). Molecular Profiling In Muscle Invasive Bladder Cancer: More Than The Sum Of Its Parts. J. Pathol.

Sontake, V., Gajjala, P.R., Kasam, R.K., and Madala, S.K. (2019). New therapeutics based on emerging concepts in pulmonary fibrosis. Expert Opin. Ther. Targets *23*, 69–81.

Spagnolo, P., Kreuter, M., Maher, T.M.M., Wuyts, W., Bonella, F., Corte, T.J.J., Kopf, S., Weycker, D., Kirchgaessler, K.-U., and Ryerson, C.J.J. (2018). Metformin Does Not Affect Clinically Relevant Outcomes in Patients with Idiopathic Pulmonary Fibrosis. Respiration.

96, 314–322.

Speca, S., Dubuquoy, L., and Desreumaux, P. (2014). Peroxisome proliferator-activated receptor gamma in the colon: inflammation and innate antimicrobial immunity. J. Clin. Gastroenterol. *48 Suppl 1*, S23-7.

Sun, H., Kim, J.K., Mortensen, R., Mutyaba, L.P., Hankenson, K.D., and Krebsbach, P.H. (2013). Osteoblast-targeted suppression of PPARgamma increases osteogenesis through activation of mTOR signaling. Stem Cells *31*, 2183–2192.

Swigris, J.J., Ogura, T., Scholand, M.B., Glaspole, I., Maher, T.M., Kardatzke, D., Kaminski, J., Castro, M., Owen, R., Neighbors, M., et al. (2018). The RIFF Study (Cohort A): A Phase II, Randomized, Double-Blind, Placebo-Controlled Trial of Lebrikizumab as Monotherapy in Patients with Idiopathic Pulmonary Fibrosis. In D12. IMMUNOTHERAPY IN LUNG DISEASE, (American Thoracic Society), pp. A6167–A6167.

Tahedl, D., Wirkes, A., Tschanz, S.A., Ochs, M., and Mühlfeld, C. (2014). How common is the lipid body-containing interstitial cell in the mammalian lung? Am. J. Physiol. Cell. Mol. Physiol. *307*, L386–L394.

Tanjore, H., Xu, X.C., Polosukhin, V. V, Degryse, A.L., Li, B., Han, W., Sherrill, T.P., Plieth, D., Neilson, E.G., Blackwell, T.S., et al. (2009). Contribution of epithelial-derived fibroblasts to bleomycin-induced lung fibrosis. Am. J. Respir. Crit. Care Med. *180*, 657–665.

Tashiro, J., Rubio, G.A., Limper, A.H., Williams, K., Elliot, S.J., Ninou, I., Aidinis, V., Tzouvelekis, A., and Glassberg, M.K. (2017). Exploring Animal Models That Resemble Idiopathic Pulmonary Fibrosis. Front. Med. *4*, 118.

Teresi, R.E., Shaiu, C.-W., Chen, C.-S., Chatterjee, V.K., Waite, K.A., and Eng, C. (2006). Increased PTEN expression due to transcriptional activation of PPARgamma by Lovastatin and Rosiglitazone. Int. J. Cancer *118*, 2390–2398.

Todd, N.W., Luzina, I.G., and Atamas, S.P. (2012). Molecular and cellular mechanisms of pulmonary fibrosis. Fibrogenes. Tissue Repair *5*, 11.

Tomaru, T., Steger, D.J., Lefterova, M.I., Schupp, M., and Lazar, M.A. (2009). Adipocyte-

specific expression of murine resistin is mediated by synergism between peroxisome proliferator-activated receptor gamma and CCAAT/enhancer-binding proteins. J. Biol. Chem. *284*, 6116–6125.

Tontonoz, P., and Spiegelman, B.M. (2008). Fat and beyond: the diverse biology of PPARgamma. Annu. Rev. Biochem. *77*, 289–312.

Torday, J., Hua, J., and Slavin, R. (1995). Metabolism and fate of neutral lipids of fetal lung fibroblast origin. Biochim. Biophys. Acta *1254*, 198–206.

Tordet, C., Marin, L., and Dameron, F. (1981). Pulmonary di-and-triacylglycerols during the perinatal development of the rat. Experientia *37*, 333–334.

Tzouvelekis, A., Ntolios, P., Karampitsakos, T., Tzilas, V., Anevlavis, S., Bouros, E., Steiropoulos, P., Koulouris, N., Stratakos, G., Froudarakis, M., et al. (2017). Safety and efficacy of pirfenidone in severe Idiopathic Pulmonary Fibrosis: A real-world observational study. Pulm. Pharmacol. Ther. *46*, 48–53.

Tzouvelekis, A., Tzilas, V., Dassiou, M., and Bouros, D. (2018). Metformin in Idiopathic Pulmonary Fibrosis "Seeking the Holy-Grail through Drug-Repositioning". Respiration. 1–3.

Vallee, A., Vallee, J.-N., Guillevin, R., and Lecarpentier, Y. (2018). Interactions Between the Canonical WNT/Beta-Catenin Pathway and PPAR Gamma on Neuroinflammation, Demyelination, and Remyelination in Multiple Sclerosis. Cell. Mol. Neurobiol. *38*, 783–795.

Varisco, B.M., Ambalavanan, N., Whitsett, J.A., and Hagood, J.S. (2012). Thy-1 signals through PPARγ to promote lipofibroblast differentiation in the developing lung. Am. J. Respir. Cell Mol. Biol. *46*, 765–772.

Viollet, B., Guigas, B., Sanz Garcia, N., Leclerc, J., Foretz, M., and Andreelli, F. (2012). Cellular and molecular mechanisms of metformin: an overview. Clin. Sci. (Lond). *122*, 253–270.

Wang, L., Yin, Y., Hou, G., Kang, J., and Wang, Q. (2018). Peroxisome Proliferator-Activated Receptor (PPARgamma) Plays a Protective Role in Cigarette Smoking-Induced

Inflammation via AMP-Activated Protein Kinase (AMPK) Signaling. Med. Sci. Monit. *24*, 5168–5177.

Wang, Y., Liu, B., Yang, Y., Wang, Y., Zhao, Z., Miao, Z., and Zhu, J. (2019). Metformin exerts antidepressant effects by regulated DNA hydroxymethylation. Epigenomics.

White, E.S., Atrasz, R.G., Hu, B., Phan, S.H., Stambolic, V., Mak, T.W., Hogaboam, C.M., Flaherty, K.R., Martinez, F.J., Kontos, C.D., et al. (2006). Negative regulation of myofibroblast differentiation by PTEN (Phosphatase and Tensin Homolog Deleted on chromosome 10). Am. J. Respir. Crit. Care Med. *173*, 112–121.

Yan, F., Wen, Z., Wang, R., Luo, W., Du, Y., Wang, W., and Chen, X. (2017). Identification of the lipid biomarkers from plasma in idiopathic pulmonary fibrosis by Lipidomics. BMC Pulm. Med. *17*, 174.

Yoon, H.-Y., Kim, D.S., and Song, J.W. (2018). Efficacy and Safety of Pirfenidone in Advanced Idiopathic Pulmonary Fibrosis. Respiration. 1–10.

Yu, T., Wang, C., Yang, J., Guo, Y., Wu, Y., and Li, X. (2017). Metformin inhibits SUV39H1-mediated migration of prostate cancer cells. Oncogenesis *6*, e324.

Yuan, T., Volckaert, T., Chanda, D., Thannickal, V.J., and De Langhe, S.P. (2018). Fgf10 Signaling in Lung Development, Homeostasis, Disease, and Repair After Injury. Front. Genet. *9*, 418.

Zhang, B., Berger, J., Zhou, G., Elbrecht, A., Biswas, S., White-Carrington, S., Szalkowski, D., and Moller, D.E. (1996a). Insulin- and Mitogen-activated Protein Kinase-mediated Phosphorylation and Activation of Peroxisome Proliferator-activated Receptor γ. J. Biol. Chem. *271*, 31771–31774.

Zhang, H.Y., Gharaee-Kermani, M., Zhang, K., Karmiol, S., and Phan, S.H. (1996b). Lung fibroblast alpha-smooth muscle actin expression and contractile phenotype in bleomycin-induced pulmonary fibrosis. Am. J. Pathol. *148*, 527–537.

Zhao, Y.D., Yin, L., Archer, S., Lu, C., Zhao, G., Yao, Y., Wu, L., Hsin, M., Waddell, T.K., Keshavjee, S., et al. (2017). Metabolic heterogeneity of idiopathic pulmonary fibrosis: a metabolomic study. BMJ Open Respir. Res. *4*.

10. Acknowledgment

During this long journey, I was always surrounded by people which without their help, advice and encouragement accomplishing this task would be very hard if not impossible. Hence in this section I would like to express my gratitude and appreciation to them.

Initially, I would like to express my appreciation to my professor, Saverio Bellusci, which has provided me with the opportunity to do my thesis in his lab. Furthermore, his scientific support, positive mentality, great vision and optimism, his flat hierarchy in his lab and his inspiration power was phenomenal. When I look back now and think about the past couple of years, I notice how much I have learnt from him and how invaluable is this experience.

I would like to also thank Prof. Werner Seeger and Dr. Rory E. Morty for providing me the invaluable experience of joining the Molecular Biology and Medicine of Lung (MBML). During my time in the program, I always enjoyed very productive and interesting seminars, lectures and also tutorial sessions which provided me with ample opportunities to learn more and more, finding new colleagues and even greater friends, participate in the annual retreats to present my work to the top in the line scientists in the world which altogether was a fantastic experience. I would also like to thank the committee of International Giessen GraduateSchool for the Life Sciences (GGL) and Prof. Eveline Baumgart-Vogt for great seminars and events and also for establishing a huge social network of biologists.

I would also express my special gratitude to Dr. Elie El Algha as my mentor in the lab and tutor in the MBML program which supported me during the whole journey. he was always there to teach me different aspects of work ranging from wet lab techniques to publication of papers, long discussions about methodologies, data collection and interpretation, constructing manuscripts and so on. Furthermore, his constructive criticisms, insightful ideas, optimism, open mind for considering new ideas set an example for me to how to be more successful and made crushing the obstacles and solving the challenges easier and much more pleasant.

I would like to also thank my parents and my family which helped me with their emotional and spiritual support all the way until the end. Their kindness, encouragement to success

made me believe that the problems are always much smaller than the solutions. I thank them for believing me and always being there for me and lightening up my life all the time.

I would like to also thank my colleagues from Bellusci lab and other groups which helped me greatly during y thesis. I would like to thank Alena, Amit and Cho for being good colleagues and also fantastic friends' during all the up and downs of this path. I would like to also thank Ana Ivonne Vazquez-Armendariz which helped me a lot in our FACS core. I also express my gratitude toward my colleague and friend Alireza Saraji for his support during my thesis.

I would like to also thank all the people in the Bellusci lab which have always helped with different aspects of lab life and work which with without them, it would not be possible for me to keep pushing ahead and following the roads.

Thanking everybody who selflessly supported and aided me during my PhD studies, will require more than couple of pages. Hens, I would like to thank all the people who aided me during this path again.

Der Lebenslauf wurde aus der elektronischen Version der Arbeit entfernt.

The curriculum vitae was removed from the electronic version of the paper.